

ROTAVIRUS INTERACTIONS WITH SILICA AND NATURAL ORGANIC MATTER

BY

LEONARDO GUTIERREZ GARCES

DISSERTATION

Submitted in partial fulfillment of the requirements
for the degree of Doctor of Philosophy in Environmental Engineering in Civil Engineering
in the Graduate College of the
University of Illinois at Urbana-Champaign, 2013

Urbana, Illinois

Doctoral Committee:

Assistant Professor Thanh Huong Nguyen, Chair
Professor Benito Jose Mariñas
Professor Charles Werth
Professor Steve Granick

ABSTRACT

Rotavirus is a leading cause of gastrointestinal infections worldwide resulting in severe diarrhea and dehydration among children (Parashar et al., 2006). Rotavirus “ubiquitous” occurrence in water systems raises fundamental questions regarding interactions with surfaces that may affect its fate and transport. Consequently, the main objectives of this study were: 1) investigate the mechanisms that govern rotavirus interactions with environmental surfaces; and 2) examine the role of solution chemistry on these mechanisms.

Interactions between rotavirus particles under different solution chemistries were studied by time-resolved dynamic light scattering. No rotavirus aggregation was observed in NaCl solutions of up to 600 mM whether in the presence or absence of Suwannee River natural organic matter (SRNOM). Rotavirus aggregation was detected in SRNOM and divalent cation-containing solutions, and was faster than in the solely presence of divalent cations. Calculated attachment efficiencies were always higher in CaCl_2 than MgCl_2 solutions of the same concentration. Deposition of rotavirus on silica or SRNOM-coated silica surface was studied using quartz crystal microbalance technique. Experimental attachment efficiencies for rotavirus adsorption to silica or SRNOM-coated surface in MgCl_2 solution were lower than in CaCl_2 of the same concentration. No rotavirus deposition on both surfaces was observed in NaCl solutions. Atomic force microscopy (AFM) was used as a complementary technique to study interaction forces at the nano-scale. Decay lengths at different NaCl concentrations showed non-electrostatic repulsive forces as mainly responsible for eliminating rotavirus aggregation. Stronger adhesion forces were measured for rotavirus-rotavirus and rotavirus-SRNOM interactions in CaCl_2 compared to those in MgCl_2 solutions of the same concentration.

Rotavirus interactions with two NOM isolates of different characteristics in NaCl

solutions were studied by AFM. Colorado River-NOM (CRW) and SRNOM were selected as model non-humic and humic NOM, respectively. Rotavirus showed repulsive forces to SRNOM during approaching regime and no adhesion during retraction even at high ionic strength. Attractive forces were observed between rotavirus and CRW during approaching and high adhesion during retraction. These results indicate two different mechanisms based on the dissimilar characteristics of the two NOM isolates. Additional control experiments suggest ionic hydrogen bond-based and electrosteric-based interactions as major mechanism between rotavirus-CRW and rotavirus-SRNOM, respectively.

Besides electrostatics, results from this study suggest that steric repulsion, acid-base interactions, and divalent cation complexation with carboxylate groups on rotavirus surface and NOM are important mechanisms controlling rotavirus deposition and aggregation. In addition, the specific surface characteristics of NOM and solution ionic composition have a profound effect on the interactions with rotavirus that might affect its fate and transport in water systems.

This thesis is dedicated to my grandmother, mom, aunt Irais and Maria, and Stefanie for their
love and support throughout these years.

ACKNOWLEDGEMENTS

I would like to express my eternal gratitude to my advisor, Professor Helen Nguyen, for her academic guidance, personal support, endless patience, and mentoring throughout my Master and Doctorate studies. I just could not be prouder of my academic roots, research values, training, and knowledge that Helen has given to me. Also, I would like to extent my sincere appreciation to the members of my committee, Professors Benito Marinas, Charles Werth, and Steve Granick for their time, constructive feedback, and dedication to my research project.

To my dear comrades and members in the Nguyen research group, to the former members, and undergrad assistants (Dao, Nanxi, Yuanyuan, Ofelia, Qinwei, Mai, Ian, King, Nick, Heather, Jay, Ray, Sahid, Annia, Toni, Hanting, Baoling, Chia-Cheng, Tommy, Bridget, Brittany, and Sheila), and to Shaoying, thanks so much for your constant help in the lab and useful feedback to my research during group meetings. Thanks you so much Professor Vern for sharing with students your experience and wisdom, and to all the wonderful people at Newmark's 4th floor to whom I am honored to call my friends. You all have been my surrogate family throughout all these years. Special thanks to Dr. Mark S. Kuhlenschmidt and Theresa K Kuhlenschmidt and to Scott McLaren for the insightful discussion and suggestion regarding microbiology and atomic force microscopy; and to every single staff member at Frederick Seitz Material Science Research Laboratory (MRL) for their priceless training in microscopy techniques. In addition, I acknowledge National Science Foundation (NSF), The Center of Advanced Materials for the Purification of Water with Systems under the National Science Foundation (Water CAMPWS), Fulbright Commission, and Frederick Seitz Material Science Research Laboratory.

This research work and every future professional achievement in my career are dedicated to those brave women in my family without whom this thesis might not have been written, and to whom I am greatly indebted. To my mother and my Aunt Blanca, who always offered me unconditional love and support. To my Aunt Irais, who dedicated long hours to teach me the richness of learning. Finally, to my Grandmother and my Aunt Maria, who taught courage and dedication by example throughout their entire lives, and now serve as a source of inspiration and motivation to the rest of my family. Finally, I express my deepest gratitude and endless love to Stefanie for her constant support and faith in me during my PhD studies. Although I am not sure if I will ever be able to pay you back for all the things that you have done for me, please know that I will always be there for you. Along with God, thank you all for been my “footprints in the sand”.

TABLE OF CONTENTS

| | |
|---|-----|
| CHAPTER 1 – INTRODUCTION | 1 |
| CHAPTER 2 – DEPOSITION AND AGGREGATION KINETICS OF ROTAVIRUS IN DIVALENT CATION SOLUTIONS | 13 |
| CHAPTER 3 – INTERACTIONS BETWEEN ROTAVIRUS AND SUWANNEE RIVER ORGANIC MATTER: AGGREGATION, DEPOSITION, AND ADHESION FORCE MEASUREMENT | 38 |
| CHAPTER 4 – INTERACTIONS BETWEEN ROTAVIRUS AND NATURAL ORGANIC MATTER ISOLATES OF DIFFERENT PHYSICOCHEMICAL CHARACTERISTICS | 86 |
| CHAPTER 5 – CONCLUSIONS | 132 |
| CHAPTER 6 – FUTURE RESEARCH..... | 134 |
| APPENDIX – PROTOCOLS FOLLOWED | 136 |

CHAPTER 1

INTRODUCTION

1.1 Background

Enteric viruses (e.g., norovirus, sapovirus, adenovirus, astrovirus, or rotavirus) are a major causative of gastrointestinal infections worldwide mainly in developing countries due to socioeconomic and epidemiological reasons.^{1,2} Specifically, rotavirus is responsible for approximately 600,000 annual deaths of children and it is considered a leading cause of diarrhea among children, elderly, and immunocompromised.³⁻⁶ Fairly successful vaccines have been already developed.^{7,8} However, the availability of these vaccines in economically-sensitive regions is limited. Besides fecal-oral route, contaminated water represents an important vector of rotavirus transmission. In fact, documented rotavirus waterborne outbreaks have been reported worldwide (e.g., Sweden, Brazil, Russia, USA, Germany, Israel, China, etc.).⁶ Using different techniques, rotavirus has been detected in every natural and engineered water system such as: raw and treated sewage, surface water, groundwater, marine waters, recreational waters, and even drinking water treatment plants (of poor infrastructure).^{6,9-14} This “ubiquitous” occurrence raises fundamental questions regarding the interacting mechanisms occurring between rotavirus and surfaces that may affect rotavirus fate and transport in water systems.

Interactions between environmentally relevant surfaces (e.g., silica, iron oxides/hydroxides, mica, sand, etc.) and enteric viruses or bacteriophages (i.e., widely used as surrogates for enteric viruses) have been extensively studied.^{10,15} These studies have provided essential information regarding transport and fate phenomena. Electrostatic interactions have

proven important during virus adsorption to surfaces. For instance, in laboratory studies (batch and column experiments), MS2 was electrostatically adsorbed to positively-charged iron oxides (magnetite particles and hematite nanoparticles) at environmental pH.^{15, 16} Similarly, in field experiments electrostatic interactions between iron oxide-coated sand and bacteriophage PRD1 or MS2 were proposed to control virus transport.¹⁷⁻²¹ Other studies also suggested electrostatics to play an important role during the adsorption of MS2, T2 bacteriophage, poliovirus 1, reovirus type 1, and reovirus type 3 (all below their isoelectric points) to negatively-charged silica surfaces.²² Using quartz crystal microbalance (QCM), MS2 deposition rate on silica surfaces was observed to increase with increasing monovalent (Na^+) or divalent cation (Ca^{2+} or Mg^{2+}) concentration in solution, indicating an active role of solution chemistry during MS2-silica interaction. Nevertheless, several comparative studies have clearly remarked the importance of the surface characteristics of viruses on their interaction with different surfaces. For instance, different adsorption behaviors were observed for PRD1, MS2, poliovirus, and ΦX174 bacteriophage to soils in groundwater during batch and column experiments.²³ Similarly, MS2 was filtered less than recombinant Norwalk virus in quartz sand during column experiments.²⁴ This remarked differences would be attributed to the dissimilar surface characteristics of the viruses used in these investigations. These characteristics may widely vary between different type of viruses and even between different strains of the same type of virus (e.g., protein structure of outermost capsids of rotavirus or MS2, different isoelectric points of different strains of poliovirus, and different surface distribution of hydrophobic/hydrophilic neutral/charged residues among different rotavirus strains).^{10, 25-29} Consequently, the abovementioned investigations give us a clear insight of the importance and implications of the selection of a model virus as a function of its surface properties.

Similarly, due to the ever-present nature of natural organic matter (NOM) in water systems, interactions between viruses and NOM have received wide attention by recent studies. Firstly, NOM has been defined as a complex and heterogeneous mixture of decayed polyfunctional organic compounds, present in nature at wide concentrations and molecular weights.³⁰⁻³³ NOM have been extensively proposed to change the surfaces properties of mineral surfaces by means of adsorption (e.g., oxide-coated quartz, mica, or feldspar grains) and to compete with viruses for available attachment sites.^{16, 17, 20, 34} For instance, the presence of natural organic matter was observed to inhibit the adsorption of MS2 to hematite and magnetite, and of PRD1 to goethite in laboratory studies (batch experiments) and to hinder the deposition of MS2 and PRD1 to mineral surfaces in field experiments (iron oxide-coated sand aquifer).^{16, 35, 36}

¹⁷⁻²¹ Additionally, steric interactions have been widely suggested to arise between MS2 and NOM, due to the complex polymeric structures of NOM itself.^{37, 38} Conversely, other studies have proposed hydrophobicity to promote the interaction between PRD1 or MS2 and NOM.^{39, 40}

Another investigation observed no significant influence of dissolved organic matter on the transport of MS2 in sandy soils.⁴¹ In addition to surface properties of viruses, results from the abovementioned studies suggest that the interaction between NOM and viruses would also depend on the specific characteristics of NOM (e.g., aromaticity/aliphaticity, elemental composition, molar ratios, major functional groups, etc.) as proposed elsewhere.³⁸ Interestingly, the physicochemical characteristics of NOM are highly dependent on their origins.⁴²⁻⁴⁴ For instance, previous characterization works have found significant differences between NOM isolates collected from a variety of natural water sources.^{33, 45, 46}

Finally, recent studies have also focused on virus/virus interactions under different solution chemistries. Attractive interactions were observed among MS2 particles with

decreasing pH approaching isoelectric point (i.e., pH at which viruses carries no net electric charge).⁴⁷ In a similar study, MS2 showed high stability even at high concentration of monovalent cation in solution, suggesting strong steric and/or electrosteric effects.⁴⁸ Conversely, aggregation was induced in the presence of divalent cations, possibly due to cation bridging mechanisms between charged moieties on MS2 surface.

As described above, fate and transport of diverse viruses in water systems have been widely studied at the micro-scale (e.g. transport and recovery of viruses in iron oxide-coated sand aquifer; transport and retention of viruses in sand/modified sand/iron oxide/iron hydroxides/gravy/sandy soils columns simulating porous media). However, the development of new procedures for studying and quantifying interactions at the nano-scale between virus-virus and virus-environmentally relevant surfaces are of great importance. In addition, considering the high impact of rotavirus in our society, there has been (to the best of our knowledge) very limited research involving this pathogen as a model virus. Consequently, additional studies are essential to improve our understanding of this phenomenon, as well as the fundamental mechanisms that govern those interactions.

1.2 Objectives

The central objectives of this study were to:

- Develop a methodology to study surface interactions at the nano-scale between rotavirus particles, and rotavirus and environmental surfaces (e.g., mica, silica, quartz, and NOM-coated surfaces). These systems are representative of fate and transport of rotavirus in subsurface.
- Elucidate the specific mechanisms (electrostatic screening, steric repulsion, cation bridging, hydrogen bonding, etc.) that govern the interactions between rotavirus and NOM as a

function of the physicochemical characteristics of NOM. This central objective had a special focus on NOM due to its ubiquitous presence and high impact in every ecosystem in the planet.

- Examine the role and influence of solution ionic composition (ionic strength, presence of monovalent/divalent cations) on the main interacting mechanisms between rotavirus and surfaces.

To accomplish these objectives, the tools used and methods developed were specially adapted to mimic natural and engineered water system under very controlled experimental conditions.

1.3 Experimental approach

This investigation was conducted using multiple sensitive techniques to study the interactions between rotavirus particles and between rotavirus and environmental surfaces at different solution chemistries. Time-resolved dynamic light scattering technique was used to determine the aggregation kinetics of rotavirus at different solution chemistries (e.g., 0.1 mM to 200 mM CaCl_2 or MgCl_2 , and up to 600 mM NaCl). The incidence of NOM in solution (e.g., up to 20 mg C/L) in the aggregation kinetics of rotavirus was also examined. On the other hand, deposition kinetics of rotavirus on silica surface and Suwannee River NOM-coated surfaces were determined by quartz crystal microbalance technique at different electrolyte solutions (e.g., up to 1 mM CaCl_2 , or MgCl_2 , or NaCl solutions). The interpretation of the resulting data followed well-established theories developed deposition and aggregation of colloid and nanoparticles. Atomic force microscopy (AFM-contact mode) has proved to be a powerful technique that allows measuring specific and non-specific interactions at the very interface. In addition, bio-modification of AFM cantilever probes has been a great development for exploring interactions in water research. In the current study, AFM colloidal probes were bio-modified to measure the

interaction forces between rotavirus particles, and between rotavirus and silica, mica, or NOM coated-surfaces at different solution chemistries. Results from the abovementioned techniques were complemented with micrographs generated by transmission electron microscopy and atomic force microscopy-tapping mode, and measurement of electrophoretic mobility. Finally, a detailed description of the protocol followed and developed throughout this study was included in the APPENDIX.

1.4 References

1. Cruz, J. R.; Caceres, P.; Cano, F.; Flores, J.; Bartlett, A.; Torun, B., Adenovirus types 40 and 41 and rotaviruses associated with diarrhea in children from Guatemala. *Journal of Clinical Microbiology* **1990**, 28, (8), 1780-1784.
2. LeBaron, C. W.; Furutan, N. P.; Lew, J. F.; Allen, J. R.; Gouvea, V.; Moe, C.; Monroe, S. S., Viral agents of gastroenteritis. Public health importance and outbreak management. *Morbidity and Mortality Weekly Report* **1990**, 39, (RR-5), 24pp.-24pp.
3. Fields, B. N.; Knipe, D. M.; Howley, P. M.; Griffin, D. E., *Fields' Virology*. Lippincott-Raven: 2001.
4. Gentsch, J. R.; Woods, P. A.; Ramachandran, M.; Das, B. K.; Leite, J. P.; Alfieri, A.; Kumar, R.; Bhan, M. K.; Glass, R. I., Review of G and P typing results from a global collection of rotavirus strains: Implications for vaccine development. *Journal of Infectious Diseases* **1996**, 174, S30-S36.
5. Parashar, U. D.; Gibson, C. J.; Bresee, J. S.; Glass, R. I., Rotavirus and severe childhood diarrhea. *Emerging Infectious Diseases* **2006**, 12, (2), 304-306.
6. Gerba, C. P.; Rose, J. B.; Haas, C. N.; Crabtree, K. D., Waterborne rotavirus: A risk assessment. *Water Research* **1996**, 30, (12), 2929-2940.

7. Estes, M. K.; Cohen, J., ROTAVIRUS GENE STRUCTURE AND FUNCTION. *Microbiological Reviews* **1989**, 53, (4), 410-449.
8. Angel, J.; Franco, M. A.; Greenberg, H. B., Rotavirus vaccines: recent developments and future considerations. *Nature Reviews Microbiology* **2007**, 5, (7), 529-U18.
9. Villena, C.; Gabrieli, R.; Pinto, R. M.; Guix, S.; Donia, D.; Buonomo, E.; Palombi, L.; Cenko, F.; Bino, S.; Bosch, A.; Divizia, M., A large infantile gastroenteritis outbreak in Albania caused by multiple emerging rotavirus genotypes. *Epidemiology and Infection* **2003**, 131, (3), 1105-1110.
10. Havelaar, A. H.; Butler, M.; Farrah, S. R.; Jofre, J.; Marques, E.; Ketratanakul, A.; Martins, M. T.; Ohgaki, S.; Sobsey, M. D.; Zaiss, U., BACTERIOPHAGES AS MODEL VIRUSES IN WATER-QUALITY CONTROL. *Water Research* **1991**, 25, (5), 529-545.
11. Abbaszadegan, M.; Lechevallier, M.; Gerba, C., Occurrence of viruses in US groundwaters. *Journal American Water Works Association* **2003**, 95, (9), 107-120.
12. Villena, C.; El-Senousy, W. M.; Abad, F. X.; Pinto, R. M.; Bosch, A., Group a rotavirus in sewage samples from Barcelona and Cairo: Emergence of unusual genotypes. *Applied and Environmental Microbiology* **2003**, 69, (7), 3919-3923.
13. Borchardt, M. A.; Bertz, P. D.; Spencer, S. K.; Battigelli, D. A., Incidence of enteric viruses in groundwater from household wells in Wisconsin. *Applied and Environmental Microbiology* **2003**, 69, (2), 1172-1180.
14. Borchardt, M. A.; Haas, N. L.; Hunt, R. J., Vulnerability of drinking-water wells in La Crosse, Wisconsin, to enteric-virus contamination from surface water contributions. *Applied and Environmental Microbiology* **2004**, 70, (10), 5937-5946.

15. Atherton, J. G.; Bell, S. S., ADSORPTION OF VIRUSES ON MAGNETIC PARTICLES .2. DEGRADATION OF BACTERIOPHAGE-MS2 BY ADSORPTION TO MAGNETITE. *Water Research* **1983**, 17, (8), 949-953.
16. Gutierrez, L.; Li, X.; Wang, J. W.; Nangmenyi, G.; Economy, J.; Kuhlenschmidt, T. B.; Kuhlenschmidt, M. S.; Nguyen, T. H., Adsorption of rotavirus and bacteriophage MS2 using glass fiber coated with hematite nanoparticles. *Water Research* **2009**, 43, (20), 5198-5208.
17. Abudalo, R. A.; Bogatsu, Y. G.; Ryan, J. N.; Harvey, R. W.; Metge, D. W.; Elimelech, M., Effect of ferric oxyhydroxide grain coatings on the transport of bacteriophage PRD1 and *Cryptosporidium parvum* oocysts in saturated porous media. *Environmental Science & Technology* **2005**, 39, (17), 6412-6419.
18. Harvey, R. W.; Ryan, J. N., Use of PRD1 bacteriophage in groundwater viral transport, inactivation, and attachment studies. *Fems Microbiology Ecology* **2004**, 49, (1), 3-16.
19. Ryan, J. N.; Harvey, R. W.; Metge, D.; Elimelech, M.; Navigato, T.; Pieper, A. P., Field and laboratory investigations of inactivation of viruses (PRD1 and MS2) attached to iron oxide-coated qauartz sand. *Environmental Science & Technology* **2002**, 36, (11), 2403-2413.
20. Ryan, J. N.; Elimelech, M.; Ard, R. A.; Harvey, R. W.; Johnson, P. R., Bacteriophage PRD1 and silica colloid transport and recovery in an iron oxide-coated sand aquifer. *Environmental Science & Technology* **1999**, 33, (1), 63-73.
21. Pieper, A. P.; Ryan, J. N.; Harvey, R. W.; Amy, G. L.; Illangasekare, T. H.; Metge, D. W., Transport and recovery of bacteriophage PRD1 in a sand and gravel aquifer: Effect of sewage-derived organic matter. *Environmental Science & Technology* **1997**, 31, (4), 1163-1170.
22. Zerda, K. S.; Gerba, C. P.; Hou, K. C.; Goyal, S. M., ADSORPTION OF VIRUSES TO CHARGE-MODIFIED SILICA. *Applied and Environmental Microbiology* **1985**, 49, (1), 91-95.

23. Davis, J. A.; Farrah, S. R.; Wilkie, A. C., Adsorption of viruses to soil: impact of anaerobic treatment. *Water Science and Technology* **2006**, 54, (3), 161-167.
24. Redman, J. A.; Grant, S. B.; Olson, T. M.; Hardy, M. E.; Estes, M. K., Filtration of recombinant Norwalk virus particles and bacteriophage MS2 in quartz sand: Importance of electrostatic interactions. *Environmental Science & Technology* **1997**, 31, (12), 3378-3383.
25. Berg, G., *Viral Pollution of the Environment*. Taylor & Francis: 1983.
26. Golmohammadi, R.; Valegard, K.; Fridborg, K.; Liljas, L., THE REFINED STRUCTURE OF BACTERIOPHAGE-MS2 AT 2-CENTER-DOT-8-ANGSTROM RESOLUTION. *Journal of Molecular Biology* **1993**, 234, (3), 620-639.
27. Aoki, S. T.; Settembre, E. C.; Trask, S. D.; Greenberg, H. B.; Harrison, S. C.; Dormitzer, P. R., Structure of Rotavirus Outer-Layer Protein VP7 Bound with a Neutralizing Fab. *Science* **2009**, 324, (5933), 1444-1447.
28. Dormitzer, P. R.; Sun, Z. Y. J.; Wagner, G.; Harrison, S. C., The rhesus rotavirus VP4 sialic acid binding domain has a galectin fold with a novel carbohydrate binding site. *Embo Journal* **2002**, 21, (5), 885-897.
29. Monnier, N.; Higo-Moriguchi, K.; Sun, Z. Y. J.; Prasad, B. V. V.; Taniguchi, K.; Dormitzer, P. R., High-resolution molecular and antigen structure of the VP8*core of a sialic acid-independent human rotavirus strain. *Journal of Virology* **2006**, 80, (3), 1513-1523.
30. Cabaniss, S. E.; Shuman, M. S., COPPER-BINDING BY DISSOLVED ORGANIC-MATTER .1. SUWANNEE RIVER FULVIC-ACID EQUILIBRIA. *Geochimica Et Cosmochimica Acta* **1988**, 52, (1), 185-193.

31. Cabaniss, S. E.; Shuman, M. S., COPPER-BINDING BY DISSOLVED ORGANIC-MATTER .2. VARIATION IN TYPE AND SOURCE OF ORGANIC-MATTER. *Geochimica Et Cosmochimica Acta* **1988**, 52, (1), 195-200.
32. Thurman, E. M., *Organic geochemistry of natural waters*. Martinus Nijhoff/Dr. W. Junk Publishers: The Netherlands, 1985.
33. Ma, H. Z.; Allen, H. E.; Yin, Y. J., Characterization of isolated fractions of dissolved organic matter from natural waters and a wastewater effluent. *Water Research* **2001**, 35, (4), 985-996.
34. Walshe, G. E.; Pang, L.; Flury, M.; Close, M. E.; Flintoft, M., Effects of pH, ionic strength, dissolved organic matter, and flow rate on the co-transport of MS2 bacteriophages with kaolinite in gravel aquifer media. *Water Research* **2010**, 44, (4), 1255-1269.
35. Atherton, J. G.; Bell, S. S., ADSORPTION OF VIRUSES ON MAGNETIC PARTICLES .1. ADSORPTION OF BACTERIOPHAGE-MS2 AND THE EFFECT OF CATIONS, CLAY AND POLY-ELECTROLYTE. *Water Research* **1983**, 17, (8), 943-948.
36. Foppen, J. W. A.; Oklety, S.; Schijven, J. F., Effect of goethite coating and humic acid on the transport of bacteriophage PRD1 in columns of saturated sand. *Journal of Contaminant Hydrology* **2006**, 85, (3-4), 287-301.
37. Yuan, B. L.; Pham, M.; Nguyen, T. H., Deposition Kinetics of Bacteriophage MS2 on a Silica Surface Coated with Natural Organic Matter in a Radial Stagnation Point Flow Cell. *Environmental Science & Technology* **2008**, 42, (20), 7628-7633.
38. Zhuang, J.; Jin, Y., Virus retention and transport as influenced by different forms of soil organic matter. *Journal of Environmental Quality* **2003**, 32, (3), 816-823.

39. Bales, R. C.; Hinkle, S. R.; Kroeger, T. W.; Stocking, K.; Gerba, C. P., Bacteriophage adsorption during transport through porous media: chemical perturbations and reversibility. *Environmental Science & Technology* **1991**, 25, (12), 2088-2095.
40. Kinoshita, T.; Bales, R. C.; Maguire, K. M.; Gerba, C. P., Effect of pH on bacteriophage transport through sandy soils. *Journal of Contaminant Hydrology* **1993**, 14, (1), 55-70.
41. Cheng, L.; Chetochine, A. S.; Pepper, I. L.; Brusseau, M. L., Influence of DOC on MS-2 bacteriophage transport in a sandy soil. *Water, Air, and Soil Pollution* **2007**, 178, (1-4), 315-322.
42. Aiken, G. R., *Humic substances in soil, sediment, and water: geochemistry, isolation, and characterization*. Wiley: 1985.
43. Imai, A.; Fukushima, T.; Matsushige, K.; Kim, Y. H.; Choi, K., Characterization of dissolved organic matter in effluents from wastewater treatment plants. *Water Research* **2002**, 36, (4), 859-870.
44. Gu, B.; Schmitt, J.; Chen, Z.; Liang, L.; McCarthy, J. F., Adsorption and desorption of different organic matter fractions on iron oxide. *Geochimica Et Cosmochimica Acta* **1995**, 59, (2), 219-229.
45. Croue, J. P.; Benedetti, M. F.; Violleau, D.; Leenheer, J. A., Characterization and copper binding of humic and nonhumic organic matter isolated from the South Platte River: Evidence for the presence of nitrogenous binding site. *Environmental Science & Technology* **2003**, 37, (2), 328-336.
46. Hwang Cordelia, J.; Kranser, S. W.; Amy, G.; Bruchet, A.; Croue, J. P.; Leenheer Jerry, A., *Polar NOM: Characterization, DBPs, Treatment*. AWWA Research Foundation: 2001.

47. Langlet, J.; Gaboriaud, F.; Gantzer, C.; Duval, J. F. L., Impact of chemical and structural anisotropy on the electrophoretic mobility of spherical soft multilayer particles: The case of bacteriophage MS2. *Biophysical Journal* **2008**, 94, (8), 3293-3312.
48. Mylon, S. E.; Rinciog, C. I.; Schmidt, N.; Gutierrez, L.; Wong, G. C. L.; Nguyen, T. H., Influence of Salts and Natural Organic Matter on the Stability of Bacteriophage MS2. *Langmuir* **2010**, 26, (2), 1035-1042.

CHAPTER 2

DEPOSITION AND AGGREGATION KINETICS OF ROTAVIRUS IN DIVALENT CATION SOLUTIONS¹

2.1 *Abstract*

Aggregation kinetics of rotavirus in aqueous solutions and its deposition kinetics on silica surface in the presence of divalent (Ca^{2+} , Mg^{2+}) cations were studied using complementary techniques of time-resolved dynamic light scattering (TR-DLS) and quartz crystal microbalance (QCM). Within a reasonable temporal window of 4 hours, aggregation could be observed at levels as low as 10 mM of Ca^{2+} and 20 mM of Mg^{2+} . Attachment efficiencies were always greater in Ca^{2+} solutions of the same concentration, and the critical coagulation concentration (CCC) for rotavirus in Ca^{2+} solutions was slightly smaller than that in Mg^{2+} solutions. No aggregation was detected in Na^+ solution within the temporal window of four hours. Deposition experiments showed higher attachment coefficients in solutions containing Ca^{2+} , compared to those obtained in Mg^{2+} solution. The classic Derjaguin, Landau, Verwey and Overbeek (DLVO) theory failed to predict both the aggregation behavior of rotavirus and its deposition on silica surface. Besides electrostatic interactions, steric repulsions and specific interaction with divalent cations were important mechanisms in controlling rotavirus deposition and aggregation. Experimental results presented here suggest that rotavirus is not expected to aggregate in groundwater with typical hardness (up to 6mM Ca^{2+}) and rotavirus deposition on silica soil would be more favorable in the presence of Ca^{2+} than Mg^{2+} .

¹Reprinted, with permission, from Gutierrez, L.; Mylon, S. E.; Nash, B.; Nguyen, T. H., 2010, "Deposition and Aggregation Kinetics of Rotavirus in Divalent Cation Solutions," *Environmental Science & Technology* 44(12): 4552-4557.

2.2 *Introduction*

Viruses are bionanoparticles responsible for a wide array of diseases in bacteria, plants, and animals, and cause a number of waterborne diseases.^{1, 2} While the number and diversity of viruses in soils, sediments and freshwaters varies with host abundance and activity,³ they are routinely detected in private household wells, municipal wells and even deep confined aquifers,⁴⁻⁶ and due, in part, to their small of size, viruses (20 – 80 nm) are generally more mobile than bacteria (0.5 – 3 μm) and protozoan parasites (4 – 15 μm).¹ In light of this, it is reasonable to conclude that viruses played a central role in the 76% of waterborne disease outbreaks in the United States that were linked to ground water contamination⁷ between 1991 and 2002.

Studies on virus fate and transport in natural aquatic systems have focused on the interaction of viruses at important environmental interfaces, specifically the mineral/water interface and the virus/virus interface. Results from examples of the former demonstrated the importance of electrostatic interactions in the specific situation of viral adsorption to solid interfaces. Using bacteriophages as surrogates for enteric viruses, the field data obtained in an aquifer containing iron oxide-coated sands suggested that electrostatic interactions control virus transport.⁸⁻¹² In laboratory studies, the deposition of MS2 onto both bare silica and organic matter coated silica, Yuan et al.¹³ showed that increasing ionic strength resulted in increasing deposition rates due to the higher degree of charge screening. Virus/virus net attractive interactions were postulated by Langlet et al.¹⁴ as they observed decreases in the mean apparent diffusion coefficient of virus suspensions with decreases in pH. As the pH approached the virus isoelectric point (IEP), or pH at which viruses carries no net electric charge, aggregation resulted from decreases in electrostatic repulsive interactions. Most recently, Mylon et al.¹⁵ showed that

the bacteriophage MS2 exhibited extreme stability against aggregation in the presence of high concentrations of monovalent cations suggesting strong steric and electrosteric stabilization of MS2. In this study, however, divalent cations had a profound effect on the aggregation behavior of MS2 most likely because of complexation to charged moieties on the MS2 surface.

Groundwater contamination by enteric virus may cause serious public health concern,⁴ and therefore there is a need to study the interfacial interactions of these specific viruses. Some experimental evidence suggested that the use of MS2 and other well-studied bacteriophages as surrogates for enteric viruses may not be fully justified. For example, filtration experiments with bacteriophage MS2 and recombinant Norwalk virus particles suggest that bacteriophages may not be a suitable surrogate for virus transport experiments because of the different surface properties.¹⁶ Additionally, Gerba and Lance¹⁷ observed that high concentrations of dissolved organic matter did not reduce attachment of polio virus where recent laboratory and field studies have demonstrated that under similar conditions bacteriophage attachment^{12, 18} is reduced. The differences here most likely reflect the differences in surface properties between the bacteriophages MS2 and poliovirus.

Even though the use of MS2 as a model virus allows us to obtain a fundamental understanding of survivability and transport of viruses, there are important physical differences between bacteriophage MS2 and enteric viruses, including rotavirus resulting in an obvious need for more studies using enteric viruses. For example, the protein capsid of MS2 is constructed from 180 single polypeptides. Each polypeptide consists of 129 amino acids.¹⁹ Intact rotavirus is a complex dsRNA triple-layered capsid (TLP) virus. Glycoprotein VP7 (calcium dependent trimer with a T=13 icosahedral packing) and protein VP4 (60 monomers protruding as spikes) make up the outer capsid.^{20, 21} More important than the higher order structure differences

between MS2 and rotavirus is the distribution of the charged amino acids glutamic acid, aspartic acid and lysine about the outer most capsid. For rotavirus, there are 21 charged amino acids (6 aspartic acid, 9 Glutamic acid and 6 lysine) in one of the N-terminal proteins, VP8 (located on the tip of VP4). The specific chemistry of these charged moieties in aqueous solutions give rise to the unique characteristics of each type of virus, such as pH- dependent surface potential and isoelectric point (i.e. pH_{IEP} of RV is ~ 4.5 while pH_{IEP} of MS2 is ~ 3.5).²²

The objectives of this study were to probe the interfacial interactions of an enteric virus at the mineral/water interface quartz crystal microbalance technique and the virus/virus interface using time-resolved dynamic light scattering and to determine how important components of groundwater such as Ca^{2+} and Mg^{2+} might affect these interactions. Data interpretation was based on physical and chemical characteristics of viruses and theories developed for colloid and nanoparticle deposition and aggregation. For this study rotavirus was selected because it is the most common enteric virus resulting in severe gastroenteritis among children worldwide.²³

2.3 *Materials and Methods*

Solution chemistries. Solutions were prepared using deionized (DI) water of a resistivity of 18.2 M Ω cm (Millipore, Barnstead, USA). Electrolyte solutions (i.e. NaCl, NaHCO₃, MgCl₂, CaCl₂) were prepared using analytical grade reagents and filtered using a sterile vacuum bottle-top 0.22 μ m PES membrane filter (Millipore, Barnstead, USA). HEPES buffer was prepared with 100 mM NaCl and 10 mM HEPES (N-(2-hydroxyethyl) piperazine-N'-2-ethanesulfonic acid) at a final pH of 5.9. Poly-L-Lysine (PLL) hydrobromide solution was prepared in HEPES buffer at a final concentration of 0.1 g/L. An unbuffered pH of 5.9 was selected for this study.

Rotavirus preparation and infectivity assays. Group A porcine rotavirus OSU strain

(ATCC # VR892) was propagated by MA-104 cells (African green monkey kidney cells) following the protocols described previously.²⁴ Rotavirus was purified by centrifugation and micro and nanofiltration.²² Focus forming assay (FFU) using MA-104 cells²⁵ was used for rotavirus enumeration. The final stock of rotavirus was stored at 4°C at a final concentration of $\sim 5 \times 10^6$ FFU/ml in 1 mM NaCl and 0.1 mM CaCl_2 which is required to prevent rotavirus dissolution due to structural changes in the outer most capsid of rotavirus. The critical free Ca^{2+} concentration that leads to the dissociation of the outermost capsid proteins (VP4 and VP7) of porcine OSU rotavirus was quantified as 100 nM.²⁶

Measurement of electrophoretic mobility (EPM) for rotavirus. A Zetasizer ZS90 (Malvern, UK) with 1 mL clear disposable zeta cells (DTS1060C, Malvern, UK) was used for measuring the electrophoretic mobility of rotavirus. Rotavirus was added to desired electrolyte solutions (NaCl, NaHCO_3 , MgCl_2 or CaCl_2) and DI water to a final concentration of $\sim 8 \times 10^5$ FFU/ml. At least 3 measurements per sample were made. Zeta potential was obtained by converting EPM using the Smoluchowski equation by Dispersion Technology Software (v5.10, 2008, Malvern, UK). The lowest concentrations of Ca^{2+} and Mg^{2+} employed in this study (0.1 mM to 10 mM) represents the hardness conditions found in natural groundwater in USA.²⁷ However aggregation rates for both divalent cations concentrations of 0.1mM and 10mM were still lower than the diffusion-limited aggregation rate. Therefore, for aggregation experiments we needed to employ even greater concentrations of Ca^{2+} to reach the critical coagulation concentration (CCC).¹⁵

Transmission electron microscopy (TEM). Micrographs of rotavirus were obtained by a cryo TEM (JEM-2100, JEOL, Tokyo, Japan) operating at 200 kV to ensure the integrity of rotavirus particles. Rotavirus pellets were obtained after centrifugation at $48,500 \times g$ for one hour.

These pellets were recovered and re-suspended using a few drops of Karnovsky's fixative for 20 minutes. The virus suspensions were applied to holey-carbon-coated copper grids of 300 mesh, and stained with uranyl acetate.

Measurement of hydrodynamic diameter of rotavirus by dynamic light scattering (DLS). Using a ZS90 Zetasizer (Malvern, UK) the initial hydrodynamic diameter of rotavirus was measured before every experiment which served as baseline measurements. This ZS90 Zetasizer utilizes a 4 mW HeNe laser operating at a wavelength of 633 nm. Low volume plastic cuvettes (ZEN0112, Malvern, UK) were used for each experiment and disposed after a single use. Scattered light intensity was measured by a photodiode positioned at a scattering angle of 90° from the incident laser beam. Autocorrelation functions were accumulated for 20 seconds and the corresponding intensity-weighted hydrodynamic diameter of the rotavirus particles was determined through second-order cumulant analysis by Dispersion Technology Software (v5.10, 2008, Malvern, UK). Rotavirus solutions were prepared by diluting stock suspensions with DI water until a final concentration of $\sim 8 \times 10^5$ FFU/mL. This initial concentration ensured an attenuator setting on the ZS90 Zetasizer of 10, (*i.e.*, 30% of maximum laser power transmitted). At least 3 measurements per solution condition were made.

Time-resolved dynamic light scattering was used to determine the aggregation kinetics of rotavirus in solutions of various concentration of either Na^+ , Mg^{2+} or Ca^{2+} . For each experiment, a rotavirus solution was prepared at the desired concentration of electrolyte solution. The solution was given a gentle shake and placed into the Zetasizer instrument as quickly as possible. Measurements began immediately and extended over a time period of 4 hours to allow for an increase in the intensity-weighted hydrodynamic diameter by 38% of the initial hydrodynamic diameter (D_{ho}).²⁸

Determination of virus/virus attachment efficiency (1/W). Rotavirus aggregation kinetics were determined by measuring the increase in hydrodynamic diameter (D_h) over time. The slope of the initial portion of this curve is directly proportional to the product of the aggregation rate constant (commonly, k_{11}) and the initial concentration of rotavirus.^{28, 29} From the initial slope, the attachment efficiency or inverse stability ratio, $1/W$, was calculated by normalizing the experimental aggregation rate constant, $k_{11\text{exp}}$, to the diffusion limited aggregation rate constant, $k_{11\text{rapid}}$ ($1/W = k_{11\text{exp}}/k_{11\text{rapid}}$).

Determination of deposition kinetics by quartz crystal microbalance (QCM). We employed a QCM-D D-300 instrument (Q-Sense, Gothenburg, Sweden) to monitor deposition kinetics experiments of rotavirus on silica and functionalized silica surfaces. For a detailed method was reported in our earlier studies on the deposition of bacteriophage MS2.^{13, 30} Briefly, QCM-D was used to determine the initial deposition rates of rotavirus in electrolyte solutions on silica surfaces in a radial stagnation flow point cell. As a proxy for naturally occurring silica surfaces, ultrasensitive silica sensors (Q-Sense, QSX 303 silica, batch 070117) coated with 50 nm amorphous silicon dioxide (SiO_2) were used. We confirmed that the oscillating frequency was proportional to the total adsorbed mass, in separate experiments where the concentration of rotavirus in solution was doubled from 8×10^5 FFU/mL. We found that the deposition rate of rotavirus at the higher condition was twice that of the lower at the same concentration of background electrolyte (1 mM Ca^{2+}) confirming that the shift of frequency in time is directly proportional to the concentration of viruses adsorbed on the silica surface of the oscillating sensor. The frequency variations were monitored at 3 overtones ($n = 3, 5, 7$). For all the experiments, the initial shift of frequency as a function of time, or slope of the curve at the third overtone $f_{(3)}$, was calculated as rotavirus adsorption rate. For fair comparison, each rotavirus

adsorption rate at a given electrolyte concentration condition is normalized by the rate of deposition onto PLL functionalized silica at the same electrolyte concentration (favorable deposition rate).

To ensure data quality and reproducibility of results, the quartz sensors were soaked for 2 hours in a 2% Hellmanex II cleaning solution (Hellma GmbH & Co. KG, Mullheim, Germany). Afterwards the sensor was rinsed with DI water, dried with ultrapure N₂ and exposed to Ozone/UV for 30 minutes (BioForce Nano-sciences, Inc., Ames, IA). The sensor was only used 5 times to ensure that experiments were performed with silica surface (see SI for more information).

The flow rate for all experiments was 0.1 mL/min using a precision syringe pump (Kd Scientific Inc., Holliston, MA) operating in withdrawal mode. Prior to all experiments, the sensors were equilibrated with DI water for at least 30 minutes until a stable baseline of no more than 2 Hz in change in frequency over 1 hour was achieved. For deposition experiments on silica surface, 2 mL of our choice of electrolyte solution (NaCl, MgCl₂, or CaCl₂) at the concentration of interest was injected to the sensor chamber for equilibration. Following this step, deposition experiments were conducted by flowing 2mL of rotavirus suspension at a concentration of $\sim 8 \times 10^5$ FFU/ml with the same electrolyte concentration as the previous step.

To create favorable deposition conditions the sensor was first functionalized with a PLL layer. After the equilibration period with DI water, 2 mL of HEPES buffer was injected to the sensor chamber. Once a stable baseline was achieved (ca 20 minutes), the sensor was coated by flowing PLL in HEPES solution a final concentration of 0.1 g/L. After functionalizing the sensor with PLL, 2 mL of HEPES buffer was flowed through the chamber and followed by 2 mL of the electrolyte solution at the concentration of interest.

DLVO energy profiles. The total interaction energy between rotavirus and the silica plate surface or between rotavirus particles was calculated as the sum of repulsive electrostatic and retarded van der Waals interactions.^{31, 32} Virus-virus interaction in aggregation experiments and virus-collector interaction in deposition experiments were calculated based on the DLVO energy profiles for sphere-sphere and sphere-plate, respectively. For the calculation, the zeta potential values were used as surface potential of the rotavirus and we used a mean value for proteins in water, 4×10^{-21} J, for the rotavirus Hamaker constant (A).³³

Softness of rotavirus and Ohshima approximation. For nanoparticles consisting of heterogeneous polyelectrolyte macromolecules (“soft” charged particles) which describes functionalized hard particles, some bacterial cells and other biological particles including some viruses, the calculated zeta potential can be a poor descriptor of the surface potential for the particle because the electrohydrodynamic interactions of soft charged particles are complicated by the unrelated anisotropies of both hydrodynamic permeability and charge density.^{14, 34} Therefore zeta potential, widely used for describing the electrokinetic behavior of “hard” particles, loses its meaning and instead the Donnan potential is used to determine the electrokinetics of “soft” particles. The theory developed by Ohshima³⁵ has been used to account for these differences. From this theory, two important parameters, electrophoretic softness and the outer surface potential can be determined. Electrophoretic softness ($1/\lambda$) is defined as the thickness of the soft layer and outer surface potential is the potential at the boundary of the soft layer and the solution.³⁵ When $1/\lambda$ approaches to zero, the particle can be considered rigid. These parameters have been reported for bacteria, *Cryptosporidium* oocysts and bacteriophage MS2.^{13, 15, 36, 37} We calculated the electrophoretic softness of rotavirus by applying a curve-fitting procedure for the EPM data of rotavirus measured in Na^+ solution to the Ohshima equation.

2.4 Results and Discussion

Characterization of rotavirus: size, electrophoretic mobility (EPM), surface potential, and softness. TEM micrographs of the rotavirus stock solution (Fig. 2.1A) confirmed suspensions of intact viral particles with a mean diameter of 75 ± 1 nm (total rotavirus particles measured=14) which is the same as previously reported.^{22, 38} No apparent structural damage of rotavirus protein capsid was observed as the VP4 proteins (commonly referred to as spikes) remained intact. The mean hydrodynamic diameter of rotavirus in aqueous solutions measured before each aggregation and deposition experiment was 113 ± 3 nm (Fig 2.1B). The mean polydispersity index < 0.25 of the cumulant analysis indicated that the rotavirus suspensions were monodisperse prior to each experiment. Differences between hydrodynamic and TEM diameters are well known and result from the hydration of rotavirus in solution during DLS measurements contrasted to the cryogenic process required for TEM imaging.^{22, 39}

With increasing cation concentration, the EPM of rotavirus became less negative (Fig. 2.2A and 2.2B), and reached a limit close to $0 \mu\text{ms}^{-1}/\text{Vcm}^{-1}$ at an IS of 450 mM for divalent cations. The EPM of rotavirus in Na^+ solution was always more negative than in divalent cation solution at the same ionic strength (IS) (Table 2.1). Differences between the EPM of rotavirus in solutions of divalent vs. monovalent cations are from the complexation of divalent cations with deprotonated carboxylic groups located on exposed polar charged amino acids (lysine, glutamic acid or aspartic acid) present on the outermost capsids (glycoprotein VP7 and protein VP4) of rotavirus,^{20, 25} as previously observed in similar systems.¹⁵

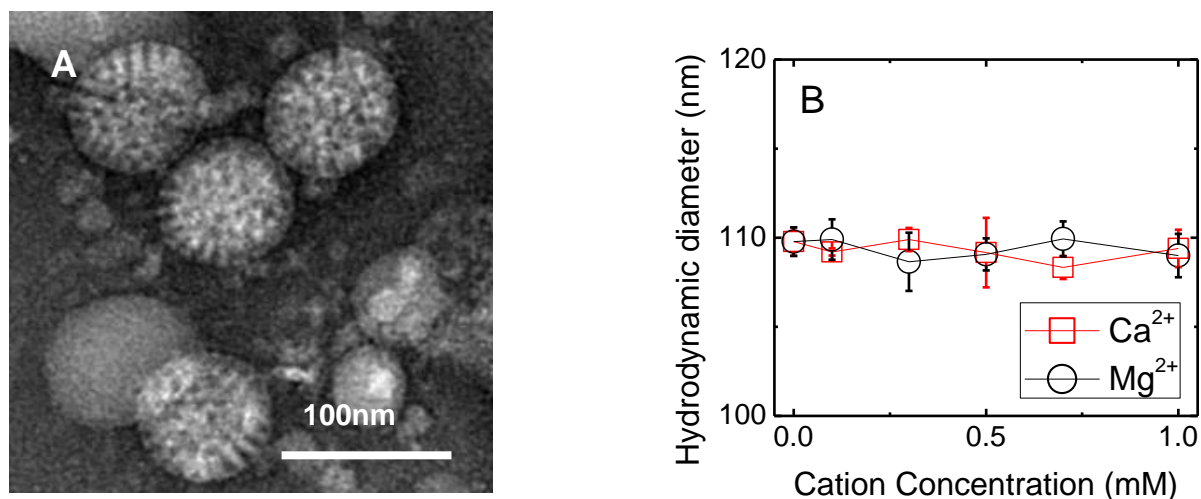


Figure 2.1 a) TEM micrograph of rotavirus. Micrographs of rotavirus were obtained using a Cryo TEM at 200 kV accelerated voltage by conventional negative staining using Uranyl acetate. The diameter of rotavirus based on TEM was *ca.* 75 nm. b) Monodispersivity of rotavirus at low concentration of divalent cations: Hydrodynamic diameter of rotavirus at 25°C and pH ~5.9 was measured at low concentrations of Mg^{2+} and Ca^{2+} (0 to 1 mM) prior to QCM experiments. The hydrodynamic diameter of virus particles in each suspension remained constant over the temporal window of our experiments (4 hours).

| IS (mM) | Ca^{2+} | | Mg^{2+} | | Na^{+} | |
|------------|------------------|--------|------------------|--------|-----------------|--------|
| | Mob | St Dev | Mob | St Dev | Mob | St Dev |
| 30 | -0.78 | 0.03 | -0.62 | 0.07 | -1.62 | 0.13 |
| 90 | -0.32 | 0.08 | -0.36 | 0.04 | -0.77 | 0.07 |
| 150 | -0.29 | 0.05 | -0.34 | 0.04 | -0.68 | 0.07 |
| 210 | -0.21 | 0.05 | -0.23 | 0.02 | -0.64 | 0.16 |
| 300 | -0.28 | 0.12 | -0.14 | 0.03 | -0.36 | 0.07 |
| 450 | -0.05 | 0.04 | -0.11 | 0.03 | -0.28 | 0.15 |
| 600 | -0.02 | 0.06 | -0.08 | 0.09 | -0.28 | 0.24 |

Table 2.1 Electrophoretic mobility of rotavirus under different solution conditions

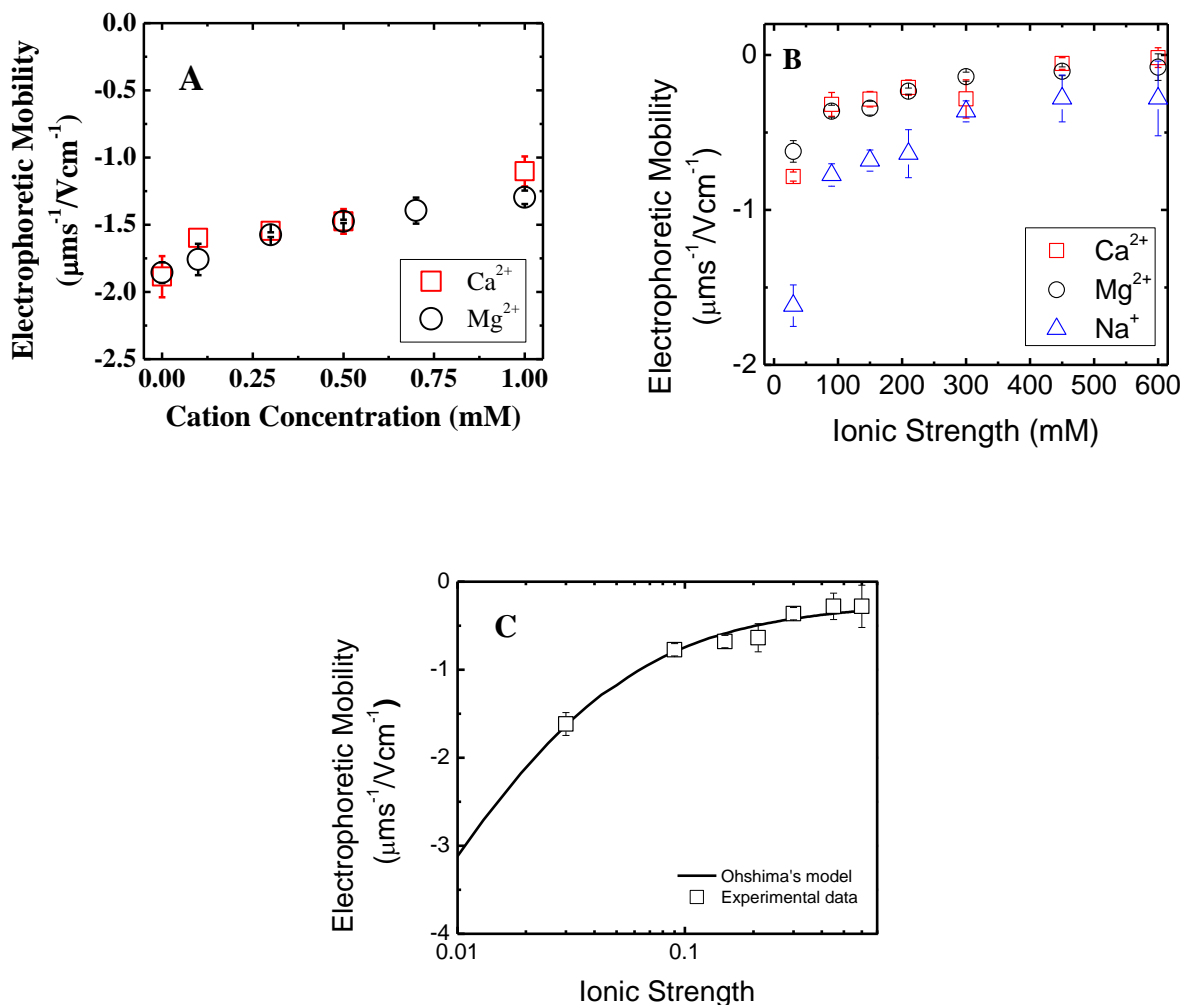


Figure 2.2 Electrophoretic mobility of a) rotavirus in solutions of low concentrations of Ca^{2+} or Mg^{2+} and of b) rotavirus in solutions with different background cations across a range of ionic strengths. All the EPM experiments were conducted at 25°C and $\text{pH} \sim 5.9$ with an initial rotavirus concentration of $\sim 8 \times 10^5$ FFU/ml. c) Experimental electrophoretic mobility (open symbols), fitted electrophoretic mobility by Ohshima's theory (solid lines) for rotavirus. The error bars are standard deviation for the measured electrophoretic mobility data in Table 2.1

The electrophoretic mobility of rotavirus as a function of ionic strength was used to calculate the outer surface potentials and electrophoretic softness using Ohshima's equation³⁵ for soft particles and zeta potentials using Smoluchowski's equation.⁴⁰ Fits to Ohshima's equation were obtained for electrophoretic mobility data only at ionic strengths above 10 mM with the fixed charge density and electrophoretic softness used as fitting parameters. The electrophoretic

softness, $1/\lambda$, is described in terms of length units where $\lambda = \sqrt{\gamma/\eta}$ and η is the viscosity and γ is the frictional coefficient of the soft layer.³⁵ For rotavirus, the $1/\lambda = 0.5$ nm (Figure 2.2C). As a first approximation the difference in electrophoretic softness of rotavirus compared to that of MS2 ($1/\lambda = 2.3$ nm)¹⁵ indicates that rotavirus behaves more like a hard sphere than MS2 and therefore DLVO theory is an appropriate choice for modeling its aggregation and deposition behavior. In a recent study for silica particles ($R_H \sim 1.6$ μ m in diameter) which are commonly used as model hard spheres, $1/\lambda$ was calculated as 0.32 nm.³⁶

Aggregation kinetics of rotavirus in monovalent or divalent cation solutions.

Rotavirus stability was investigated under a wide range of solution conditions. We employed Na^+ , Ca^{2+} or Mg^{2+} cations as supporting electrolytes at a pH = 5.9. In Na^+ solution across an IS from 30 mM to 600mM, rotavirus remained stable against aggregation over the 4 hours experimental window. The same trend was observed in our previous research using the bacteriophage MS2.¹⁵ Like MS2, the stability of rotavirus is inconsistent with the predictions of DLVO theory for sphere/sphere interactions. Based on experimental surface potentials for rotavirus, diffusion-limited aggregation should be observed at $[\text{Na}^+] > 90$ mM (Table 2.2). Our results suggest non-DLVO forces are primarily responsible for these stable suspensions of rotavirus. We posit that the VP4 proteins on the capsid contribute steric repulsive forces that prevent the aggregation of rotavirus even at very large Na^+ concentrations. Steric interactions in microorganisms have been extensively studied.⁴¹⁻⁴³ In these systems the long-range repulsive forces are primarily steric in nature consistent with polyelectrolyte brush layer in microorganisms surfaces. Similar protein loops on the MS2 surface may be responsible for its stability as well.^{30,33} Steric and electrosteric interactions have been invoked to explain the significant decrease in the aggregation rates of polystyrene latex, organic matter coated hematite,

and C₆₀ in the presence of monovalent cations Na⁺ and K^{+28, 29, 44} but in these systems aggregation has never been eliminated as it is in the case of rotavirus and MS2 in the monovalent electrolytes.

| Ionic Strength (mM) | Energy barrier (kT) | | |
|------------------------|---------------------|------------------|-----------------|
| | Ca ²⁺ | Mg ²⁺ | Na ⁺ |
| 0.3 (sphere-plate) | 65.1 | 75.9 | NA |
| 0.9 (sphere-plate) | 64 | 64.7 | NA |
| 2.1 (sphere-plate) | 59.5 | 61.5 | NA |
| 3 (sphere-plate) | 57.7 | 57 | NA |
| 30 (sphere-sphere) | NE | NE | 11.3 |
| 90 (sphere-sphere) | NE | NE | NE |

Table 2.2 Classic DLVO theory and calculation of energy barriers. NA: not available; NE: non-existence

In contrast to its stability in the presence of Na⁺, rotavirus aggregates in both Mg²⁺ and Ca²⁺ solutions (Fig. 2.3A-B). The aggregation rate of rotavirus increased as the Mg²⁺ concentration was increased from 20 to 100 mM indicating reaction limited or unfavorable aggregation of rotavirus. At Mg²⁺ concentrations above *ca.* 120 mM, the aggregation rate remained constant which is indicative of favorable aggregation. Defined by the cross-over region between favorable and unfavorable aggregation regimes, the critical coagulation concentration (CCC) for rotavirus in Mg²⁺ was 120 mM. In Ca²⁺ solution, aggregation of rotavirus could also be induced although the CCC is slightly lower compared to the case of Mg²⁺. The results shown in Figure 2.3A are the calculated stability ratios (1/W) obtained for rotavirus in both Ca²⁺ and Mg²⁺ solutions.

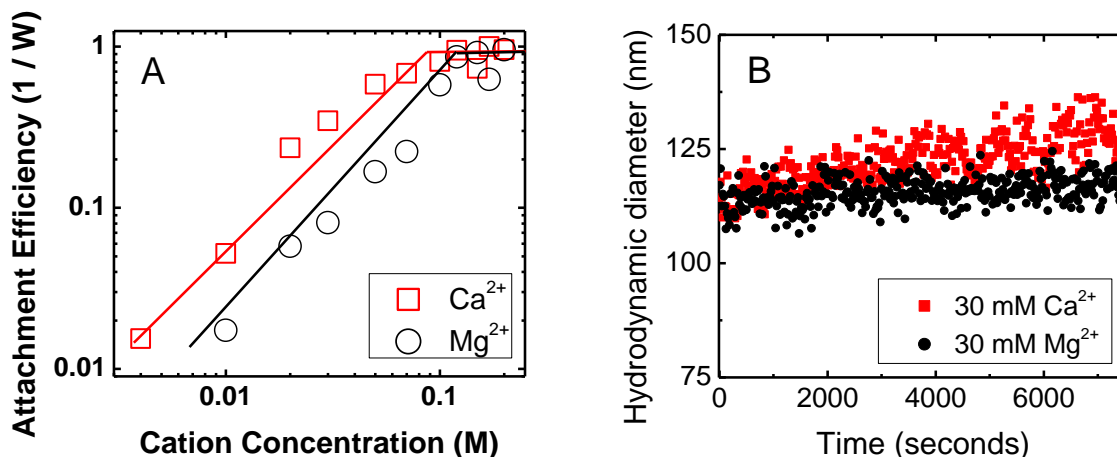


Figure 2.3 a) Attachment efficiency (1/W) of rotavirus in the presence of divalent cations. Aggregation rates for rotavirus were measured at various cation concentrations ranging from 4 mM to 200 mM in Ca^{2+} and 10 mM to 200 mM in Mg^{2+} and normalized as attachment efficiency with respect to the fastest measured aggregation rate (the lines are meant to delineate the regions between favorable and unfavorable aggregation). b) Change of hydrodynamic diameter of rotavirus with time in the presence of divalent cations. Aggregation rate of rotavirus was measured in the presence of 30 mM Ca^{2+} and 30 mM Mg^{2+} . Measurements were recorded every 20 seconds. These TR-DLS experiments were conducted at 25°C and pH ~5.9.

The results of molecular dynamic simulation suggest that cation-NOM binding takes place predominantly with carboxylate groups and the strength of the cation-carboxylate complexation can be described using the ratio of charge/radius of the cation involved. Although Ca^{2+} and Mg^{2+} has the same charge, Ca^{2+} is expected to interact strongly than Mg^{2+} because of a larger ionic radius ($R_{\text{Ca}^{2+}}=1.61 \text{ \AA}$, $R_{\text{Mg}^{2+}}=0.92 \text{ \AA}$).^{45, 46} As a smaller cation, Mg^{2+} has a strongly-held hydration sphere and thus only weak outer sphere complexes to the organic moiety can be expected. The larger Ca^{2+} cation can exchange water more easily forming inner sphere complexes with carboxylate groups. Glycoprotein VP7 and protein VP4 on the outermost capsids of rotavirus are known to contain the amino acids glutamic acid or aspartic acid both of which contain carboxylate moieties.^{20, 21, 26} Thus, inner sphere and outer sphere complexation of Ca^{2+} and Mg^{2+} respectively with carboxylate groups on rotavirus surface leads to higher

aggregation in Ca^{2+} compared to Mg^{2+} solution.

We also employed DLVO theory to predict the energy barrier to aggregation for the system of rotavirus in both Ca^{2+} and Mg^{2+} solutions. Based on these calculations no energy barrier to aggregation was predicted (i.e. diffusion limited aggregation, $1/W = 1$) was expected at all the experimental concentrations. The theory of DLVO, however, does not consider steric or electrosteric interactions,⁴⁰ and the enhanced stability cannot be predicted within the DLVO paradigm. This discrepancy between the stability of rotavirus suspensions where the supporting electrolyte is monovalent compared to those suspensions in divalent cations is most likely due to the formation of complexes between divalent cations and functional groups on rotavirus outermost capsid. Complexation of divalent cations to the charged functional groups of the rotavirus capsid probably alters the structure of key components to the protein capsid which must have a diminishing effect on the steric forces that are responsible the stability of rotavirus. Enhanced aggregation of nanoparticles due to specific interactions between divalent cations and organic matter has been previously studied,^{47, 48} and in there divalent cations (Ba^{2+} , Ca^{2+} , Sr^{2+}) were hypothesized to complex with charged functional groups from materials (NOM, alginate) that were adsorbed to the surface of the colloids. In some cases, this has resulted in substantial increase aggregation rates compared to the same solutions in monovalent electrolytes.^{47, 48}

Rotavirus deposition kinetics to silica surface. Prior to all deposition experiments the monodispersity of rotavirus suspensions in Ca^{2+} and Mg^{2+} (0.1 to 1 mM) solution were measured using DLS. As shown in Fig 2.1B, the suspensions were stable against aggregation and remained so for at least 30 minutes.

We defined favorable deposition as the rotavirus/PLL system because at the pH 5.9 rotavirus is negatively charged²² while PLL is positively charged. Deposition rates of rotavirus

under favorable conditions to PLL-coated silica surface in the presence of Ca^{2+} remained reasonably stable over the range of concentrations employed (Fig. 2.4A). Deposition kinetics of rotavirus to the bare silica surface (repulsive conditions) in the presence of Ca^{2+} was shown in Fig. 2.4A. At a concentration of 0.1 mM Ca^{2+} the deposition rate was approximately 14 times lower than favorable conditions at the same Ca^{2+} concentration. We observed an increase in the adsorption rate of rotavirus with concomitant increase in Ca^{2+} concentration. At 0.3 mM Ca^{2+} , the deposition rate increased to 7 times lower than those on PLL surface, and an apparent maximum deposition rate was reached by 0.5 mM Ca^{2+} . The fact that the maximum deposition rate was still lower (2.3 times) than that measured under favorable attachment conditions has been observed in previous studies where attachment efficiencies measured under experimental conditions never reach unity. For example, the maximum attachment efficiency of 0.7 was measured for bacteriophage MS2 deposition on silica surface coated with Suwannee River Natural Organic Matter³⁰ and bacteriophage lambda on sand collector.³³

While DLVO theory predicts similar energy barrier for adsorption of rotavirus to bare silica in Ca^{2+} and Mg^{2+} solutions of the same concentration (Table 2.2), our experimental attachment efficiencies for rotavirus adsorption to silica surface in Mg^{2+} solution was always lower than the corresponding solution in Ca^{2+} solution (Fig 2.4B). This contrasts some earlier studies where the adsorption rate in Ca^{2+} compared to Mg^{2+} were greater for plasmid DNA and bacteriophage MS2 adsorption.^{30, 49} The differences in the solution chemistry and complexation characteristics between Mg^{2+} and Ca^{2+} that were discussed previously are most likely responsible for these differences between rotavirus attachment efficiencies.

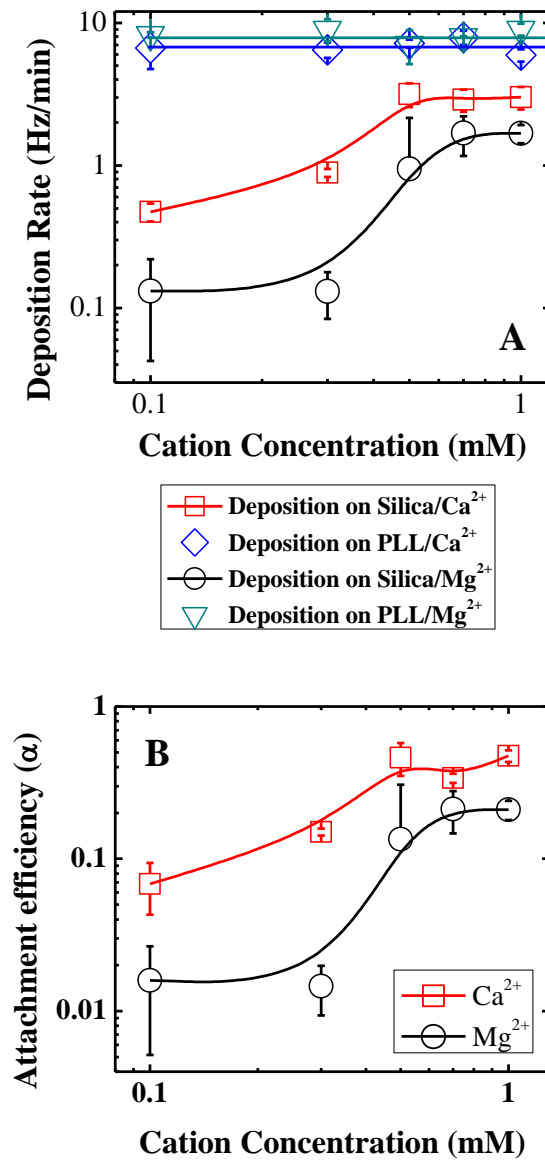


Figure 2.4 a) Deposition kinetics of rotavirus on silica surface and PLL-coated silica surface in the presence of divalent cations. The cation concentration (Ca^{2+} and Mg^{2+}) ranged from 0.1 to 1 mM for all the experiments. The temperature of the experiments was 25°C at an initial rotavirus concentration of 8×10^5 FFU/ml and a pH of 5.9. The deposition rates were expressed in Hz/min (all lines are draw as guides). b) Attachment efficiencies of rotavirus on silica surface. Deposition rates of rotavirus on silica surface were normalized by the deposition rate on PLL surface for each cation condition (Ca^{2+} and Mg^{2+}).

Environmental implications of rotavirus deposition and aggregation kinetics. This and other studies show that van der Waals and electrostatic interactions alone do not govern the interactions of viruses at interfaces (virus/virus or virus/solid).^{13, 15, 30} Rotavirus aggregation was not measurable under the solution conditions that typify groundwater hardness in the USA (up to 6 mM Ca^{2+} and Mg^{2+}),²⁷ and even at much higher levels of hardness the rotavirus concentrations even in contaminated groundwater do not reach the concentrations that we employed in these aggregation experiments. Therefore, the aggregation of rotavirus is unlikely the common fate in natural aquatic systems. Deposition of rotavirus on silica surface, however, was significant at these concentrations, and therefore, the interactions of rotavirus at the mineral/water interface are more likely to govern their fate and transport in the subsurface media. The stability of viruses against aggregation and to some extent deposition reported in this study together with other field studies^{4-6, 27} suggest that viruses (infectious and non-infectious) are uniquely mobile in aquatic systems.

Acknowledgements. This work was partially supported by the WaterCAMPWS NSF grant CTS-0120978 and USDA grant no. 2008-35102-19143 and NSF-MRI Grant 0619409.

2.5 References

1. Abbaszadegan, M.; Lechevallier, M.; Gerba, C., Occurrence of viruses in US groundwaters. *Journal American Water Works Association* **2003**, 95 (9), 107-120.
2. Yoder, J. S.; Hlavsa, M. C.; Craun, G. F.; Hill, V.; Roberts, V.; Yu, P. A.; Hicks, L. A.; Alexander, N. T.; Calderon, R. L.; Roy, S. L.; Beach, M. J. *Surveillance for Waterborne Disease and Outbreaks Associated with Recreational Water Use and Other Aquatic Facility-Associated Health Events - United States, 2005-2006*; CDC: 2008.
3. Masen, E. L., *Environmental Microbiology: From Genomes to Biogeochemistry*. Wiley-

Blackwell 2008.

4. Borchardt, M. A.; Bertz, P. D.; Spencer, S. K.; Battigelli, D. A., Incidence of enteric viruses in groundwater from household wells in Wisconsin. *Appl. Environ. Microbiol.* **2003**, 69 (2), 1172-1180.
5. Borchardt, M. A.; Haas, N. L.; Hunt, R. J., Vulnerability of drinking-water wells in La Crosse, Wisconsin, to enteric-virus contamination from surface water contributions. *Appl. Environ. Microbiol.* **2004**, 70 (10), 5937-5946.
6. Borchardt, M. A.; Bradbury, K. R.; Gotkowitz, M. B.; Cherry, J. A.; Parker, B. L., Human enteric viruses in groundwater from a confined bedrock aquifer. *Environ. Sci. Technol.* **2007**, 41 (18), 6606-6612.
7. Hoffman, R.; Marshall, M. M.; Gibson, M. C.; Rochelle, P. A., Prioritizing Pathogens for Potential Future Regulation in Drinking Water. *Environ. Sci. Technol.* **2009**, 43 (14), 5165-5170.
8. Abudalo, R. A.; Bogatsu, Y. G.; Ryan, J. N.; Harvey, R. W.; Metge, D. W.; Elimelech, M., Effect of ferric oxyhydroxide grain coatings on the transport of bacteriophage PRD1 and *Cryptosporidium parvum* oocysts in saturated porous media. *Environ. Sci. Technol.* **2005**, 39 (17), 6412-6419.
9. Harvey, R. W.; Ryan, J. N., Use of PRDI bacteriophage in groundwater viral transport, inactivation, and attachment studies. *Fems Microbiology Ecology* **2004**, 49 (1), 3-16.
10. Ryan, J. N.; Harvey, R. W.; Metge, D.; Elimelech, M.; Navigato, T.; Pieper, A. P., Field and laboratory investigations of inactivation of viruses (PRD1 and MS2) attached to iron oxide-coated quartz sand. *Environ. Sci. Technol.* **2002**, 36 (11), 2403-2413.
11. Ryan, J. N.; Elimelech, M.; Ard, R. A.; Harvey, R. W.; Johnson, P. R., Bacteriophage PRD1 and silica colloid transport and recovery in an iron oxide-coated sand aquifer. *Environ.*

Sci. Technol. **1999**, 33 (1), 63-73.

12. Pieper, A. P.; Ryan, J. N.; Harvey, R. W.; Amy, G. L.; Illangasekare, T. H.; Metge, D. W., Transport and recovery of bacteriophage PRD1 in a sand and gravel aquifer: Effect of sewage-derived organic matter. *Environ. Sci. Technol.* **1997**, 31 (4), 1163-1170.

13. Yuan, B. L.; Pham, M.; Nguyen, T. H., Deposition Kinetics of Bacteriophage MS2 on a Silica Surface Coated with Natural Organic Matter in a Radial Stagnation Point Flow Cell. *Environ. Sci. Technol.* **2008**, 42 (20), 7628-7633.

14. Langlet, J.; Gaboriaud, F.; Gantzer, C.; Duval, J. F. L., Impact of chemical and structural anisotropy on the electrophoretic mobility of spherical soft multilayer particles: The case of bacteriophage MS2. *Biophys. J.* **2008**, 94 (8), 3293-3312.

15. Mylon, S. E.; Rinciog, C. I.; Schmidt, N.; Gutierrez, L.; Wong, G. C. L.; Nguyen, T. H., Influence of Salts and Natural Organic Matter on the Stability of Bacteriophage MS2. *Langmuir* **2010**, 26 (2), 1035-1042.

16. Redman, J. A.; Grant, S. B.; Olson, T. M.; Hardy, M. E.; Estes, M. K., Filtration of recombinant Norwalk virus particles and bacteriophage MS2 in quartz sand: Importance of electrostatic interactions. *Environ. Sci. Technol.* **1997**, 31 (12), 3378-3383.

17. Gerba, C. P.; Lance, J. C., Poliovirus Removal from Primary and Secondary Sewage Effluent by Soil Filtration. *Appl. Environ. Microbiol.* **1978**, 36 (2), 247-251.

18. Zhuang, J.; Jin, Y., Virus retention and transport as influenced by different forms of soil organic matter. *Journal of Environmental Quality* **2003**, 32 (3), 816-823.

19. Golmohammadi, R.; Valegard, K.; Fridborg, K.; Liljas, L., The Refined Structure of Bacteriophage-Ms2 at 2-Center-Dot-8-Angstrom Resolution. *J. Mol. Biol.* **1993**, 234 (3), 620-639.

20. Aoki, S. T.; Settembre, E. C.; Trask, S. D.; Greenberg, H. B.; Harrison, S. C.; Dormitzer, P. R., Structure of Rotavirus Outer-Layer Protein VP7 Bound with a Neutralizing Fab. *Science* **2009**, 324 (5933), 1444-1447.
21. Dormitzer, P. R.; Sun, Z. Y. J.; Wagner, G.; Harrison, S. C., The rhesus rotavirus VP4 sialic acid binding domain has a galectin fold with a novel carbohydrate binding site. *EMBO J.* **2002**, 21 (5), 885-897.
22. Gutierrez, L.; Li, X.; Wang, J.; Nangmenyi, G.; Economy, J.; Kuhlenschmidt, T. B.; Kuhlenschmidt, M. S.; Nguyen, T. H., Adsorption of rotavirus and bacteriophage MS2 using glass fiber coated with hematite nanoparticles. *Water Res.* **2009**, 43 (20), 5198-5208
23. Parashar, U. D.; Gibson, C. J.; Bresee, J. S.; Glass, R. I., Rotavirus and severe childhood diarrhea. *Emerging Infectious Diseases* **2006**, 12 (2), 304-306.
24. Rolsma, M. D.; Gelberg, H. B.; Kuhlenschmidt, M. S., Assay for Evaluation of Rotavirus-Cell Interactions - Identification of an Enterocyte Ganglioside Fraction That Mediates Group-a Porcine Rotavirus Recognition. *J. Virol.* **1994**, 68 (1), 258-268.
25. Rolsma, M. D.; Kuhlenschmidt, T. B.; Gelberg, H. B.; Kuhlenschmidt, M. S., Structure and function of a ganglioside receptor for porcine rotavirus. *J. Virol.* **1998**, 72 (11), 9079-9091.
26. Ruiz, M. C.; Charpilienne, A.; Liprandi, F.; Gajardo, R.; Michelangeli, F.; Cohen, J., The concentration of Ca²⁺ that solubilizes outer capsid proteins from rotavirus particles is dependent on the strain. *J. Virol.* **1996**, 70 (8), 4877-4883.
27. Yates, M. V.; Gerba, C. P.; Kelley, L. M., Virus Persistence in Groundwater. *Appl. Environ. Microbiol.* **1985**, 49 (4), 778-781.
28. Holthoff, H.; Egelhaaf, S. U.; Borkovec, M.; Schurtenberger, P.; Sticher, H., Coagulation rate measurements of colloidal particles by simultaneous static and dynamic light scattering.

Langmuir **1996**, 12 (23), 5541-5549.

29. Chen, K. L.; Mylon, S. E.; Elimelech, M., Aggregation kinetics of alginate-coated hematite nanoparticles in monovalent and divalent electrolytes. *Environ. Sci. Technol.* **2006**, 40 (5), 1516-1523.
30. Pham, M.; Nguyen, T. H., Deposition Kinetics of Bacteriophage MS2 to Natural Organic Matter: Role of Divalent Cations. *J. Colloid Interface Sci.* **2009**, 338 (1), 1-9.
31. Gregory, J., Approximate Expressions for Retarded Van der Waals Interaction. *J. Colloid Interface Sci.* **1981**, 83 (1), 138-145.
32. Hogg, R.; Healy, T. W.; Fuersten.Dw, Mutual Coagulation of Colloidal Dispersions. *Transactions of the Faraday Society* **1966**, 62 (522P), 1638-&.
33. Penrod, S. L.; Olson, T. M.; Grant, S. B., Deposition kinetics of two viruses in packed beds of quartz granular media. *Langmuir* **1996**, 12 (23), 5576-5587.
34. Langlet, J.; Gaboriaud, F.; Duval, J. F. L.; Gantzer, C., Aggregation and surface properties of F-specific RNA phages: Implication for membrane filtration processes. *Water Res.* **2008**, 42 (10-11), 2769-2777.
35. Ohshima, H., Electrokinetics of soft particles. *Colloid Polym. Sci.* **2007**, 285 (13), 1411-1421.
36. de Kerchove, A. J.; Elimelech, M., Relevance of electrokinetic theory for "soft" particles to bacterial cells: Implications for bacterial adhesion. *Langmuir* **2005**, 21 (14), 6462-6472.
37. Liu, Y. Y.; Janjaroen, D.; Kuhlenschmidt, M. S.; Kuhlenschmidt, T. B.; Nguyen, T. H., Deposition of *Cryptosporidium parvum* Oocysts on Natural Organic Matter Surfaces: Microscopic Evidence for Secondary Minimum Deposition in a Radial Stagnation Point Flow Cell. *Langmuir* **2009**, 25 (3), 1594-1605.

38. Estes, M. K.; Cohen, J., Rotavirus Gene Structure and Function. *Microbiological Reviews* **1989**, 53 (4), 410-449.
39. Lute, S.; Aranha, H.; Tremblay, D.; Liang, D. H.; Ackermann, H. W.; Chu, B.; Moineau, S.; Brorson, K., Characterization of coliphage PR772 and evaluation of its use for virus filter performance testing. *Appl. Environ. Microbiol.* **2004**, 70 (8), 4864-4871.
40. Elimelech, M.; Gregory, J.; Jia, X.; Williams, R. A., *Particle Deposition and Aggregation: Measurement, Modeling, and Simulation*. Butterworth-Heinemann, Oxford 1995.
41. Kuznar, Z. A.; Elimelech, M., Adhesion kinetics of viable *Cryptosporidium parvum* oocysts to quartz surfaces. *Environ. Sci. Technol.* **2004**, 38 (24), 6839-6845.
42. Kuznar, Z. A.; Elimelech, M., Role of surface proteins in the deposition kinetics of *Cryptosporidium parvum* oocysts. *Langmuir* **2005**, 21 (2), 710-716.
43. Byrd, T. L.; Walz, J. Y., Investigation of the interaction force between *Cryptosporidium parvum* oocysts and solid surfaces. *Langmuir* **2007**, 23 (14), 7475-7483.
44. Chen, K. L.; Elimelech, M., Relating Colloidal Stability of Fullerene (C-60) Nanoparticles to Nanoparticle Charge and Electrokinetic Properties. *Environ. Sci. Technol.* **2009**, 43 (19), 7270-7276.
45. Kalinichev, A. G.; Kirkpatrick, R. J., Molecular dynamics simulation of cationic complexation with natural organic matter. *European Journal of Soil Science* **2007**, 58 (4), 909-917.
46. Xu, X.; Kalinichev, A. G.; Kirkpatrick, R. J., ¹³³Cs and Cl-35 NMR spectroscopy and molecular dynamics modeling of Cs⁺ and Cl⁻ complexation with natural organic matter. *Geochim. Cosmochim. Acta* **2006**, 70 (17), 4319-4331.
47. Mylon, S. E.; Chen, K. L.; Elimelech, M., Influence of natural organic matter and ionic

composition on the kinetics and structure of hematite colloid aggregation: Implications to iron depletion in estuaries. *Langmuir* **2004**, 20 (21), 9000-9006.

48. Chen, K. L.; Mylon, S. E.; Elimelech, M., Enhanced aggregation of alginate-coated iron oxide (hematite) nanoparticles in the presence of calcium, strontium, and barium cations. *Langmuir* **2007**, 23 (11), 5920-5928.

49. Nguyen, T. H.; Chen, K. L., Role of divalent cations in plasmid DNA adsorption to natural organic matter-coated silica surface. *Environ. Sci. Technol.* **2007**, 41 (15), 5370-5375.

CHAPTER 3

INTERACTIONS BETWEEN ROTAVIRUS AND SUWANNEE RIVER ORGANIC MATTER: AGGREGATION, DEPOSITION, AND ADHESION FORCE MEASUREMENT²

3.1 *Abstract*

Interaction between rotavirus and Suwannee River natural organic matter (NOM) was studied by time-resolved dynamic light scattering, quartz crystal microbalance, and atomic force microscopy. In NOM-containing NaCl solutions of up to 600 mM, rotavirus suspension remained stable for over 4 hours. Atomic force microscopy (AFM) measurement for interaction force decay length at different ionic strengths showed that non-electrostatic repulsive forces were mainly responsible for eliminating aggregation in NaCl solutions. Aggregation rates of rotavirus in solutions containing 20 mg C/L increased with divalent cation concentration until reaching a critical coagulation concentration of 30 mM CaCl₂ or 70 mM MgCl₂. Deposition kinetics of rotavirus on NOM-coated silica surface was studied using quartz crystal microbalance. Experimental attachment efficiencies for rotavirus adsorption to NOM-coated surface in MgCl₂ solution were lower than in CaCl₂ solution at a given divalent cation concentration. Stronger adhesion force was measured for virus-virus and virus-NOM interactions in CaCl₂ solution compared to those in MgCl₂ or NaCl solutions at the same ionic strength. This study suggested that divalent cation complexation with carboxylate groups in NOM and on virus surface was an important mechanism in the deposition and aggregation kinetics of rotavirus.

²Reprinted, with permission, from Gutierrez, L.; Nguyen, T. H., 2012, "Interactions between Rotavirus and Suwannee River Organic Matter: Aggregation, Deposition, and Adhesion Force Measurement," *Environmental Science & Technology* 46(16): 8705-8713.

3.2 *Introduction*

The most recent study by the Centers for Disease Control and Prevention (CDC) reported 48 waterborne disease outbreaks during 2007-2008 in the US.¹ More than half of the outbreaks associated with drinking water were related to groundwater.¹ Virus, parasites, and bacteria have been identified as causes for most of the outbreaks.^{2, 3} The most comprehensive study on groundwater contamination in the US collected samples from 448 sites in 35 states.⁴ Of these samples, 4.8% and 31.5% contained infectious viruses, determined by cell culture assay, and viral nucleic acid, determined by polymerase chain reaction (PCR).⁴ A newer study conducted in South Korea in 2008 reported that norovirus was found in 21.7% of 300 groundwater samples.⁵ Thus, groundwater contamination by viruses from animal and human waste remains a public health concern in the US and other countries.³⁻⁹

Field research in an iron oxide-coated sand aquifer suggested the importance of electrostatic forces in the transport of bacteriophage PRD1 through uncontaminated and sewage contaminated zones, where NOM played an important role in grain surface properties and bacteriophage PRD1 attachment.^{10, 11} In laboratory studies, the presence of positively charged metal hydroxide/oxyhydroxide surfaces and the effect of humic acid on bacteriophage transport were investigated for sands, gravel, and sandy soils.^{12, 13} NOM has been reported to hinder the deposition of viruses to mineral surfaces due to competition for available adsorption sites.^{11, 14, 15} At pH typical for groundwater (e.g. 7.3 to 8.3)¹⁶ NOM adsorbs to positively charged metal oxide-coated quartz, mica, or feldspar grains, and influences the interaction of viruses and mineral surfaces. In addition to bacteriophages, a few studies have conducted transport experiments with enteric viruses. For example, minimal transport of human adenovirus in undisturbed soil cores was reported.¹⁷ Another study reported MS2 to be generally more mobile

than poliovirus 1 and Norwalk virus.¹⁸ In addition, the differential adsorption of MS2, PRD1, and poliovirus 1 to soils was suggested to be related to their isoelectric points.¹⁹ Strong electrostatic attractions were identified to be mainly responsible for aichi virus removal in iron oxide-coated sand.²⁰

A theory developed by Derjaguin, Landau, Verwey and Overbeek, i.e., DLVO theory, that includes van der Waals and electrostatic interactions, has been used to explain surface interaction of hard colloids.²¹ However, a number of studies have reported non-DLVO behavior for viruses. Divalent cation complexation with negatively charged carboxylate groups on both NOM and MS2 phage were suggested as the main mechanisms governing MS2 deposition to silica and NOM surfaces in a radial stagnation point flow cell.²² Steric interactions were suggested to maintain MS2 stability even at high Li^+ , Na^+ , or K^+ concentrations in solution.²³ Steric interactions were also attributed to less deposition of MS2 phage or norovirus capsids on silica surface than expected if only van der Waals and electrostatic interactions were considered.²⁴⁻²⁶ Besides steric interaction and divalent cation complexation, a novel electrokinetic theory, which considers MS2 as particles consisting of an impermeable hard core and a charged permeable soft shell, was developed to describe electrophoretic mobility of MS2 at different pH and ionic strengths.²⁷⁻²⁹

The objective of this study was to investigate interactions between rotavirus and a model aquatic natural organic matter isolated from Suwannee River water. The deposition kinetics of rotavirus to NOM-coated silica surfaces were studied using quartz crystal microbalance. Rotavirus aggregation kinetics in NOM and divalent cation solutions were studied by time-resolved dynamic light scattering. Adhesion force between rotavirus and rotavirus in NOM solution and between rotavirus and NOM-coated surface was measured by AFM technique to

complement the deposition and aggregation studies. Rotavirus was selected for this study because it is the leading cause of severe gastroenteritis among young children,³⁰⁻³² and it is routinely detected in wastewater, surface water, drinking water, and groundwater worldwide.³³

3.3 *Materials and Methods*

Solution chemistries and reagents. Deionized (DI) water (Millipore, Barnstead, USA) of an 18 M Ω -cm resistivity was used for preparing all the solutions for deposition, aggregation, and AFM experiments. The unadjusted pH of fresh DI water remained stable for the entire duration of the QCM, TR-DLS, and AFM experiments (3 hours, 4 hours, and 1 hour respectively). Analytical grade NaCl, CaCl₂, MgCl₂, poly-L-lysine (PLL) hydrobromide, and HEPES buffer were utilized in this research. HEPES buffer was prepared with 100 mM NaCl and 10 mM N-(2-hydroxyethyl) piperazine-N'-2-ethanesulfonic acid at a final pH of 5.9. PLL hydrobromide solution was prepared in HEPES buffer at a final concentration of 0.1 g/L. All electrolyte solutions and HEPES buffer were filtered through a 0.22 μ m sterile cellulose acetate membrane and sonicated for 30 minutes before use. The polyglutamic sodium salt (PLG) with a molecular weight ranging from 50,000–100,000 g/mol (Cat# P4886, Sigma) was prepared in solution by adding 25 mg of PLG to 4.2 g of DI water.

Suwannee river natural organic matter (NOM, International Humic Substances, IHSS, St. Paul, MN) was used as a dissolved organic matter model. The procedure for NOM solution preparation was previously described.⁴³ Total dissolved organic carbon (DOC) concentration of the NOM stock solution was measured using a Phoenix 8000 TOC analyzer (Dohrmann, USA) at 101.4 mg C/L. The NOM stock was stored at 4°C and covered from light by aluminum foil. All the solutions were kept at pH 5.9 with the exception of the solutions used for studying the effect

of pH. For these experiments, pH was adjusted to 8.3 using NaOH. The average D_h of NOM in 1 mM NaCl solution measured every 20 seconds for 240 minutes was 2 nm and 1 nm for 2 consecutive TR-DLS experiments. However, due to the small size of NOM and its fluorescent nature we believe that fluorescence correlation spectroscopy would be a more sensitive technique for estimating the size of NOM in solution.⁸⁸

Rotavirus preparation and focus forming unit (FFU) infectivity assays. Briefly, group A porcine OSU rotavirus (ATCC VR892) were grown in the presence of trypsin in embryonic African green monkey kidney cells (MA-104) as the host.³⁴ Purification of rotavirus was conducted by sequential centrifugation and filtration as described previously.¹⁴ This stock of rotavirus is referred to as membrane-purified rotavirus. While care was taken for virus purification, it is possible that protein contamination remained in the virus stock used for this study. Due to the biological nature of virus, it is impossible to obtain pure virion without influencing virus infectivity or causing aggregation.⁸⁹⁻⁹¹ Enumeration of rotavirus was carried out using FFU infectivity assays.⁹² The stock concentration was $\sim 5 \times 10^6$ FFU/ml and was stored at 4°C in a 1 mM NaCl and 0.1 mM CaCl_2 solution. Calcium in rotavirus stock was kept above the critical free calcium concentration to avoid solubilization of outer capsid proteins VP4 and VP7.⁹³ This membrane-purified rotavirus stock was also used in our previous study.³⁶ After preparation the virus stock was carefully aliquoted and stored for almost 2 years with no significant change in infectivity or hydrodynamic diameter. Another rotavirus stock was grown and purified using CsCl gradient method described previously³⁴ to a final concentration of $\sim 10^8$ FFU/mL. This stock is referred to as CsCl-purified rotavirus. Standard SDS-PAGE was carried out for the rotavirus stock using 7.5% Mini-PROTEAN TGX Precast minigels stained overnight using SYPRO Ruby protein gel stain according to the manufacturer's instructions (Bio-Rad,

Hercules, CA). Bands were analyzed for molecular weight using a Gel-Doc imager (Bio-Rad, Hercules, CA).

Electrophoretic mobility (EPM) measurements. A ZS90 Zetasizer instrument and clear disposable cells (Malvern, UK) were used to determine the EPM of membrane-purified rotavirus in solution containing 20 mg C/L and a broad range of salt concentrations (5 mM to 600 mM for NaCl, 5 mM to 200 mM for CaCl₂ and MgCl₂) at an unadjusted pH of 5.9 at room temperature (~25°C). At least three measurements were conducted for each salt concentration. Membrane-purified rotavirus was added to these solutions to a final concentration of 8×10^5 FFU/mL, which ensured an optimal signal for EPM measurements. For comparison purposes, EPM of membrane-purified rotavirus and CsCl-purified rotavirus was measured at 1 mM NaCl and at pH 3, 4, 5.9 and 8.3 at room temperature (~25°C). pH was adjusted by the addition of NaOH and HCl. Silica beads coated sequentially with PLL and NOM or poly-L-glutamic sodium salt (PLG) were used as surrogates for NOM-coated and PLG-coated surfaces. The coating protocol was described in our previous study.^{22, 35} EPM was measured for these beads in solutions containing 1 mM CaCl₂ at pH 5.9 or 8.3.

Aggregation kinetics of rotavirus by time-resolved dynamic light scattering (TR-DLS). Aggregation kinetics of rotavirus in NOM-containing electrolyte solutions were measured by a ZS90 Zetasizer and disposable plastic cuvettes (Malvern, UK) as described previously.³⁶ For comparison purposes, aggregation kinetics of both membrane-purified and CsCl-purified rotavirus in 20 mg C/L NOM solutions at pH 5.9 were measured at 1, 5, 15, 50, and 100 mM CaCl₂. These two stocks of rotavirus were added to the electrolyte NOM-containing solution so that the DLS photon counting was similar (~20 kcps).

The aggregation kinetics of rotavirus in solution was determined as the initial rate of

increase in the hydrodynamic diameter (D_h) with respect to time. This rate is directly proportional to rotavirus initial concentration and the initial aggregation rate constant (k_{11}).^{23, 37, 38} The aggregation rate was obtained by calculating the initial slope of the D_h vs. time plot up to the point at which D_h reaches the relative hydrodynamic diameter of $1.38D_{ho}$. However, when the salt concentration is very low during reaction-limited regime, this linear region would end before reaching $1.38D_{ho}$; the slope was fitted only for the linear portion, allowing that the fitted line intercepts the y axis no more than 3 nm in excess of D_{ho} .^{37, 39} The inverse stability ratio ($1/W$), ranging from 0 to 1, was calculated by normalizing the initial aggregation rate constant k_{11} obtained at different electrolyte concentrations for the reaction limited regime by the aggregation rate constant k_{fast} determined during the diffusion-limited regime.⁴⁰⁻⁴²

Control experiments were conducted to measure the hydrodynamic diameters and aggregation rates of NOM in NaCl, CaCl₂, and MgCl₂ solutions. These results were compared to the corresponding results for the rotavirus-salt-NOM aggregation experiments at the same electrolyte concentration to determine which aggregates dominate the TR-DLS intensity signal. The procedures and the range of salt concentration used were the same as for the rotavirus aggregation experiments described above.

Determination of rotavirus deposition kinetics by quartz crystal microbalance (QCM). A QCM-D D-300 instrument (Q-Sense, Sweden) was used to study the initial deposition rates of rotavirus in electrolyte solutions on NOM-coated silica surface in a radial stagnation flow point cell. Previous studies have used this technique for deposition experiments of MS2 on silica and NOM surfaces^{22, 24} and its procedure has been described.^{22, 43} Following well-established methods in colloid deposition,⁴⁴⁻⁴⁹ the QCM experiments were conducted for a short-pulse injection of virus suspension. This method allows estimation of deposition kinetics

based on the first-order kinetics region of the deposition curve, which is relevant for virus transport study because of low concentration of virus present in groundwater.^{4, 5, 50, 51} Control experiments were conducted with solutions containing different concentrations of rotavirus. The deposition rate increased twice when the rotavirus concentration was doubled from 8×10^5 FFU/ml in the same background salt concentration (tested with 1 mM CaCl_2 and 0.1 mM CaCl_2). The results of these control experiments confirmed that the frequency shift is proportional with the virus concentration, indicating first order kinetics. Rotavirus deposition rate was determined as the slope of the initial frequency shift vs. time curve for the third overtone ($d\Delta f_{(3)}/dt$). Ultrasensitive silica sensors (Q-Sense, QSX 303 silica, batch 070117) were used. The solutions were introduced into the chamber at the rate of 0.1 mL/min. Before conducting QCM experiments, hydrodynamic diameter of membrane-purified RV in solution was measured by DLS showing a single peak at 100 nm for rotavirus monodispersed population. Similar observation was obtained for rotavirus stocks purified with CsCl gradient centrifugation or with membrane filtration. This observation showed that rotavirus was present in the stock, and protein contamination was not detected by DLS.

As commonly used in colloid literature, deposition kinetics is presented as attachment efficiency.^{39, 52} The attachment efficiency (α) was calculated by normalizing rotavirus deposition rate on NOM surface at a given electrolyte concentration by the rate obtained for the same electrolyte concentration under non-repulsive conditions. The deposition rate was determined as the slope of the linear portion of the frequency shift vs. time plots, as in previous studies.^{36, 39, 53} Fitting examples for the deposition rate are shown in Figures 3.1a-b.

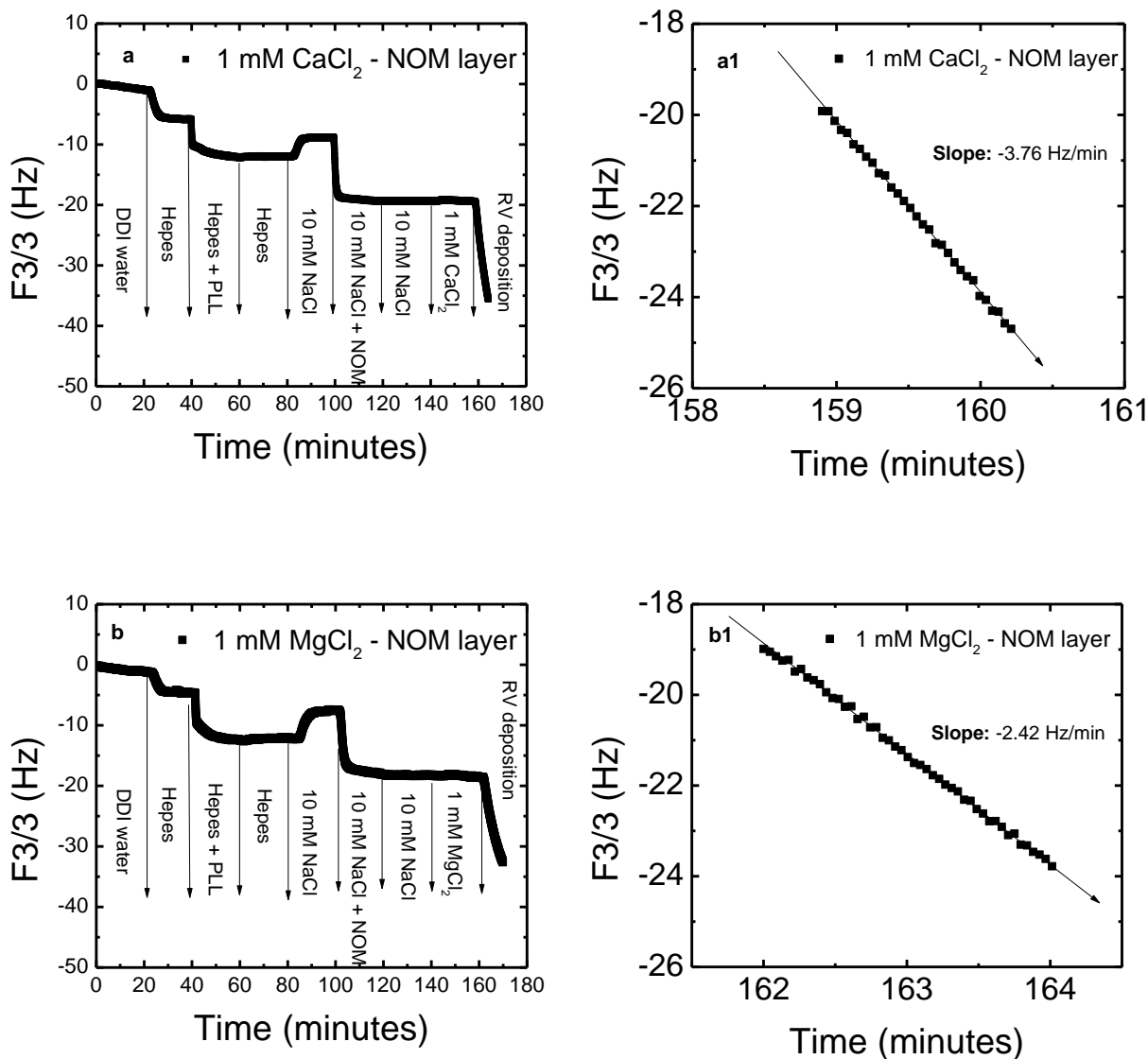


Figure 3.1 Measurement of deposition of RV on SRNOM layer in solution containing a) 1 mM CaCl_2 or b) 1 mM MgCl_2 with their corresponding deposition rate calculation (a1 and b1). Rotavirus concentration was $\sim 8 \times 10^5$ FFU/mL in solution at 25°C.

QCM sensor cleaning and QCM deposition protocol. Cleaning protocol before each experiment was as follows: quartz sensors were soaked for 2 hours in a 2% Hellmanex II cleaning solution (Hellma GmbH & Co. KG, Mullheim, Germany), thoroughly rinsed with DI water, dried with ultrapure N_2 , and oxidized in an Ozone/UV chamber for 30 minutes (BioForce Nano-sciences, Inc., Ames, IA). The electrolyte solutions were injected into the QCM system

using a precision syringe pump (Kd Scientific Inc., Holliston, MA) operating at a withdrawal mode at a 0.1 mL/min flow rate. After a stable baseline was established in water, the QCM sensors were sequentially coated with PLL and then NOM as described previously.^{43, 22} After coating, the system was equilibrated with 2 mL of electrolyte solution (NaCl, CaCl₂, MgCl₂) at the concentration of interest (i.e., 0.1, 0.3, 0.5, 0.7, or 1 mM). Equilibrium (frequency shift with time <0.1 Hz/min) was obtained after the addition of this 2 ml of electrolyte solution. This step was followed immediately by virus adsorption experiments, which were performed by flowing 2 mL of rotavirus suspensions at a concentration of 8×10^5 FFU/ml and in the same electrolyte concentration as the previous step. For non-repulsive conditions, rotavirus deposition rates on PLL-coated silica surface in MgCl₂ and CaCl₂ solutions from our previous research³⁶ were used in this investigation.

Surface preparation for AFM experiments. The quartz and silica surfaces were first cleaned by immersion in 2% Hellmanex (Hellma Analytics, USA) solution for 30 minutes and subsequently rinsed in excess with DI water. Next, approximately 300 μ L of 98% sulfuric acid with 30 g/L nochromix solution were pipetted on top of the surfaces for 24 hours and then removed. The surfaces were finally rinsed in excess with DI water. NOM-coated surfaces were prepared following the layer-by-layer protocol introduced previously.^{22, 35} The PLL coating protocol of the silica surface (QCM sensor) was conducted by pipetting 300 μ L of PLL hydrobromide solution prepared in HEPES buffer at a final concentration of 0.1 g/L and left undisturbed for 24 hours. Next, the PLL solution was removed and the surface was rinsed with DI water. Similarly, PLL layer was coated by pipetting 300 μ L of approximately 240 mg C/L SRNOM solution or 6 g/L of PLG solution and left undisturbed for 24 hours. The SRNOM solution was then removed and the surface was rinsed with DDI water. For some selected

experiments, the PLL layer was coated by pipetting 300 μL of solution containing $\sim 1 \times 10^8$ FFU/ml rotavirus and left undisturbed for 8 hours. The viral solution was then removed and the surface rinsed with DI water.

Rotavirus-coated membranes were prepared following a modified procedure previously used for oocysts.⁵⁶ Briefly, 10 mL of $\sim 5 \times 10^6$ FFU/ml rotavirus solution were vacuum-filtered onto a 13 mm in diameter piece of 0.05 μm polycarbonate track-etched membrane (Whatman Nucleopore, USA) and afterwards carefully rinsed with DI water. A layer of water was maintained to prevent rotavirus exposure to air. After this filtration step, the membrane was immediately glued by the edges to a glass slide. Rotavirus coating of the membrane was checked by tapping mode imaging at a scan rate of 0.5 Hz with a chromium-gold-coated silicon nitride probe with a spring constant of ~ 0.27 N/m (Budget Sensors, Bulgaria).

Samples of rotavirus-coated silica probe were similarly prepared by the layer-by-layer method described above.^{22, 35} Twenty μL of PLL hydrobromide solution prepared in HEPES buffer at a final concentration of 0.1 g/L were added as a drop on top of the glass slide. Using a DMI5000M Leica inverted microscope (Leica, Germany) and a 10 \times lens, only the probe was carefully introduced to the PLL drop and allowed to coat for 6 hours. The probe was then removed from the PLL drop and rinsed with DI water. Following the same procedure, the probe was carefully introduced in a 20 μL $\sim 5 \times 10^6$ FFU/ml rotavirus drop and allowed to coat for 6 hours. The probe was then removed from the virus solution drop and rinsed with DI water. The preparation for the rotavirus-coated silica surface was described above.

AFM force measurement protocol and data analysis. Interaction force was measured using a MFP-3D AFM (Asylum Research, CA, USA). The following sets of experiments were conducted: 1) control experiments for testing the coating completeness of silica and membrane

surfaces; 2) approaching force measurements between silica probe and silica surface in solutions with and without NOM; 3) approaching and retracting force measurements between rotavirus and silica surfaces or NOM-coated surfaces, and between rotavirus and rotavirus.

For the first set of control experiments, the coating completeness of surfaces was tested using a silicon nitride (Si₃N₄) tip with 20 nm tip radius (0.24 N/m, NP series, Bruker, USA). The approaching curves were separately measured in 1 mM NaHCO₃ solution at a buffered pH of 8.3 with the following surfaces: a) ultra-pure quartz; b) QCM silica sensors (i.e., silica surface); c) silica surface coated with PLL; d) silica surface coated sequentially with PLL and then NOM or PLG or rotavirus. Ultrapure quartz surface (Cat # 26016, 19×19×0.5 mm thick, Ted Pella, USA) was used as a reference for negatively charged surface. Note that zeta potential of this surface has been measured in our previous work (-2.53 to -0.18 $\mu\text{mcmV}^{-1}\text{s}^{-1}$ at 1 and 200 mM NaCl, respectively).³⁵ QCM silica sensor surface (Qsx 303 silica sensor, Q-Sense, Sweden) was used in most AFM experiments because this surface was also used in deposition experiments.

For the second set of control experiments, a 1 μm silica sphere mounted on a silicon nitride tip-less cantilever with a spring constant of ~ 0.06 N/m (Novascan Technologies, USA) was used. For the first subset of this control set, we obtained approaching force curves for the silica sphere probe with quartz surface in solution with and without 20 mg C/L NOM. The solution also contained either 1 or 10 or 100 mM NaCl at unadjusted pH 5.9. For the second subset of this control, we obtained approaching force curves for the following cases: 1) silica probe and rotavirus-coated membrane; 2) silica probe and rotavirus-coated silica surface; 3) rotavirus-coated silica probe and silica surface. This 1 μm silica sphere was used for AFM force measurement as recommended in previous studies reviewed by Butt et al.,⁵⁵ so that nanometer scale roughness of the substrate did not influence AFM force measurement.

For the third set of experiments, approaching and retracting force was obtained for rotavirus-coated silica probe with one of the following surfaces: 1) rotavirus-coated membrane; 2) NOM-coated silica surfaces; and 3) PLG-coated silica surfaces. We used unadjusted pH 5.9 solution containing 0 or 20 mg C/L NOM and 1 or 10 or 100 mM NaCl, or 33.3 mM MgCl₂, or 33.3 mM CaCl₂ to study interactions between rotavirus and rotavirus. The interaction between rotavirus and NOM was studied using solution composition similar to the ones used for QCM experiments, i.e., solution containing 3 mM NaCl or 1 mM MgCl₂ or 1 mM CaCl₂. For the experiment using 1 mM CaCl₂, we used two pH conditions: unadjusted pH 5.9 or 1 mM bicarbonate buffered solution at pH 8.3. The interaction between rotavirus and PLG was studied using solution containing 1 mM CaCl₂ at unadjusted pH 5.9 or 1 mM bicarbonate buffered solution at pH 8.3.

The spring constant of the cantilevers was calibrated before each experiment using thermal tuning method, and these values were used to convert deflection to force according to Hooke's law.⁵⁴ Approaching and retracting force profiles were measured at a scan rate of 0.35 Hz using AR-MFP-3D v.101010 software (Asylum Research, USA). At least 5 force profile curves per location at 5 different locations were sampled for every solution condition. For the control experiments, a minimum of 25 approaching force curves were recorded at different locations within an approximate circular area of 0.7 cm² of each surface. Based on the approaching curves, the interaction force can be described by the following equation: $F = B \exp(-\kappa h)$, where h is the separation distance, F is the interaction force, B is a pre-exponential constant, and κ^{-1} is the interaction force decay length.⁵⁵⁻⁵⁸ The value of κ was determined as the slope of the linear region of a repulsion force profile as a function of separation distance in a semi-natural logarithm plot. The observed decay lengths were calculated based on the approaching force

curves. The adhesion forces were determined using the retracting force curves based on the maximum force measured before total detachment of the silica probe from the substrate. The adhesion forces were further normalized by the silica probe radius (0.5 μm) as in previous studies.⁵⁹ The adhesion distance was defined in this study as the maximum separation distance during the retraction of the probe, where the interaction between the colloidal probe and substrate disappears.

3.4 *Results and Discussion*

Electrophoretic mobility (EPM). Intensity and volume analysis conducted by Dispersion Technology Software (v5.10, 2008, Malvern, UK) for membrane-purified RV suspension immediately after EPM measurement indicated monodispersed population of viruses even at high concentration of NaCl, CaCl₂, or MgCl₂ (Table 3.1). CsCl-purified rotavirus and membrane-purified rotavirus showed similar EPM and at the range of studied pH (Fig. 3.2a). For both stocks of rotavirus, the value of isoelectric points determined in 1 mM NaCl solution was 4. This value of isoelectric point is within the range of most frequently observed for different viruses.⁶⁰ Thus, for pH 5.9 and 8.3 of the aggregation and deposition studies described below, rotavirus is negatively charged. As shown in Fig 3.2b, in NOM solutions at pH 5.9, rotavirus EPM became less negative with increasing cation concentration (Na⁺, Ca²⁺, or Mg²⁺) until asymptotically reaching a finite lower limit at high concentrations. However, EPM was always more negative in NaCl than in CaCl₂ solutions at the same ionic strength. This trend was previously reported for MS2 and rotavirus.^{23, 36, 61} EPM of SRNOM-coated silica particles of 1.6 μm in diameter changed from -3.21 to -1.00 $\mu\text{mcmV}^{-1}\text{s}^{-1}$ as ionic strength increased from 1 to 200 mM. This observation shows a decrease in negative charge of SRNOM with increasing ionic strength, suggesting simple charge screening.³⁵ The EPM and D_h results presented here suggest

that the reduction in EPM of rotavirus in NaCl solutions was caused by charge screening, while the reduction of EPM of rotavirus in CaCl_2 or MgCl_2 was caused by charge screening and cation complexation.

| Concentration mM | D_h (nm) | |
|---------------------|-----------------|-----------------|
| | CaCl_2 | MgCl_2 |
| 1 | 115 | |
| 2 | 116 | |
| 3 | 114 | |
| 5 | 121 | 118 |
| 7.5 | 120 | |
| 10 | 120 | 119 |
| 20 | 127 | 122 |
| 30 | 147 | 124 |
| 50 | 167 | 129 |
| 100 | 177 | 138 |
| 200 | 202 | 146 |

Table 3.1 Hydrodynamic diameter of RV-NOM aggregates in divalent cation solutions after EPM measurements by intensity analysis

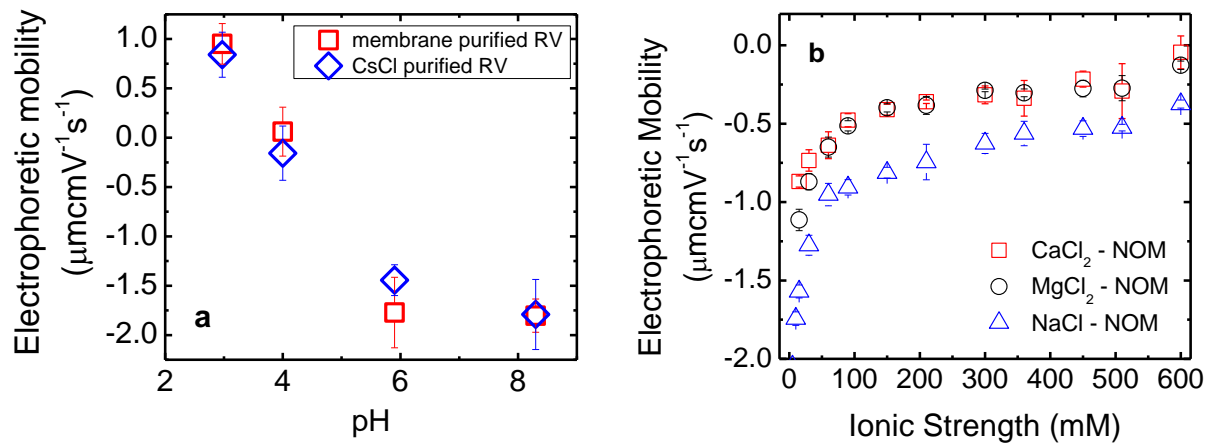


Figure 3.2 a) EPM of rotavirus purified following CsCl gradient method or dialysis-concentration with 1 mM NaCl solution. b) EPM of rotavirus in 20 mg C/L NOM solution with different background cations. All the experiments were conducted at a pH ~ 5.9 with a rotavirus concentration of $\sim 8 \times 10^5$ FFU/ml. Both volume and intensity analysis showed monodispersed populations of rotavirus up to 600 mM NaCl, 200 mM MgCl_2 , and 30 mM CaCl_2 .

Aggregation kinetics of rotavirus in NOM solutions. The mean hydrodynamic diameter in 1mM NaCl solution containing 20 mg C/L for rotavirus was measured as 117 ± 5 nm for a total of 26 samples (Fig. 3.3a). The mean polydispersity index (PDI), i.e., width parameter of the cumulant analysis for the DLS measurements, was measured as 0.25 ± 0.06 , indicating a monodispersed virus population before aggregation experiments. The diameter of rotavirus measured by TEM was reported in previous studies as approximately $75 \text{ nm} \pm 1 \text{ nm}$.^{14, 32, 36} Differences between hydrodynamic and TEM diameters due to dehydration during TEM sample preparation have been documented in previous work.^{14, 62} The mean hydrodynamic diameter for rotavirus purified following CsCl gradient method, in 1mM NaCl solution containing 20 mg C/L, was 111 ± 3.1 nm and PDI of 0.17 ± 0.02 for a total of 7 samples (Fig. 3.3b). This measurement suggests a monodispersed population comparable to membrane-purified rotavirus.

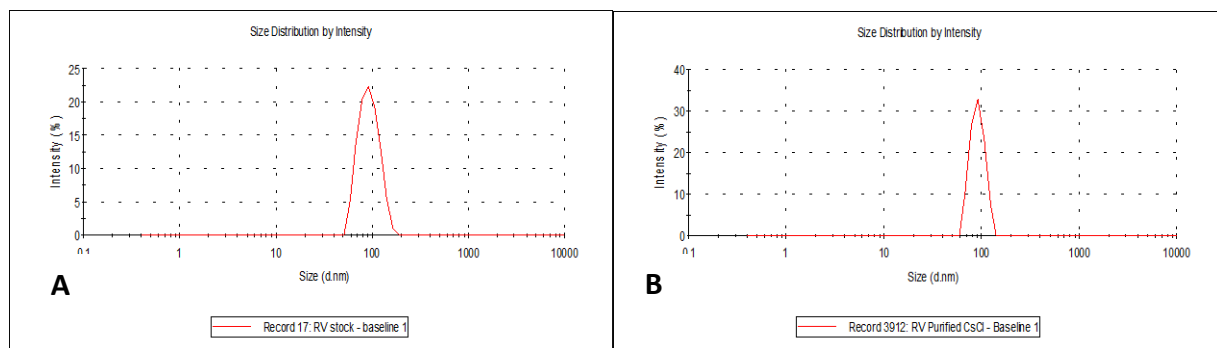


Figure 3.3 Measurement of hydrodynamic diameter of rotavirus purified following a) dialysis-concentration using Amicon ultrafiltration membrane cell, b) CsCl gradient method. Rotavirus aggregation was studied in NOM solutions at a pH of 5.9 for 4 hours.

No change in hydrodynamic diameter was detected even at 600 mM NaCl. Rotavirus stability in NaCl was previously observed in the absence of NOM³⁶ and was also reported for MS2.²³ The change in hydrodynamic diameters of rotavirus in MgCl_2 and CaCl_2 solutions as a function of time is shown in Figures 3.4a and 3.4b. Insignificant change in hydrodynamic

diameter of rotavirus was observed after 4 hours in solutions containing up to 5 mM MgCl_2 and 3 mM CaCl_2 . In solution containing 100 mM CaCl_2 , after 4 hours, the hydrodynamic diameter of rotavirus aggregates was more than 3 times larger than those in 100 mM MgCl_2 (e.g., 700 nm vs. 200 nm).

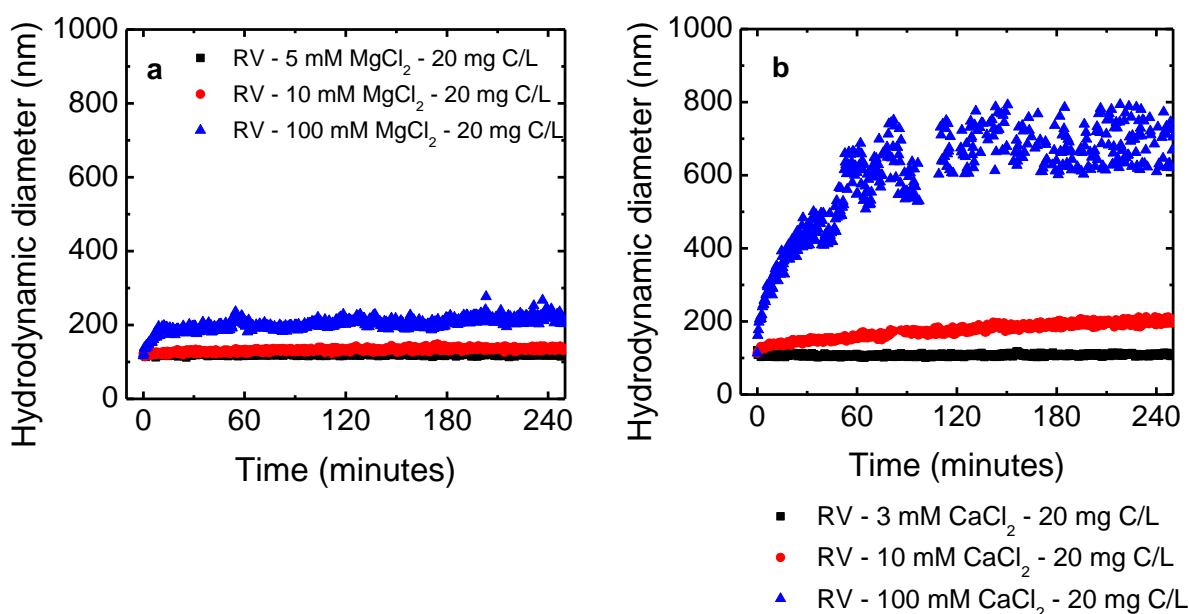


Figure 3.4 Aggregation kinetics of rotavirus in solutions containing 20 mg C/L SRNOM and a) MgCl_2 or b) CaCl_2 recorded for 250 minutes. Rotavirus concentration was $\sim 8 \times 10^5$ FFU/mL in solution at 25°C.

As shown in Figure 3.5a, the stability curve for rotavirus in MgCl_2 solution delineates clear regions of favorable or diffusion-limited regime and unfavorable or reaction-limited regime aggregation, already observed in other investigations for hematite, alginate-coated hematite, and fullerene nanoparticles.^{38, 39, 63} No change in rotavirus hydrodynamic size was detected at 5 mM MgCl_2 . Aggregation rates increased with MgCl_2 concentration until critical coagulation concentration (CCC) at 70 mM MgCl_2 . CCC for rotavirus in NOM-free MgCl_2 solutions occurred at 120 mM.³⁶ Aggregation rates of rotavirus in MgCl_2 solutions containing NOM were on average 60 times higher than the aggregation rates of rotavirus in NOM-free solutions at the

same MgCl_2 concentrations.³⁶

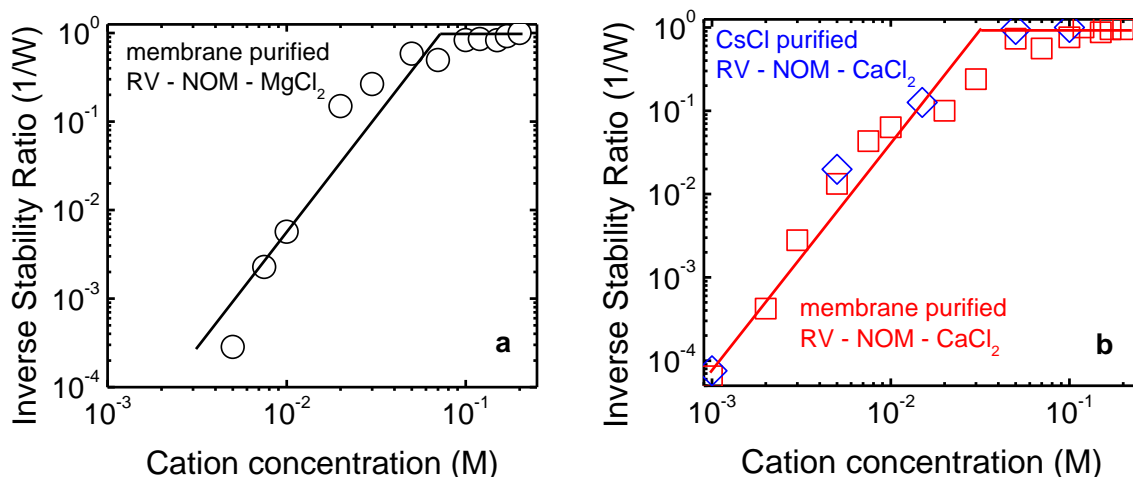


Figure 3.5 Inverse stability ratio ($1/W$) of rotavirus ($\sim 8 \times 10^5$ FFU/mL) in NOM (20 mg C/L) solutions in the presence of a) MgCl_2 and b) CaCl_2 cations at 25°C . Aggregation kinetic rates were measured at various cation concentrations ranging from 1 mM to 200 mM in CaCl_2 and from 5 mM to 200 mM in MgCl_2 (the lines are meant to delineate the regions between favorable and unfavorable aggregation). Data for membrane-purified rotavirus (i.e., circle and square symbols) are presented in Fig. 3.5a and 3.5b. Data for CsCl purified rotavirus (i.e., diamond symbols) are presented in Fig 3.5b.

The addition of CaCl_2 to rotavirus-NOM solutions caused a more pronounced effect on aggregation kinetics than MgCl_2 . Although aggregation was not observed at 1 mM CaCl_2 , aggregation rates increased with cation concentration until reaching a CCC at 30 mM, above which aggregation rates remained constant (Fig. 3.5b). The rates of rotavirus- Ca^{2+} -NOM formation were on average 566 times higher than those for the corresponding rotavirus- Ca^{2+} aggregates previously reported.³⁶ The observation of stable suspension of rotavirus in solution containing up to 600 mM NaCl, and fast aggregation of rotavirus at 70 mM MgCl_2 or 30 mM CaCl_2 , suggests that double layer compression by charge screening alone was not sufficient to control rotavirus aggregation.

Stability curves for both CsCl-purified and membrane-purified rotavirus were presented in Figure 3.5b. The difference between the inverse stability ratio ($1/W$) values was not

statistically significant for both rotavirus stocks (two-tailed t test, $p=0.05$). Thus, the results obtained for EPM and aggregation studies suggested that the purification method by membrane filtration produces rotavirus of similar characteristics to the CsCl gradient procedure.

Rotavirus aggregation rates decreased by an average factor of 82 when NOM concentration was reduced from 20 mg C/L to 4 mg C/L in 100 mM CaCl_2 concentration. This result and the previous comparison between rotavirus aggregation rates with and without 20 mg C/L (566 times higher in NOM) indicate that the presence of NOM enhanced rotavirus aggregation. For 20 mg C/L solutions, no NOM aggregation was detected in solutions containing up to 600 mM NaCl or 200 mM MgCl_2 (Fig. 3.6a). For rotavirus-free solutions containing 20 mg C/L and up to 200 mM CaCl_2 , NOM aggregation rate was 8 times lower than rotavirus aggregation rate. The size of the rotavirus-NOM aggregates used to determine the aggregation rate was 5 times larger than that of the NOM aggregates in CaCl_2 solution. At 10 mM CaCl_2 we did not observe NOM aggregate growth during the first 30 min (Fig. 3.6b). For this same time period, rotavirus-NOM aggregates grew to 150 nm. At 100 mM CaCl_2 , the increase in NOM aggregates after 30 minutes was 350 nm, while the growth of rotavirus-NOM aggregate was 450 nm (Fig 3.6c). The difference in aggregate growth for NOM and rotavirus-NOM suggest that only NOM adsorption on rotavirus surface was not enough to account for the observed D_h increase in rotavirus-NOM aggregates. However, adsorption of NOM on rotavirus surface can enhance rotavirus aggregation, similar to observation in other studies with nanoparticles.⁶³⁻⁶⁵

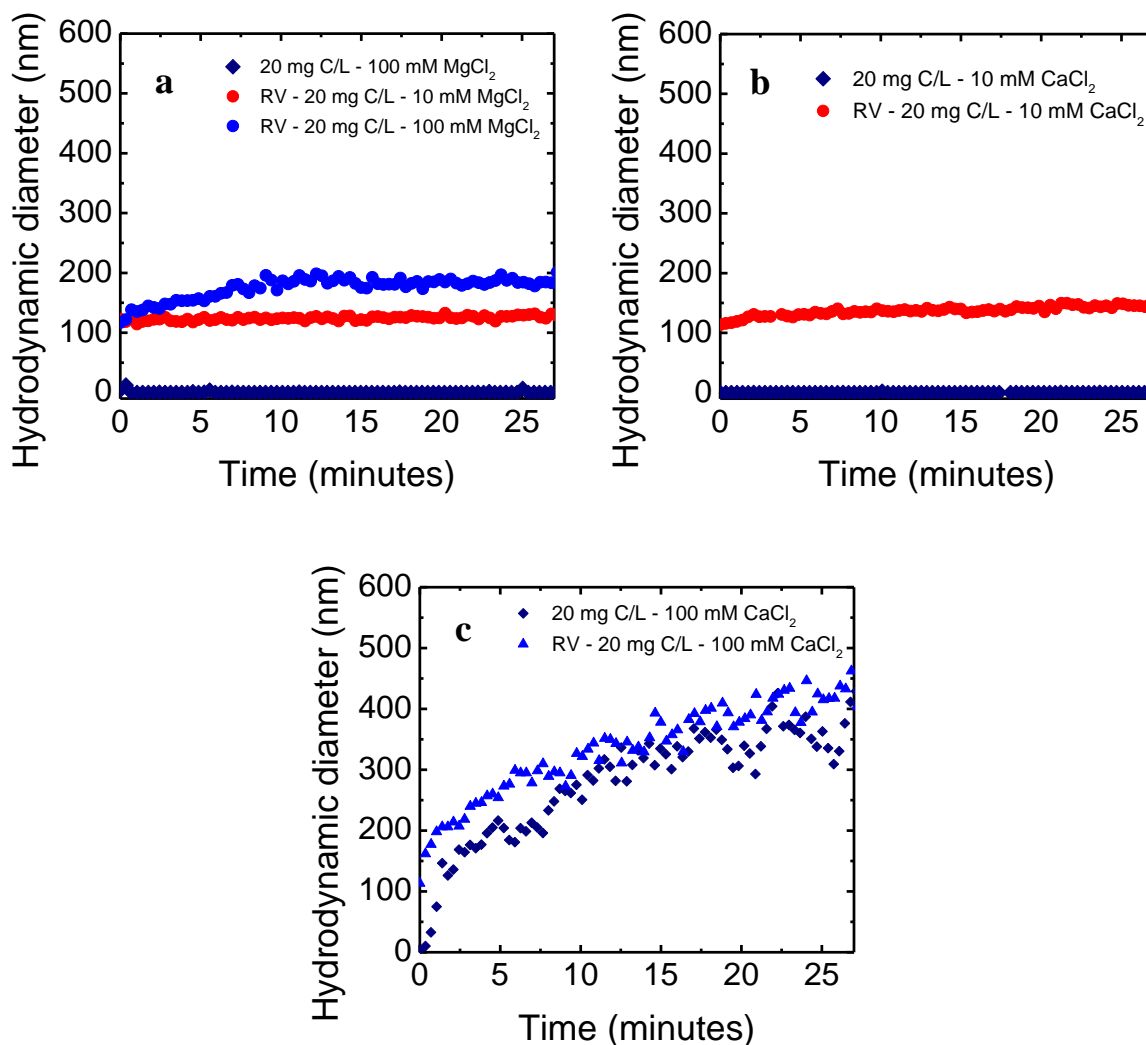


Figure 3.6 a) Aggregation kinetics of rotavirus in solutions containing 20 mg C/L SRNOM and 10 or 100 mM MgCl₂, and aggregation kinetics of 20 mg C/L SRNOM and 100 mM MgCl₂. b) Aggregation kinetics of rotavirus in solutions containing 20 mg C/L SRNOM and 10 mM CaCl₂, and aggregation kinetics of 20 mg C/L SRNOM and 10 mM MgCl₂. c) Aggregation kinetics of rotavirus in solutions containing 20 mg C/L SRNOM and 100 mM CaCl₂, and aggregation kinetics of 20 mg C/L SRNOM and 100 mM MgCl₂.

Rotavirus deposition kinetics on NOM-coated surfaces. TR-DLS results from our previous study showed that rotavirus remained stable in CaCl₂ and MgCl₂ solutions at concentrations ranging from 0.1 to 1 mM.³⁶ In addition, hydrodynamic diameter of membrane-purified RV in solution was measured by DLS showing a single peak at 100 nm for rotavirus

monodispersed population. Similar observation was obtained for rotavirus stocks purified with CsCl gradient centrifugation or with membrane filtration. This observation shows that rotavirus is present in the stock, and protein contamination is not detected by DLS. We further studied deposition kinetics of this stable suspension of rotavirus on NOM-coated surfaces. As shown in Figure 3.7a, rotavirus deposition rate on positively charged PLL-coated layer (i.e., favorable conditions) did not depend on the range of ionic strength examined (i.e., 0.1 to 1 mM). At 0.1 mM MgCl₂ or CaCl₂, rotavirus deposition rate on NOM-coated surface was 13 and 3.5 times lower than those at favorable conditions, respectively. Deposition rates increased with MgCl₂ or CaCl₂ concentration until reaching a finite lower limit at approximately 0.5 mM MgCl₂ or CaCl₂ (Fig. 3.7a), where the deposition rates were on average only 3.5 or 1.7 times lower than those for favorable conditions, respectively. This finite lower limit was also observed in MS2 deposition on NOM and silica surfaces at high IS (60 mM NaCl).²⁴ Maximum attachment efficiency of rotavirus occurred at 1 mM MgCl₂ or CaCl₂ solution (Fig. 3.7b), reaching a value of 0.2 and 0.7, respectively. A previous study of MS2 deposition on NOM surfaces reported a similar attachment behavior, i.e., attachment efficiencies were higher in CaCl₂ solution compared to those in MgCl₂ solution.²² Rotavirus deposition rate on NOM surfaces remained the same when the pH of the rotavirus suspension was increased from 5.9 to 8 for two CaCl₂ concentrations, 0.1 and 1 mM (Fig. 3.7b). As shown in Table 3.2, in 1 mM CaCl₂, both rotavirus and NOM-coated beads became slightly more negative charged (-1.6 ± 0.2 vs. -2.2 ± 0.1 $\mu\text{mcmV}^{-1}\text{s}^{-1}$ for NOM-coated beads and -0.7 ± 0.1 vs. -0.8 ± 0.2 $\mu\text{mcmV}^{-1}\text{s}^{-1}$ for rotavirus). This small change in EPM and similar deposition rate of rotavirus on NOM-coated surfaces at pH 5.9 and 8.3 suggests the role of Ca²⁺ complexation with the carboxylate groups on both rotavirus and NOM-surface. We will further discuss this observation in light of the AFM interaction force below.

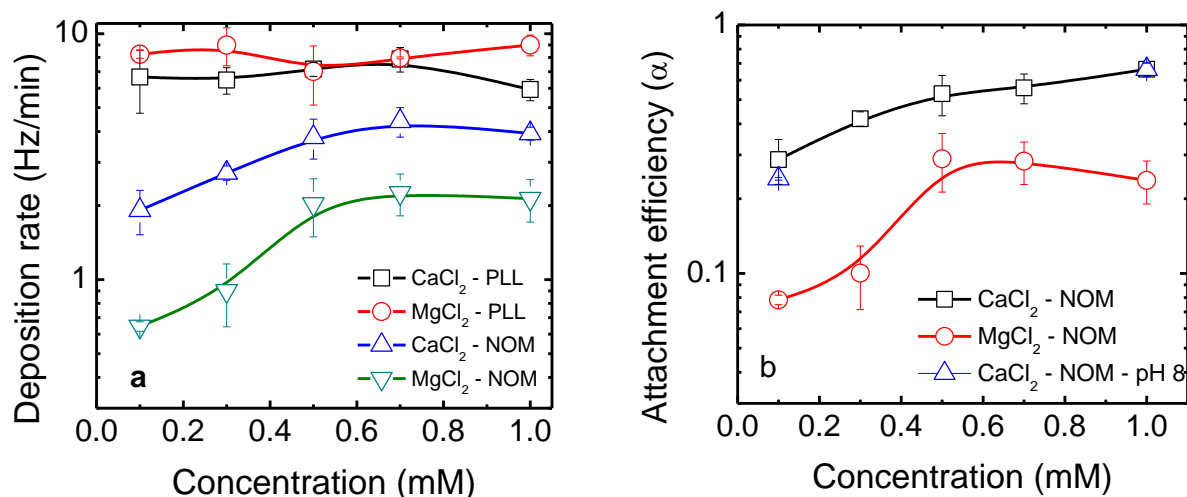


Figure 3.7 a) Deposition kinetics of rotavirus (8×10^5 FFU/ml) on NOM-coated silica surface and PLL-coated silica surface in divalent cation solutions. CaCl₂ and MgCl₂ concentrations ranged from 0.1 to 1 mM for all the experiments at 25°C. pH of solutions was 5.9 unless otherwise indicated. Deposition rates were expressed in Hz/min. b) Deposition rates of rotavirus on NOM surface were normalized by the deposition rate on PLL surface for each cation condition (CaCl₂ and MgCl₂) as Attachment efficiencies (α).

| | pH 5.9 | | pH 8.3 | |
|--|----------------------------|-------|----------------------------|-------|
| | Mob ($\mu\text{mcm/Vs}$) | StDev | Mob ($\mu\text{mcm/Vs}$) | StDev |
| Silica - 1 mM CaCl ₂ | -1.7 | 0.2 | -3.0 | 0.2 |
| NOM - 1 mM CaCl ₂ | -1.6 | 0.2 | -2.2 | 0.1 |
| PLG - 1 mM CaCl ₂ | -1.8 | 0.4 | -2.1 | 0.4 |
| Rotavirus - 1 mM NaCl | -1.6 | 0.2 | -1.8 | 0.2 |
| Rotavirus - 1 mM CaCl ₂ | -0.7 | 0.1 | -0.8 | 0.1 |
| Rotavirus - 1 mM CaCl ₂ - 20 mg C/L | -1.0 | 0.1 | -1.1 | 0.2 |

Table 3.2 Electrophoretic mobility of silica beads, NOM or PLG-coated silica beads, and rotavirus. Three measurements were conducted for each condition.

Control experiments for PLL and NOM coating completeness on silica surface.

Representative force curves are shown in Figure 3.8. As shown in Figure 3.8a, electrostatic repulsion was observed in 1 mM bicarbonate buffer solution at pH 8.3 when the SiNi tip was approaching the negatively charged quartz surface. This control experiment was conducted first

to ensure that the SiNi tip was negatively charged in 1 mM bicarbonate solution at pH 8.3. This solution condition and the SiNi tip was further used to determine the surface charge of silica sensor surface and the polycarbonate membrane. The negative charge of the silica surface and the polycarbonate (PC) membrane was evidenced because repulsive electrostatic forces were recorded (Fig. 3.8a).

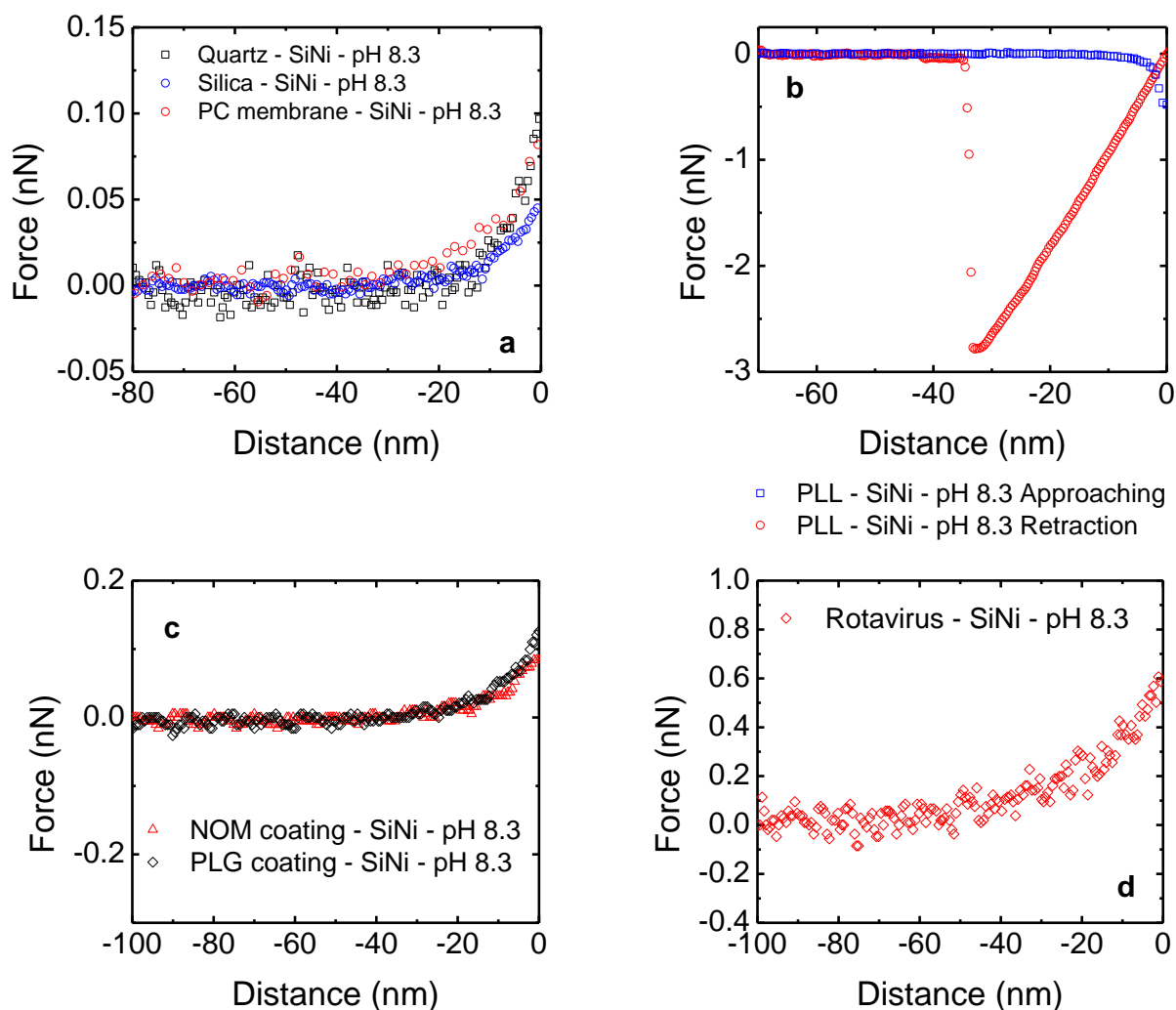


Figure 3.8 Control experiments showing a) electrostatic repulsion between quartz surface and silicon nitride probe, silica surface and silicon nitride probe, and polycarbonate surface and silicon nitride probe, b) electrostatic attraction between PLL layer and silicon nitride probe during approaching and adhesion during retraction, c) repulsion forces between NOM layer and silicon nitride probe, PLG layer and silicon nitride probe, and d) repulsion force between silicon nitride probe and rotavirus layer adsorbed on a PLL layer (1 mM NaHCO_3 buffered pH of 8.3).

Coating completeness of positively charged PLL on silica surface was confirmed for 25 approaching force curves along a 0.7 cm^2 area when attractive electrostatic forces were detected using a sharp SiNi tip of 20 nm-curvature-radius; adhesion was also always detected during retraction (Fig. 3.8b). Finally, negatively charged NOM coverage on PLL-coated silica surface was confirmed when repulsive forces were recorded during approaching force curves between the SiNi probe and NOM layer (Fig. 3.8c). Similar to NOM-coated surfaces, the PLG-coated and the rotavirus-coated silica surfaces also showed electrostatic repulsion (Fig. 3.8c and 3.8d, respectively). These results suggest that the coating protocol completely covered the positively charged PLL layer relative to the 20-nm tip radius of the SiNi probe used over 0.7 cm^2 probing area of the studied surface. Note that the SiNi probe is 2 times smaller than the rotavirus particles. Thus, the surface coating is considered complete on the length scale of the SiNi probe.

Control experiments using the spherical silica probe. We first conducted the force measurement for the uncoated silica probe with polycarbonate membrane or quartz surface at 1, 10, and 100 mM NaCl solutions. As shown in Figures 3.9a, 3.10a and Table 3.3, the interaction force decay length for silica probe with the membrane or the quartz surface closely followed the Debye length calculated based on the Debye-Hückel theory. This observation suggests the dominant role of electrostatic interactions between the probe and the membrane or the quartz surface, as expected. In solution containing 20 mg C/L NOM, the interaction force decay length between silica probe and quartz also followed closely the predicted Debye length (Fig 3.10a). In addition, the difference between measured decay lengths with and without NOM in solution was not statistically significant (two-tailed t test, $p=0.05$). This observation showed that the presence of 20 mg C/L NOM did not influence the AFM force measurement.

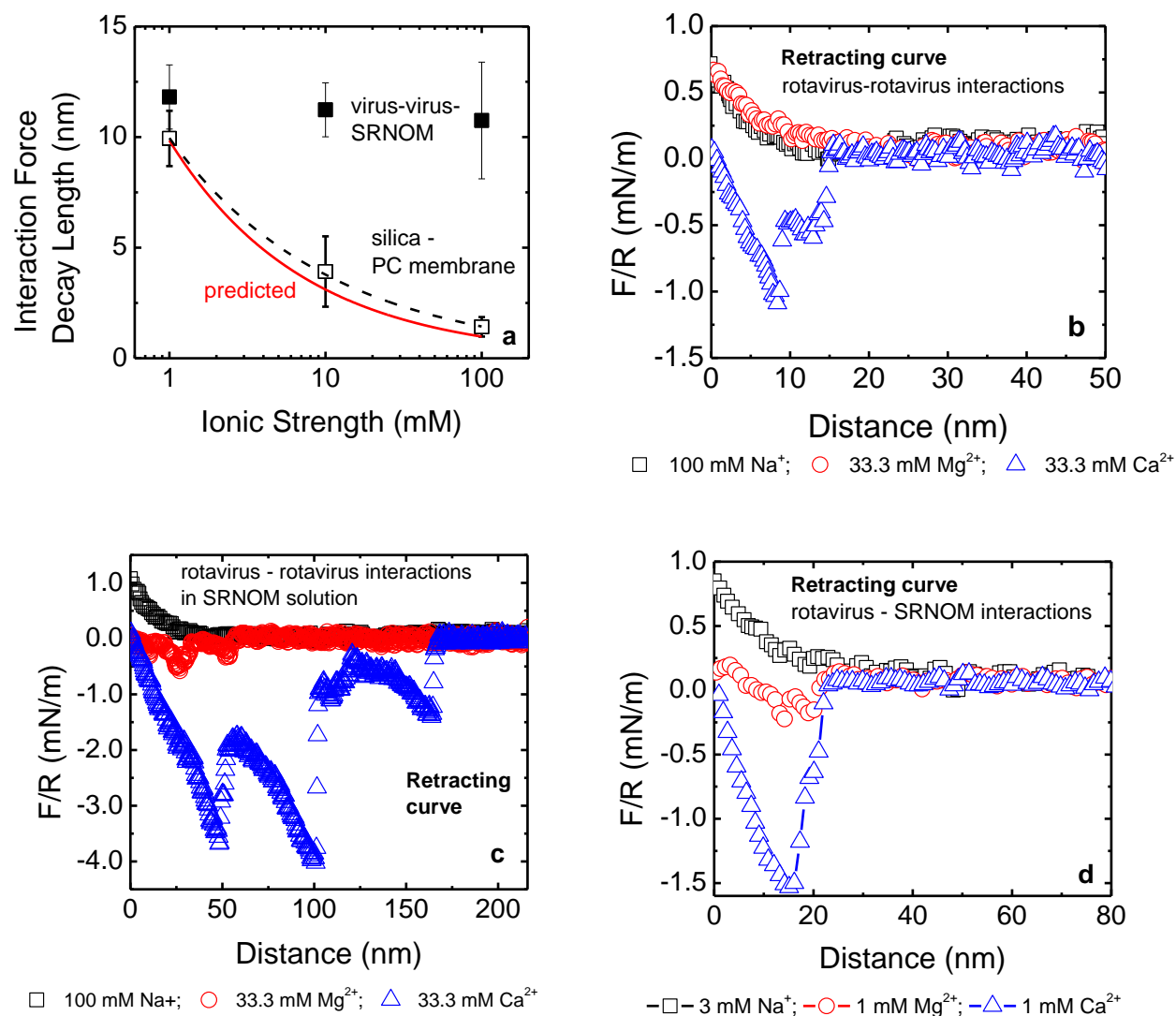


Figure 3.9 a) Interaction force decay length determined for silica probe with membrane, and rotavirus-coated probe with rotavirus-coated membrane. b) Retracting force curves for rotavirus-coated probe with rotavirus-coated membrane in solutions containing 100 mM NaCl or 33.3 mM CaCl_2 or 33.3 mM MgCl_2 . c) Retracting force curves for rotavirus-coated probe with rotavirus-coated membrane in solutions containing 20 mg C/L and 33.3 mM NaCl or 33.3 mM CaCl_2 or 33.3 mM MgCl_2 . d) Retracting force curves for rotavirus-coated probe with NOM-coated surface in solutions containing 3 mM NaCl or 1 mM MgCl_2 or 1 mM CaCl_2 .

Additional control experiments were conducted for rotavirus-coated probe with silica surface, for silica probe with rotavirus-coated silica surface, and for silica probe with rotavirus-coated polycarbonate membrane at 1 mM NaCl solutions at pH 5.9. No electrostatic attractive force was observed for these experiments (Fig. 3.11 a-b), suggesting that the rotavirus coating

protocol used for force measurement was able to completely cover the positively charged PLL layer laid between the silica sphere probe and rotavirus layer, and between the silica surface and rotavirus layer. The difference among the interaction force decay lengths measured for all three conditions (Fig. 3.10b and Table 3.3b) was not statistically significant (two-tailed t test, $p=0.05$). Thus, the decay length obtained by the AFM approaching curve between rotavirus and silica did not depend on whether the rotavirus was located on the substrate or on the probe. In addition, the decay length determined from these experiments did not follow the predicted Debye length, suggesting an additional interaction besides electrostatic interaction.

Table 3.3 Predicted Debye length and measured interaction force decay length in NaCl containing solutions for:

a) Control experiments with silica probe and hard surfaces with and without 20 mg C/L NOM.

| Ionic Strength (mM) | Debye Length predicted | Silica probe PC membrane | Silica probe quartz surface | Silica probe quartz surface 20 mg C/L NOM |
|---------------------|------------------------|--------------------------|-----------------------------|---|
| 1 | 10 | 10 ± 1.3 | 10 ± 0.5 | 10 ± 0.7 |
| 10 | 3 | 4 ± 1.6 | 3 ± 0.2 | 3 ± 0.4 |
| 100 | 1 | 1 ± 0.4 | 1 ± 0.2 | 1 ± 0.5 |

b) Rotavirus interaction with silica or rotavirus with and without 20 mg C/L NOM.

| Ionic Strength (mM) | Silica Probe rotavirus-coated PC membrane | Rotavirus-coated probe silica surface | Silica probe rotavirus-coated silica surface | Rotavirus-coated probe rotavirus-coated membrane 20 mg C/I NOM |
|---------------------|---|---------------------------------------|--|--|
| 1 | 10 ± 1.2 | 10 ± 1.7 | 11 ± 1.2 | 12 ± 1.5 |
| 10 | 8 ± 1.4 | 7 ± 1.4 | 8 ± 0.6 | 11 ± 1.2 |
| 100 | 6 ± 1.1 | 5 ± 1.1 | 6 ± 0.6 | 11 ± 2.6 |

Interaction force decay lengths were calculated from approaching force curves using AFM in contact mode.

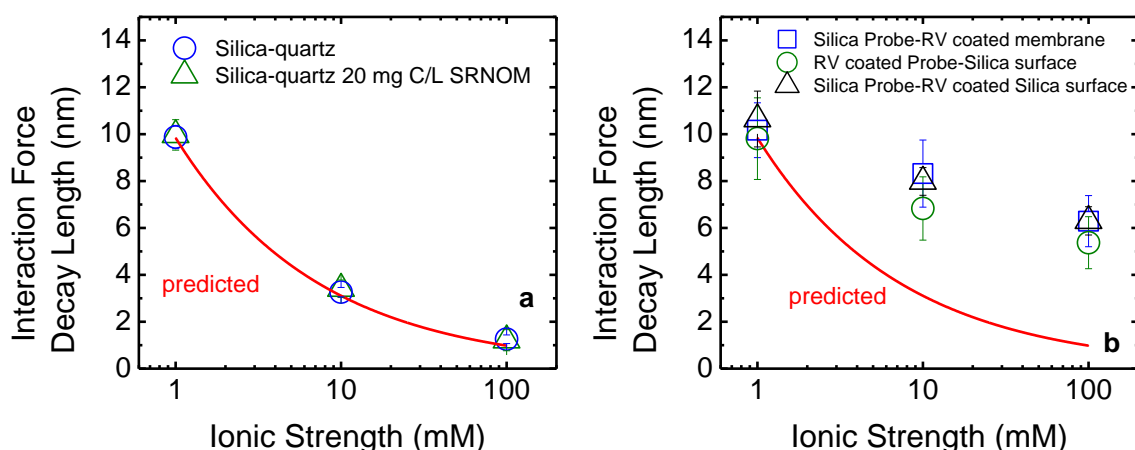


Figure 3.10 Interaction force decay length determined for a) silica probe with quartz cover slip, and silica probe with quartz cover slip in 20 mg C/L NOM and b) silica probe with rotavirus-coated membrane, and rotavirus-coated probe with silica surface, and silica probe with rotavirus-coated silica surface. Predicted Debye length is plotted for comparison purposes.

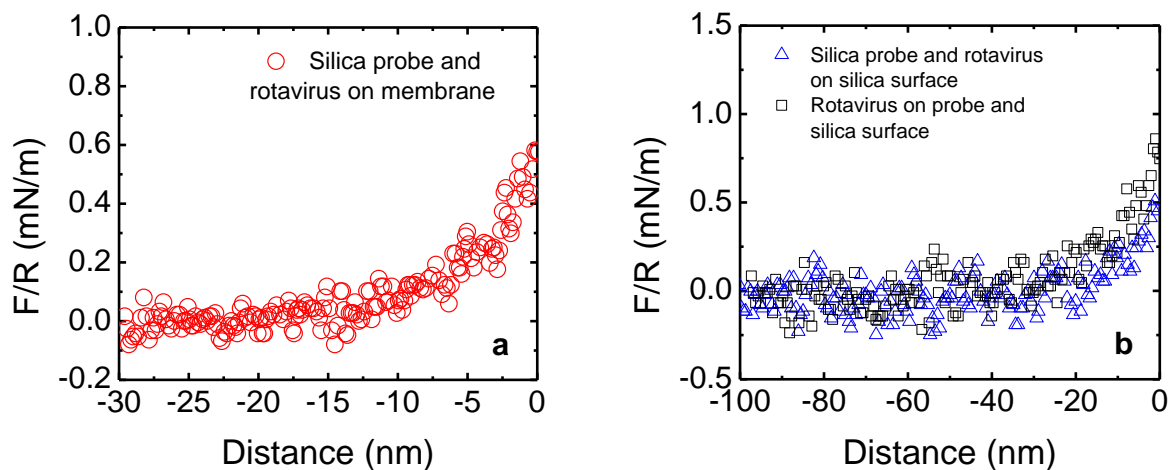


Figure 3.11 Approaching force curves for a) silica probe with rotavirus layer on polycarbonate membrane and b) silica probe with rotavirus layer on silica surface, and rotavirus on probe with silica surface.

Interaction force between rotavirus and rotavirus. The difference among interaction force decay lengths for rotavirus-rotavirus in 20 mg C/L solution was not statistically significant for 1, 10, and 100 mM NaCl ionic strength (two-tailed t test, $p=0.05$) suggesting the lack of ionic

strength dependence (Figure 3.9a). Similar to the observed rotavirus and silica interaction, an additional interaction besides electrostatic interaction was detected.

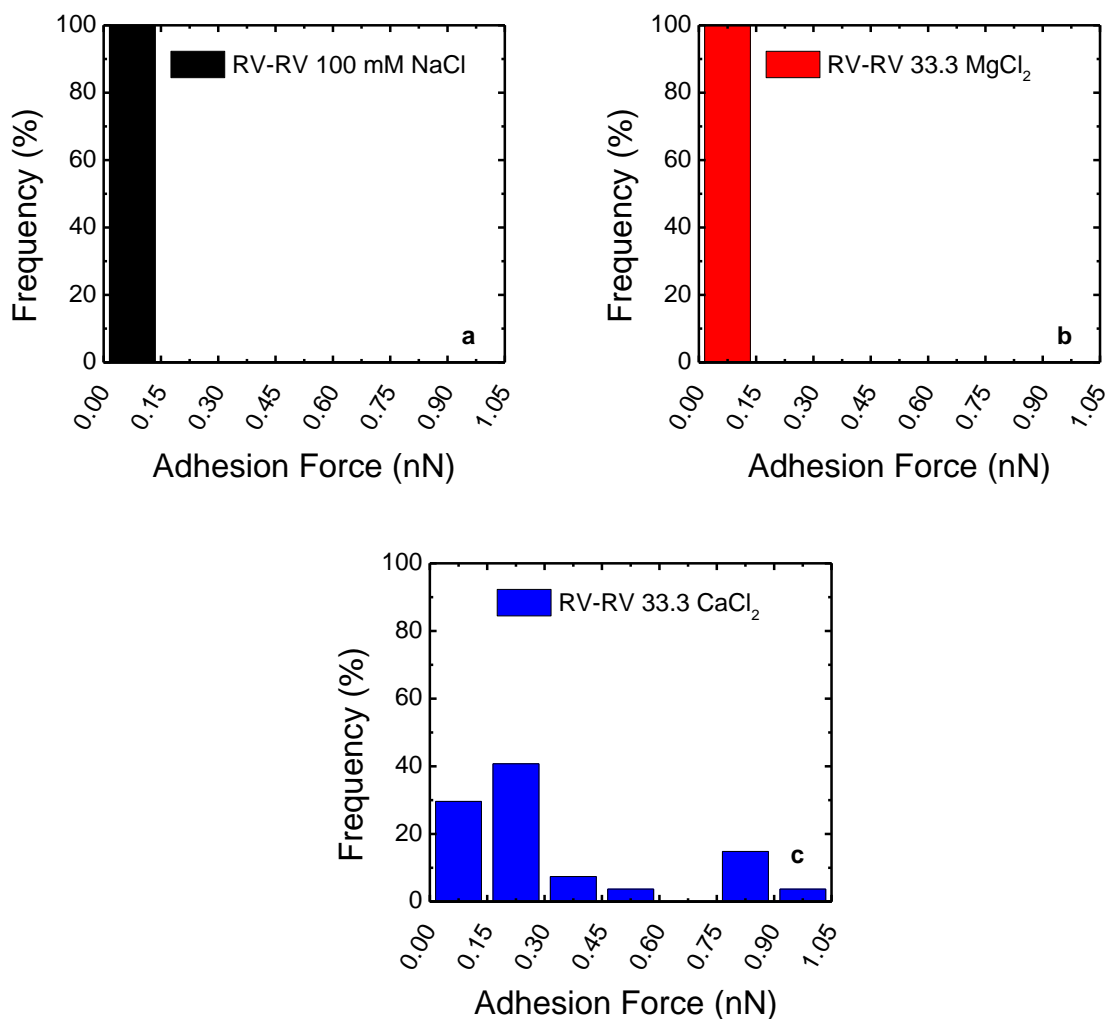


Figure 3.12 Adhesion forces of RV with RV layer in solution containing a) 100 mM NaCl or b) 33.3 mM MgCl₂ or c) 33.3 mM CaCl₂.

The adhesion force curves, determined from the retracting force profiles in 100 mM NaCl or 33.3 mM CaCl₂ or 33.3 mM MgCl₂ (Fig. 3.9b), were statistically analyzed using frequency distribution (Fig. 3.12). These salt concentrations used in the adhesion force experiments were selected because of the different aggregation results obtained during the TR-DLS experiments. 33.3 mM CaCl₂ was found in the previous section to be approximately at the CCC of rotavirus

aggregation in CaCl_2 solutions while 33.3 mM MgCl_2 was found to be below the CCC in MgCl_2 solutions. Conversely, 100 mM NaCl was selected because no aggregation was detected during TR-DLS experiments in NaCl solutions. No adhesion force was observed in the rotavirus-rotavirus system in the presence of 100 mM NaCl , and the retracting curve mirrored the approaching curve in all the experiments. In 33.3 mM MgCl_2 solutions only 10% of the retracting curves analyzed showed small adhesion forces on the order of tens of pN (0.016, 0.034, 0.040 nN or 0.032, 0.068, 0.080 mN/m); the rest of the retracting curves displayed no adhesion. Unlike the case of NaCl or MgCl_2 solutions, in CaCl_2 solutions all the force profiles displayed significant adhesion forces at different magnitudes on the order of hundreds of pN (commonly between 0 to 0.3 nN or 0 to 0.6 mN/m and a small fraction even reaching 1 nN or 2 mN/m). The adhesion force in 33.3 mM CaCl_2 solution exhibited multiple detachments at separation distance starting at ~ 10 nm. These multiple detachments have been observed previously for AFM force measurement of oocysts in 50 mg/L Ca^{2+} solution using silica probe, and for single bacteria cell probe^{66, 67} due to complex multiple discrete adsorptions on surface polymers. The diverse nature of NOM supramolecules^{68, 69} may allow part of the NOM-rotavirus or NOM-NOM connections to break. It is also likely that the 1 μm silica sphere coated with rotavirus had multiple contact points with the rotavirus layer, and the retracting force curves were the results of breaking multiple bridges formed by Ca^{2+} -complexation with rotavirus surfaces.^{70, 71} The magnitude of the adhesion forces followed the order of $\text{Ca}^{2+} > \text{Mg}^{2+} > \text{Na}^+$.

When 20 mg C/L NOM was added to the solutions containing 100 mM NaCl or 33.3 mM CaCl_2 or 33.3 mM MgCl_2 , the adhesion behavior changed dramatically, as shown in Figures 3.9c and 3.14. Thirty-three percent of the retracting curves displayed forces ranging from 0.053 to 0.292 nN (or 0.106 to 0.584 mN/m) with maximum adhesion distances of ~ 50 nm in 100 mM

NaCl. Adhesion forces in MgCl_2 solutions were observed in all experiments. Approximately 90% of these forces were below 0.75 nN (or 1.5 mN/m), and 80% of adhesion distances were below 150 nm. Highest adhesion forces were observed in CaCl_2 solutions. Specifically, the adhesion forces were usually found between 0.5 to 2 nN (or 1 to 4 mN/m) with adhesion distances commonly above ~200 nm. The longest adhesion distances were observed upon final rupture between rotavirus-coated probe and rotavirus layer in 20 mg C/L NOM and CaCl_2 . The adhesion distances that were longer than rotavirus diameter of 75 nm¹⁴ were probably caused by pulling-off rotavirus and NOM from the substrate. Long adhesion distance has already been reported for alginate-alginate interaction in CaCl_2 solution.^{59, 71} Multiple detachments were evidenced in both CaCl_2 (Fig. 3.13) and MgCl_2 solutions. Similar to the previous adhesion force experiments in the absence of NOM, the magnitude of the adhesion forces followed the same order of $\text{Ca}^{2+} > \text{Mg}^{2+} > \text{Na}^+$.

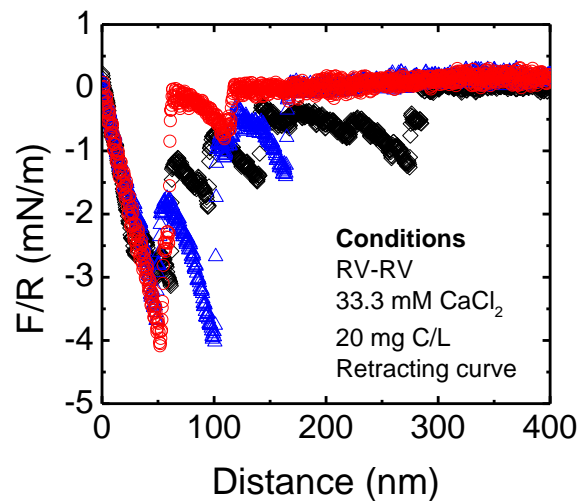


Figure 3.13 Retracting force curves for rotavirus-coated probe with rotavirus-coated membrane in solution containing 20 mg C/L and 33.3 mM CaCl_2 .

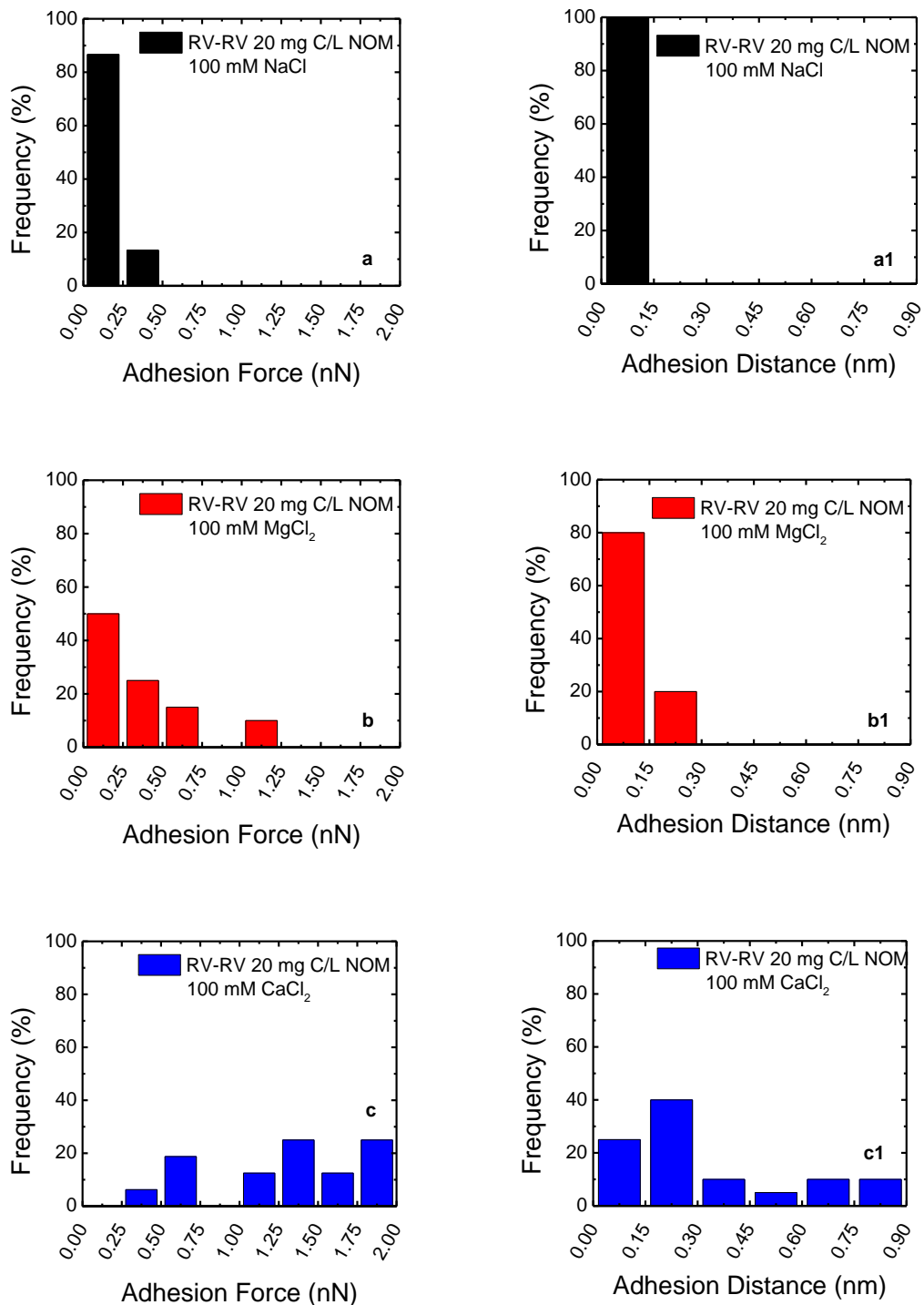


Figure 3.14 Adhesion forces and adhesion distances of RV with RV layer in solution containing 20 mg C/L SRNOM and a-a1) 100 mM NaCl or b-b1) 33.3 mM MgCl₂ or c-c1) 33.3 mM CaCl₂.

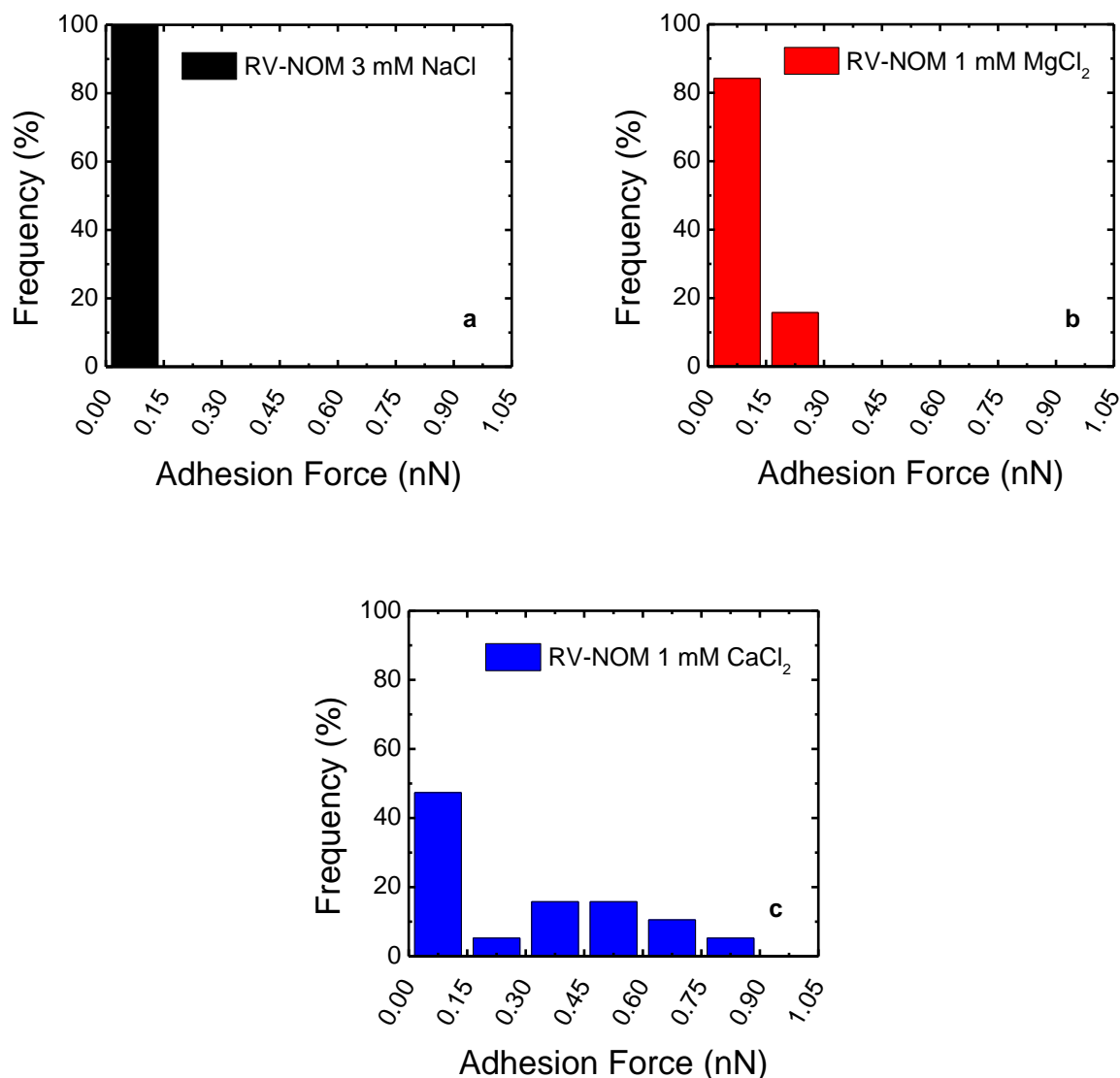


Figure 3.15 Adhesion forces of RV with SRNOM layer in solution containing a) 3 mM NaCl or b) 1 mM MgCl₂ or c) 1 mM CaCl₂.

Interaction force between rotavirus and NOM-coated surface. Retracting force profiles for the experiment with rotavirus and NOM-coated surface in solutions containing 3 mM NaCl or 1 mM CaCl₂ or 1 mM MgCl₂ are shown in Figures 3.9d and 3.15. These salt concentrations were selected because higher deposition in CaCl₂ solutions compared to that in MgCl₂ or NaCl solutions was observed by QCM experiments. No adhesion force was observed

in 3 mM NaCl solutions. In 1 mM MgCl_2 solutions, approximately half of the retracting curves showed adhesion forces ranging from 0.076 to 0.242 nN (0.152 to 0.484 mN/m) following multiple detachments with adhesion distances of commonly ~ 20 nm, although the rest of the retracting curves displayed no adhesion at all. In 1 mM CaCl_2 solutions, $\sim 50\%$ of the adhesion forces were found in the range of 0.3 to 0.9 nN (0.6 to 1.8 mN/m), all of them showing multiple detachments. The rest of the adhesion forces obtained for CaCl_2 solutions were below 0.15 nN (or 0.3 mN/m). The magnitude of the adhesion forces followed the order of $\text{Ca}^{2+} > \text{Mg}^{2+} > \text{Na}^+$. In a previous study,²⁰ the adhesion forces of MS2, ϕX174 or aichi virus to metal oxide-removed sand in artificial groundwater are in the range of the forces measured between rotavirus and NOM layer at approximately the same divalent cation concentration.

Adhesion force between rotavirus and NOM-coated surface was determined for 1 mM CaCl_2 at pH 5.9 and 8.3. As shown in Figures 3.16a-b, the most frequently observed forces were between 0.05-0.15 nN for both pH conditions. These results are consistent with the deposition results obtained in similar solution conditions for both pH. Thus, pH increase from 5.9 to 8.3 did not influence the adhesion between rotavirus and NOM-coated layer. The role of Ca^{2+} complexation with carboxylate groups was further studied based on the adhesion force measurement in 1mM CaCl_2 solution for rotavirus and silica surface coated with polyglutamic acid (PLG) at pH 5.9 and 8.3. As shown in Figures 3.17a-b, the adhesion forces determined for these two conditions were between 0.2-0.6 nN (or 0.4-1.2 mN/m). Despite expected electrostatic repulsion between rotavirus and PLG due to negative EPM for both rotavirus and PLG-coated surfaces (Table 3.2), the observed strong adhesion force again indicated the role of Ca^{2+} complexation with carboxylate groups in rotavirus deposition.

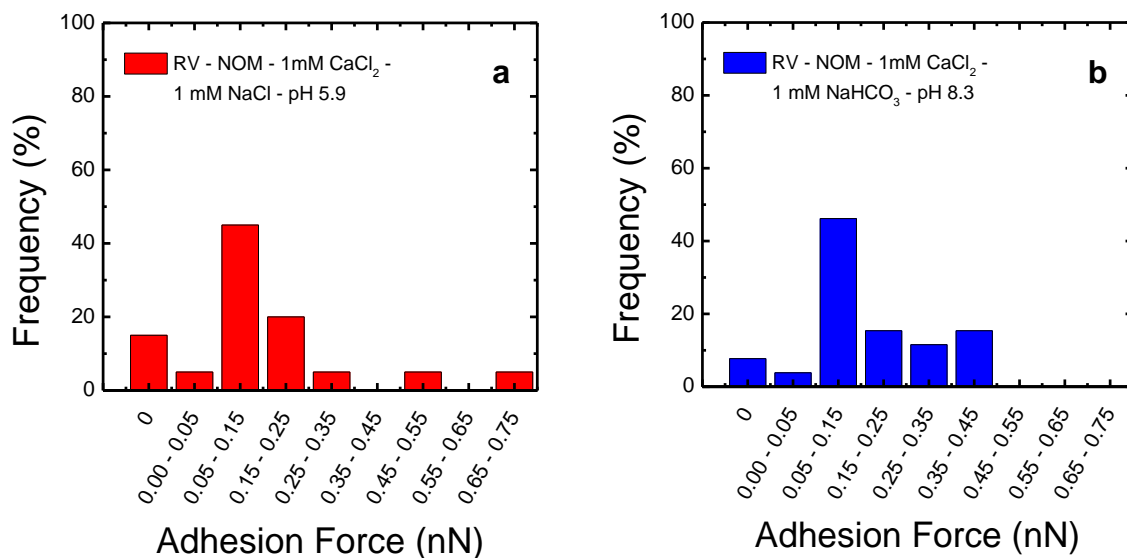


Figure 3.16 Adhesion forces of RV with SRNOM layer in solution containing 1 mM CaCl₂ at a) pH 5.9 (1 mM NaCl) or b) pH 8.3 (1 mM NaHCO₃).

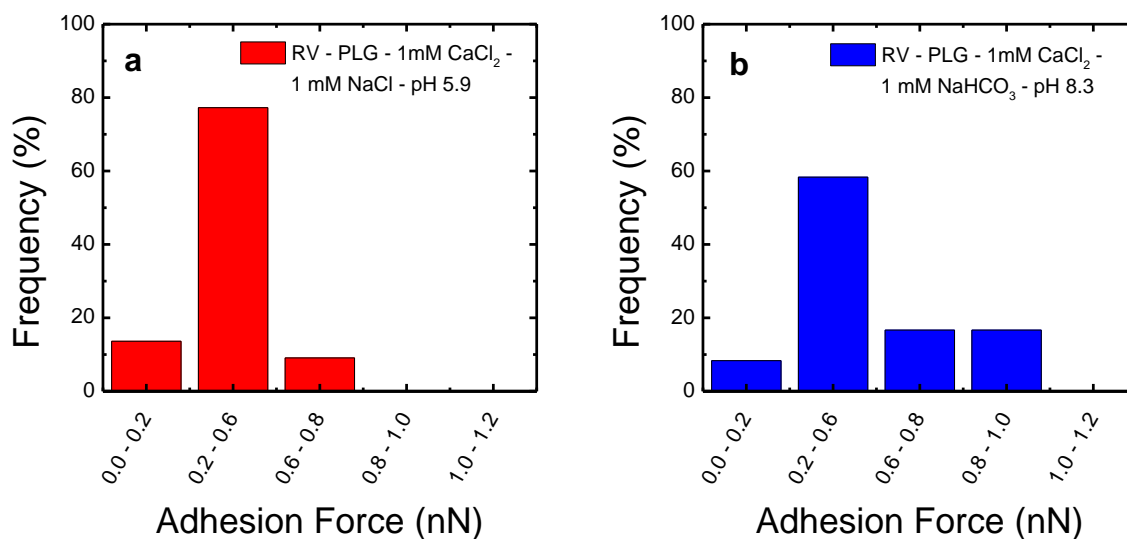


Figure 3.17 Adhesion forces of RV with PLG layer in solution containing 1 mM CaCl₂ at a) pH 5.9 (1 mM NaCl) or b) pH 8.3 (1 mM NaHCO₃).

Roles of non-DLVO interactions on rotavirus aggregation and deposition. The total interaction energy that control colloid transport has been traditionally determined based on the

classic DLVO theory as the sum of retarded van der Waals and repulsive electrostatic interactions.^{72, 73} For interaction between like charged surfaces, such as between negatively charged viruses, increasing ionic strength is expected to lead to compression of the double layer, and as a result the interaction force decay length should become smaller following the Debye equation. In contrast to this expectation, the interaction force decay length of rotavirus did not change as ionic strength increased, as shown in Figure 3.9a. In addition to the independence of decay length measured by AFM, the absence of adhesion force for the rotavirus-rotavirus retracting curves is consistent with the lack of detectable rotavirus aggregation in NaCl solutions even at 600 mM NaCl as reported previously.³⁶ Stable suspension of rotavirus at high ionic strength and independence of rotavirus interaction force decay length with ionic strength may be a result of a number of factors. Specifically, steric interaction similar to those observed for bacteria and oocysts may be the cause.^{56, 74-77} Another possibility is the combination of fast Brownian motion of nanometer size rotavirus and weak van der Waals interaction due to low Hamaker constants, which have been found to be almost 10 times lower than those for latex particles.^{26, 78-82} The third possibility may be the role of hydration force for rotavirus particles. Hydrated surface of rotavirus may prevent them from approaching each other.

Stronger adhesion forces were observed for rotavirus with rotavirus (Figures 3.9b and 3.9c), and rotavirus with NOM-coated surfaces (Figure 3.9d) in CaCl₂ solutions compared to those in MgCl₂ and NaCl solutions. This observation is consistent with higher deposition of rotavirus on NOM-coated surfaces (Fig. 3.7) and faster aggregation of rotavirus in NOM-containing solutions, both in the presence of calcium ions. Carboxylate groups have been shown to be the dominating functional groups that control NOM negative charge at the pH (~5.9) of our experiments.^{68, 83, 84} Molecular dynamics simulation of complexation between NOM and

different divalent cations suggest that NOM carboxylate groups are able to form strong inner sphere complexation with CaCl_2 and weak outer sphere complexation with MgCl_2 due to the presence of a tightly-held hydration layer in MgCl_2 cations.^{84, 85} The surface of rotavirus capsids also contains carboxylate groups located on glutamic acid and aspartic acids.^{86, 87} Stronger interactions observed for rotavirus in CaCl_2 solutions compared to MgCl_2 or NaCl solutions can be explained by the ability of CaCl_2 to form inner sphere complexation with carboxylate groups in NOM and on rotavirus surfaces. Experimental data obtained from a combination of approaches presented in this study, together with the experimental and theoretical studies for permeable microbial particles,²⁷⁻²⁹ further emphasize the importance of non-DLVO interactions in microbial adhesion.

Environmental implications of rotavirus deposition and aggregation kinetics in presence of NOM and hardness. Aggregation of rotavirus started to be detected at 2 mM CaCl_2 and 7.5 mM MgCl_2 in solutions containing NOM. Although these concentrations can be found in groundwater with very high hardness, i.e. CaCl_2 ranging from 1 to 15 mM with average of 5 mM, and MgCl_2 ranging from 0.2 to 23.8 mM with average of 5 mM,¹⁶ dissolved NOM concentration of 20 mg C/L was required for rotavirus aggregation. Lower aggregation rate of rotavirus in 4 mg C/L solution compared to 20 mg/L solution was found. Thus, in groundwater with low hardness and low dissolved organic matter, rotavirus may remain monodispersed. At environmentally relevant hardness of groundwater in the US,¹⁶ deposition of viruses on NOM surfaces was found to be higher than on clean silica surfaces measured in our previous work.³⁶ Considering the ubiquitous presence of NOM in groundwater, this study suggests that dissolved NOM concentration, NOM-coated surfaces, and the functional groups of NOM may play an important role in rotavirus aggregation and deposition in subsurface. In an aquifer with low

hardness, non-DLVO interactions among virus particles and virus with a soil surface could prevent virus aggregation and virus deposition, thus allow viruses to be more mobile than DLVO prediction.

Acknowledgements. This work was partially supported by NSF #0954501, the Academic Excellence Alliance program at King Abdullah University of Science and Technology, and the U.S. Department of Energy DE-FG02-07ER46453 and DE-FG02-07ER46471. We also acknowledge Dr. Scott McLaren, Ms. Ofelia Romero, and Mr. Tony Straub.

3.5 References

1. Brunkard, J. M.; Ailes, E.; Roberts, V. A.; Hill, V.; Hilborn, E. D.; Craun, G. F.; Rajasingham, A.; Kahler, A.; Garrison, L.; Hicks, L.; Carpenter, J.; Wade, T. J.; Beach, M. J.; Yoder, J. S. *Morbidity and Mortality Weekly Report (MMWR): Surveillance for Waterborne Disease Outbreaks Associated with Drinking Water --- United States, 2007--2008*; Centers for Disease Control and Prevention (CDC): 2011.
2. Yoder, J.; Roberts, V.; Craun, G. F.; Hill, V.; Hicks, L.; Alexander, N. T.; Radke, V.; Calderon, R. L.; Hlavsa, M. C.; Beach, M. J.; Roy, S. L. *Surveillance for Waterborne Disease and Outbreaks Associated with Drinking Water and Water not Intended for Drinking --- United States, 2005--2006*; Centers for Diseases Control and Prevention: 2008.
3. Fong, T. T.; Mansfield, L. S.; Wilson, D. L.; Schwab, D. J.; Molloy, S. L.; Rose, J. B., Massive microbiological groundwater contamination associated with a waterborne outbreak in Lake Erie, South Bass Island, Ohio. *Environ. Health Perspect.* **2007**, *115*, (6), 856-864.
4. Abbaszadegan, M.; Lechevallier, M.; Gerba, C., Occurrence of viruses in US groundwaters. *J. Am. Water Work Assoc.* **2003**, *95*, (9), 107-120.

5. Lee, S. G.; Jheong, W. H.; Suh, C. I.; Kim, S. H.; Lee, J. B.; Jeong, Y. S.; Ko, G.; Jang, K. L.; Lee, G. C.; Paik, S. Y., Nationwide Groundwater Surveillance of Noroviruses in South Korea, 2008. *Appl. Environ. Microbiol.* **2011**, 77, (4), 1466-1474.
6. Gabrieli, R.; Maccari, F.; Ruta, A.; Pana, A.; Divizia, M., Norovirus Detection in Groundwater. *Food Environ. Virol.* **2009**, 1, (2), 92-96.
7. Futch, J. C.; Griffin, D. W.; Lipp, E. K., Human enteric viruses in groundwater indicate offshore transport of human sewage to coral reefs of the Upper Florida Keys. *Environ. Microbiol.* **2010**, 12, (4), 964-974.
8. Gibson, K. E.; Schwab, K. J., Detection of Bacterial Indicators and Human and Bovine Enteric Viruses in Surface Water and Groundwater Sources Potentially Impacted by Animal and Human Wastes in Lower Yakima Valley, Washington. *Appl. Environ. Microbiol.* **2011**, 77, (1), 355-362.
9. Locas, A.; Barthe, C.; Barbeau, B.; Carrire, A.; Payment, P., Virus occurrence in municipal groundwater sources in Quebec, Canada. *Can. J. Microbiol.* **2007**, 53, (6), 688-694.
10. Pieper, A. P.; Ryan, J. N.; Harvey, R. W.; Amy, G. L.; Illangasekare, T. H.; Metge, D. W., Transport and recovery of bacteriophage PRD1 in a sand and gravel aquifer: Effect of sewage-derived organic matter. *Environ. Sci. Technol.* **1997**, 31, (4), 1163-1170.
11. Ryan, J. N.; Elimelech, M.; Ard, R. A.; Harvey, R. W.; Johnson, P. R., Bacteriophage PRD1 and silica colloid transport and recovery in an iron oxide-coated sand aquifer. *Environ. Sci. Technol.* **1999**, 33, (1), 63-73.
12. Foppen, J. W. A.; Okletey, S.; Schijven, J. F., Effect of goethite coating and humic acid on the transport of bacteriophage PRD1 in columns of saturated sand. *J. Contam. Hydrol.* **2006**, 85, (3-4), 287-301.

13. Hijnen, W. A. M.; Brouwer-Hanzens, A. J.; Charles, K. J.; Medema, G. J., Transport of MS2 phage, *Escherichia coli*, *Clostridium perfringens*, *Cryptosporidium parvum* and *Giardia intestinalis* in a gravel and a sandy soil. *Environ. Sci. Technol.* **2005**, *39*, (20), 7860-7868.
14. Gutierrez, L.; Li, X.; Wang, J.; Nangmenyi, G.; Economy, J.; Kuhlenschmidt, T. B.; Kuhlenschmidt, M. S.; Nguyen, T. H., Adsorption of rotavirus and bacteriophage MS2 using glass fiber coated with hematite nanoparticles. *Water Res.* **2009**, *43*, (20), 5198-5208
15. Zhuang, J.; Jin, Y., Virus retention and transport as influenced by different forms of soil organic matter. *J. Environ. Qual.* **2003**, *32*, (3), 816-823.
16. Yates, M. V.; Gerba, C. P.; Kelley, L. M., Virus presistence in groundwater. *Appl. Environ. Microbiol.* **1985**, *49*, (4), 778-781.
17. Horswell, J.; Hewitt, J.; Prosser, J.; Van Schaik, A.; Croucher, D.; Macdonald, C.; Burford, P.; Susarla, P.; Bickers, P.; Speir, T., Mobility and survival of Salmonella Typhimurium and human adenovirus from spiked sewage sludge applied to soil columns. *J. Appl. Microbiol.* **2009**, *108*, (1), 104-114.
18. Meschke, J. S.; Sobsey, M. D., Comparative reduction of Norwalk virus, poliovirus type 1, F+ RNA coliphage MS2 and *Escherichia coli* in miniature soil columns. *Water Sci. Technol.* **2003**, *47*, (3), 85-90.
19. Davis, J. A.; Farrah, S. R.; Wilkie, A. C., Adsorption of viruses to soil: impact of anaerobic treatment. *Water Sci. Technol.* **2006**, *54*, (3), 161-167.
20. Attinti, R.; Wei, J.; Kniel, K.; Sims, J. T.; Jin, Y., Virus' (MS2, phi X174, and Aichi) Attachment on Sand Measured by Atomic Force Microscopy and Their Transport through Sand Columns. *Environ. Sci. Technol.* **2010**, *44*, (7), 2426-2432.

21. Kretzschmar, R.; Borkovec, M.; Grolimund, D.; Elimelech, M., Mobile subsurface colloids and their role in contaminant transport. *Advances in Agronomy* **1999**, *66*, 121-193.
22. Pham, M.; Mintz, E. A.; Nguyen, T. H., Deposition kinetics of bacteriophage MS2 to natural organic matter: Role of divalent cations. *J. Colloid Interface Sci.* **2009**, *338*, (1), 1-9.
23. Mylon, S. E.; Rinciog, C. I.; Schmidt, N.; Gutierrez, L.; Wong, G. C. L.; Nguyen, T. H., Influence of Salts and Natural Organic Matter on the Stability of Bacteriophage MS2. *Langmuir* **2010**, *26*, (2), 1035-1042.
24. Yuan, B. L.; Pham, M.; Nguyen, T. H., Deposition Kinetics of Bacteriophage MS2 on a Silica Surface Coated with Natural Organic Matter in a Radial Stagnation Point Flow Cell. *Environ. Sci. Technol.* **2008**, *42*, (20), 7628-7633.
25. da Silva, A. K.; Kavanagh, O. V.; Estes, M. K.; Elimelech, M., Adsorption and Aggregation Properties of Norovirus GI and GII Virus-like Particles Demonstrate Differing Responses to Solution Chemistry. *Environ. Sci. Technol.* **2011**, *45*, (2), 520-526.
26. Penrod, S. L.; Olson, T. M.; Grant, S. B., Deposition kinetics of two viruses in packed beds of quartz granular media. *Langmuir* **1996**, *12*, (23), 5576-5587.
27. Dika, C.; Duval, J. F. L.; Ly-Chatain, H. M.; Merlin, C.; Gantzer, C., Impact of Internal RNA on Aggregation and Electrokinetics of Viruses: Comparison between MS2 Phage and Corresponding Virus-Like Particles. *Appl. Environ. Microbiol.* **2011**, *77*, (14), 4939-4948.
28. Duval, J. F. L.; Gaboriaud, F., Progress in electrohydrodynamics of soft microbial particle interphases. *Current Opinion in Colloid & Interface Science* **2010**, *15*, (3), 184-195.
29. Langlet, J.; Gaboriaud, F.; Gantzer, C.; Duval, J. F. L., Impact of chemical and structural anisotropy on the electrophoretic mobility of spherical soft multilayer particles: The case of bacteriophage MS2. *Biophys. J.* **2008**, *94*, (8), 3293-3312.

30. Parashar, U. D.; Gibson, C. J.; Bresee, J. S.; Glass, R. I., Rotavirus and severe childhood diarrhea. *Emerg. Infect. Dis* **2006**, *12*, (2), 304-306.
31. Wyn-Jones, A. P.; Sellwood, J., Enteric viruses in the aquatic environment. *J. Appl. Microbiol.* **2001**, *91*, (6), 945-962.
32. Estes, M. K.; Cohen, J., Rotavirus gene structure and function. *Microbiological Reviews* **1989**, *53*, (4), 410-449.
33. Gerba, C. P.; Rose, J. B.; Haas, C. N.; Crabtree, K. D., Waterborne rotavirus: A risk assessment. *Water Res.* **1996**, *30*, (12), 2929-2940.
34. Rolsma, M. D.; Gelberg, H. B.; Kuhlenschmidt, M. S., Assay for Evaluation of Rotavirus-Cell Interactions - Identification of an Enterocyte Ganglioside Fraction That Mediates Group-a Porcine Rotavirus Recognition. *J. Virol.* **1994**, *68*, (1), 258-268.
35. Liu, Y.; Janjaroen, D.; Kuhlenschmidt, M. S.; Kuhlenschmidt, T. B.; Nguyen, T. H., Deposition of *Cryptosporidium parvum* oocysts on natural organic matter surfaces: Microscopic evidence for secondary minimum deposition in a radial stagnation point flow cell. *Langmuir* **2009**, *25*, (3), 1594-1605.
36. Gutierrez, L.; Mylon, S. E.; Nash, B.; Nguyen, T. H., Deposition and Aggregation Kinetics of Rotavirus in Divalent Cation Solutions. *Environ. Sci. Technol.* **2010**, *44*, (12), 4552-4557.
37. Holthoff, H.; Egelhaaf, S. U.; Borkovec, M.; Schurtenberger, P.; Sticher, H., Coagulation rate measurements of colloidal particles by simultaneous static and dynamic light scattering. *Langmuir* **1996**, *12*, (23), 5541-5549.

38. Chen, K. L.; Mylon, S. E.; Elimelech, M., Aggregation kinetics of alginate-coated hematite nanoparticles in monovalent and divalent electrolytes. *Environ. Sci. Technol.* **2006**, *40*, (5), 1516-1523.
39. Chen, K. L.; Elimelech, M., Aggregation and deposition kinetics of fullerene (C-60) nanoparticles. *Langmuir* **2006**, *22*, (26), 10994-11001.
40. Hierrezuelo, J.; Sadeghpour, A.; Szilagyi, I.; Vaccaro, A.; Borkovec, M., Electrostatic Stabilization of Charged Colloidal Particles with Adsorbed Polyelectrolytes of Opposite Charge. *Langmuir* **2010**, *26*, (19), 15109-15111.
41. Kleimann, J.; Gehin-Delval, C.; Auweter, H.; Borkovec, M., Super-Stoichiometric Charge Neutralization in Particle–Polyelectrolyte Systems. *Langmuir* **2005**, *21*, (8), 3688-3698.
42. Bouyer, F.; Robben, A.; Yu, W. L.; Borkovec, M., Aggregation of Colloidal Particles in the Presence of Oppositely Charged Polyelectrolytes: Effect of Surface Charge Heterogeneities. *Langmuir* **2001**, *17*, (17), 5225-5231.
43. Nguyen, T. H.; Elimelech, M., Adsorption of plasmid DNA to a natural organic matter-coated silica surface: Kinetics, conformation, and reversibility. *Langmuir* **2007**, *23*, (6), 3273-3279.
44. Grolimund, D.; Elimelech, M.; Borkovec, M., Aggregation and deposition kinetics of mobile colloidal particles in natural porous media. *Colloid Surf. A-Physicochem. Eng. Asp.* **2001**, *191*, (1-2), 179-188.
45. Kretzschmar, R.; Barmettler, K.; Grolimund, D.; Yan, Y. D.; Borkovec, M.; Sticher, H., Experimental determination of colloid deposition rates and collision efficiencies in natural porous media. *Water Resour. Res.* **1997**, *33*, (5), 1129-1137.

46. Yan, Y. D.; Borkovec, M.; Sticher, H., Deposition and release of colloidal particles in porous media. In *Trends in Colloid and Interface Science IX*, Appell, J. P. G., Ed. 1995; Vol. 98, pp 132-135.
47. Kuznar, Z. A.; Elimelech, M., Adhesion kinetics of viable *Cryptosporidium parvum* oocysts to quartz surfaces. *Environ. Sci. Technol.* **2004**, *38*, (24), 6839-6845.
48. Walker, S. L.; Redman, J. A.; Elimelech, M., Role of cell surface lipopolysaccharides in *Escherichia coli* K12 adhesion and transport. *Langmuir* **2004**, *20*, (18), 7736-7746.
49. De Kerchove, A. J.; Elimelech, M., Bacterial swimming motility enhances cell deposition and surface coverage. *Environ. Sci. Technol.* **2008**, *42*, (12), 4371-4377.
50. Abbaszadegan, M.; Stewart, P.; LeChevallier, M., A strategy for detection of viruses in groundwater by PCR. *Appl. Environ. Microbiol.* **1999**, *65*, (2), 444-449.
51. Rodriguez, R. A.; Pepper, I. L.; Gerba, C. P., Application of PCR-Based Methods To Assess the Infectivity of Enteric Viruses in Environmental Samples. *Appl. Environ. Microbiol.* **2009**, *75*, (2), 297-307.
52. de Kerchove, A. J.; Elimelech, M., Impact of alginate conditioning film on deposition kinetics of motile and nonmotile *Pseudomonas aeruginosa* strains. *Appl. Environ. Microbiol.* **2007**, *73*, (16), 5227-5234.
53. Saleh, N.; Kim, H. J.; Phenrat, T.; Matyjaszewski, K.; Tilton, R. D.; Lowry, G. V., Ionic strength and composition affect the mobility of surface-modified Fe-0 nanoparticles in water-saturated sand columns. *Environ. Sci. Technol.* **2008**, *42*, (9), 3349-3355.
54. Gaboriaud, F.; Dufrêne, Y. F., Atomic force microscopy of microbial cells: Application to nanomechanical properties, surface forces and molecular recognition forces. *Colloid Surf. B-Biointerfaces* **2007**, *54*, (1), 10-19.

55. Butt, H. J.; Cappella, B.; Kappl, M., Force measurements with the atomic force microscope: Technique, interpretation and applications. *Surf. Sci. Rep.* **2005**, *59*, (1-6), 1-152.
56. Byrd, T. L.; Walz, J. Y., Investigation of the interaction force between *Cryptosporidium parvum* oocysts and solid surfaces. *Langmuir* **2007**, *23*, (14), 7475-7483.
57. Polyakov, P.; Soussen, C.; Duan, J. B.; Duval, J. F. L.; Brie, D.; Francius, G., Automated Force Volume Image Processing for Biological Samples. *PLoS One* **2011**, *6*, (4).
58. Adout, A.; Kang, S.; Asatekin, A.; Mayes, A. M.; Elimelech, M., Ultrafiltration Membranes Incorporating Amphiphilic Comb Copolymer Additives Prevent Irreversible Adhesion of Bacteria. *Environ. Sci. Technol.* **2010**, *44*, (7), 2406-2411.
59. de Kerchove, A. J.; Elimelech, M., Formation of polysaccharide gel layers in the presence of Ca^{2+} and K^{+} ions: Measurements and mechanisms. *Biomacromolecules* **2007**, *8*, (1), 113-121.
60. Michen, B.; Graule, T., Isoelectric points of viruses. *J. Appl. Microbiol.* **2010**, *109*, (2), 388-397.
61. Brady-Estevéz, A. S.; Nguyen, T. H.; Gutierrez, L.; Elimelech, M., Impact of solution chemistry on viral removal by a single-walled carbon nanotube filter. *Water Res.* **2010**, *44*, (13), 3773-3780.
62. Lute, S.; Aranha, H.; Tremblay, D.; Liang, D. H.; Ackermann, H. W.; Chu, B.; Moineau, S.; Brorson, K., Characterization of coliphage PR772 and evaluation of its use for virus filter performance testing. *Appl. Environ. Microbiol.* **2004**, *70*, (8), 4864-4871.
63. Chen, K. L.; Mylon, S. E.; Elimelech, M., Enhanced aggregation of alginate-coated iron oxide (hematite) nanoparticles in the presence of calcium, strontium, and barium cations. *Langmuir* **2007**, *23*, (11), 5920-5928.

64. Chen, K. L.; Elimelech, M., Influence of humic acid on the aggregation kinetics of fullerene (C60) nanoparticles in monovalent and divalent electrolyte solutions. *J. Colloid Interface Sci.* **2007**, *309*, (1), 126-134.
65. Saleh, N. B.; Pfefferle, L. D.; Elimelech, M., Influence of Biomacromolecules and Humic Acid on the Aggregation Kinetics of Single-Walled Carbon Nanotubes. *Environ. Sci. Technol.* **2010**, *44*, (7), 2412-2418.
66. Considine, R. F.; Dixon, D. R.; Drummond, C. J., Oocysts of *Cryptosporidium parvum* and model sand surfaces in aqueous solutions: an atomic force microscope (AFM) study. *Water Res.* **2002**, *36*, (14), 3421-3428.
67. Kang, S.; Elimelech, M., Bioinspired Single Bacterial Cell Force Spectroscopy. *Langmuir* **2009**, *25*, (17), 9656-9659.
68. Kalinichev, A. G.; Iskrenova-Tchoukova, E.; Ahn, W.-Y.; Clark, M. M.; Kirkpatrick, R. J., Effects of Ca²⁺ on supramolecular aggregation of natural organic matter in aqueous solutions: A comparison of molecular modeling approaches. *Geoderma* **2011**, *169*, (0), 27-32.
69. Sutton, R.; Sposito, G., Molecular structure in soil humic substances: The new view. *Environ. Sci. Technol.* **2005**, *39*, (23), 9009-9015.
70. Li, Q.; Elimelech, M., Organic fouling and chemical cleaning of nanofiltration membranes: Measurements and mechanisms. *Environ. Sci. Technol.* **2004**, *38*, (17), 4683-4693.
71. Mi, B. X.; Elimelech, M., Organic fouling of forward osmosis membranes: Fouling reversibility and cleaning without chemical reagents. *J. Membr. Sci.* **2010**, *348*, (1-2), 337-345.
72. Gregory, J., Approximate expressions for retarded van der Waals interaction. *J. Colloid Interface Sci.* **1981**, *83*, (1), 138-145.

73. Hogg, R.; Healy, T.; Fuersten, D., Mutual coagulation of colloidal dispersions. *Trans. Faraday Soc.* **1966**, *62*, 1638-1651.
74. Butt, H. J.; Kappl, M.; Mueller, H.; Raiteri, R.; Meyer, W.; Ruhe, J., Steric forces measured with the atomic force microscope at various temperatures. *Langmuir* **1999**, *15*, (7), 2559-2565.
75. Claesson, P. M.; Poptoshev, E.; Blomberg, E.; Dedinaite, A., Polyelectrolyte-mediated surface interactions. *Adv. Colloid Interface Sci.* **2005**, *114*, 173-187.
76. Romero-Cano, M. S.; Martin-Rodriguez, A.; de las Nieves, F. J., Electrosteric stabilization of polymer colloids with different functionality. *Langmuir* **2001**, *17*, (11), 3505-3511.
77. Byrd, T. L.; Walz, J. Y., Interaction force profiles between *Cryptosporidium parvum* oocysts and silica surfaces. *Environ. Sci. Technol.* **2005**, *39*, (24), 9574-9582.
78. Behrens, S. H.; Borkovec, M.; Schurtenberger, P., Aggregation in Charge-Stabilized Colloidal Suspensions Revisited. *Langmuir* **1998**, *14*, (8), 1951-1954.
79. Behrens, S. H.; Christl, D. I.; Emmerzael, R.; Schurtenberger, P.; Borkovec, M., Charging and aggregation properties of carboxyl latex particles: Experiments versus DLVO theory. *Langmuir* **2000**, *16*, (6), 2566-2575.
80. Curtis, R. A.; Ulrich, J.; Montaser, A.; Prausnitz, J. M.; Blanch, H. W., Protein-protein interactions in concentrated electrolyte solutions: Hofmeister-series effects. *Biotechnol. Bioeng.* **2002**, *79*, (4), 367-380.
81. Hahn, M. W.; Abadzic, D.; O'Melia, C. R., Aquasols: On the Role of Secondary Minima†. *Environ. Sci. Technol.* **2004**, *38*, (22), 5915-5924.

82. Nir, S., Van der Waals interactions between surfaces of biological interest. *Prog. Surf. Sci.* **1977**, 8, (1), 1-58.
83. Edwards, M.; Benjamin, M. M.; Ryan, J. N., Role of organic acidity in sorption of natural organic matter (NOM) to oxide surfaces. *Colloid Surf. A-Physicochem. Eng. Asp.* **1996**, 107, 297-307.
84. Iskrenova-Tchoukova, E.; Kalinichev, A. G.; Kirkpatrick, R. J., Metal Cation Complexation with Natural Organic Matter in Aqueous Solutions: Molecular Dynamics Simulations and Potentials of Mean Force. *Langmuir* **2010**, 26, (20), 15909-15919.
85. Kalinichev, A. G.; Kirkpatrick, R. J., Molecular dynamics simulation of cationic complexation with natural organic matter. *Eur. J. Soil Sci.* **2007**, 58, (4), 909-917.
86. Aoki, S. T.; Settembre, E. C.; Trask, S. D.; Greenberg, H. B.; Harrison, S. C.; Dormitzer, P. R., Structure of Rotavirus Outer-Layer Protein VP7 Bound with a Neutralizing Fab. *Science* **2009**, 324, (5933), 1444-1447.
87. Dormitzer, P. R.; Sun, Z. Y. J.; Wagner, G.; Harrison, S. C., The rhesus rotavirus VP4 sialic acid binding domain has a galectin fold with a novel carbohydrate binding site. *Embo Journal* **2002**, 21, (5), 885-897.
88. Lead, J. R.; Wilkinson, K. J.; Starchev, K.; Canonica, S.; Buffle, J., Determination of diffusion coefficients of humic substances by fluorescence correlation spectroscopy: Role of solution conditions. *Environmental Science & Technology* 2000, 34, (7), 1365-1369.
89. Zolotukhin, S.; Byrne, B. J.; Mason, E.; Zolotukhin, I.; Potter, M.; Chesnut, K.; Summerford, C.; Samulski, R. J.; Muzyczka, N., Recombinant adeno-associated virus purification using novel methods improves infectious titer and yield. *Gene Therapy* 1999, 6, (6), 973-985.

90. Hosokawa, M.; Hama, S.; Mandai, K.; Okuda, K.; Takashima, S.; Tajiri, H.; Eguchi, K.; Heike, Y., Preparation of purified, sterilized, and stable adenovirus vectors using albumin. *Journal of Virological Methods* 2002, 103, (2), 191-199.
91. Wright, J. F.; Le, T.; Prado, J.; Bahr-Davidson, J.; Smith, P. H.; Zhen, Z.; Sommer, J. M.; Pierce, G. F.; Qu, G., Identification of factors that contribute to recombinant AAV2 particle aggregation and methods to prevent its occurrence during vector purification and formulation. *Molecular Therapy* 2005, 12, (1), 171-178.
92. Rolsma, M. D.; Kuhlenschmidt, T. B.; Gelberg, H. B.; Kuhlenschmidt, M. S., Structure and function of a ganglioside receptor for porcine rotavirus. *Journal of Virology* 1998, 72, (11), 9079-9091.
93. Ruiz, M. C.; Charpilienne, A.; Liprandi, F.; Gajardo, R.; Michelangeli, F.; Cohen, J., The concentration of Ca^{2+} that solubilizes outer capsid proteins from rotavirus particles is dependent on the strain. *Journal of Virology* 1996, 70, (8), 4877-4883.

CHAPTER 4

INTERACTIONS BETWEEN ROTAVIRUS AND NATURAL ORGANIC MATTER ISOLATES OF DIFFERENT PHYSICOCHEMICAL CHARACTERISTICS

4.1 *Abstract*

Interactions forces between rotavirus and two well-characterized NOM isolates of different physicochemical properties were studied by atomic force microscopy (AFM) in NaCl solutions and at ambient pH (5.7-5.9). Suwanee River NOM was selected as a model humic NOM (i.e., hydrophobic acid NOM fraction) because of its aromatic structure and high presence of phenolic and carboxylic functional groups. Conversely, Colorado River NOM (CRW) was selected as a model non-humic NOM (i.e., transphilic acid NOM fraction) because of its more aliphatic structure, lower aromatic carbon and phenolic content, and considerable presence of polysaccharide moieties rich in alcohol functional groups. SRNOM showed a higher negative charge than CRW during electrophoretic mobility (EPM) measurements, suggesting a more dominant presence of deprotonated carboxylic groups at the pH of the experiments. Control experiments between mica and SRNOM showed repulsion forces closely following theoretical Debye length during approaching and no adhesion during retraction even at high ionic strength. Conversely, strong attractive forces causing jump-in to contact during approaching (i.e., therefore preventing calculation of decay lengths) were detected between mica and CRW, while high adhesion was recorded during retracting. Interestingly, CRW adhesion to mica decreased with increasing ionic strength. While for SRNOM a repulsive long ranged-electrostatic component was evident, a different mechanism of probable acid-base nature dominated the

interactions between mica and CRW (i.e., occurring between electronegative elements on mica surface and hydroxyl groups on CRW). In another control experiment, interaction force decay length measured between rotavirus and mica significantly deviated from Debye length, suggesting the presence of non-DLVO forces in this system. Similarly, strong repulsion forces between rotavirus and SRNOM were observed during approaching, and their measured decay lengths were very similar to the rotavirus-mica system. This latter result indicates rotavirus, and not SRNOM, as the main contributor to the marked deviation from theoretical Debye length. Furthermore, no adhesion was observed during retraction. Contrariwise, jump-in to contact was observed between CRW and rotavirus during approaching and high adhesion during retraction. Moreover, these adhesion forces decreased with increasing ionic strength. Based on these results, ionic hydrogen bond-based interactions are suggested as the dominant mechanisms between rotavirus and CRW, probably occurring between deprotonated carboxyl groups on rotavirus and hydroxyl functional groups on CRW. Results from this investigation would potentially advance our fundamental understanding and predictive capabilities of the dominant interacting mechanisms between viruses and NOM in specific natural ecosystems as a function of the structural and chemical properties of their surfaces.

4.2 *Introduction*

Natural organic matter (NOM) is a highly heterogeneous mixture of decayed organic compounds ever-present in soils, natural and engineered water systems in a variety of molecular sizes. NOM is considered a major constituent in the carbon cycle and its essential bio/geochemical role in every aquatic environment is undeniable.¹⁻⁴ However, the structural and chemical characteristics of NOM are highly dependent on their origin.⁵⁻⁷ Previous characterization works have shown significant differences (e.g., aromaticity/aliphaticity,

elemental composition, molar ratios, major functional groups, SUVA₂₅₄) between NOM isolates collected from a variety of natural water sources (e.g., South Platte River, Suwannee River, Newport River, Colorado River).⁸⁻¹⁰

For instance, results from previous extensive NOM characterizations indicate that humic substances constitute approximately 50% of dissolved organic matter (DOM, operationally defined as organic matter passing through a 0.45 μm filter) in surface waters.⁴ Furthermore, hydrophobic acid NOM fractions (i.e., humic substances by definition) are characterized by high content of aromatic/phenolic carbon, large C/H, C/O and C/N ratios (low nitrogen content), and carboxyl and phenol as main functional groups.^{4, 8, 11} Conversely, non-humic substances (i.e., frequently microbial/algae-derived NOM) are characterized by high content of nitrogen and aliphatic carbon, and low content of aromatic/phenolic carbon. In addition, polysaccharide moieties (i.e., carbohydrates with considerable content of alcoholic groups) are usually incorporated in transphilic (i.e., intermediate polarity between hydrophobic and hydrophilic NOM) acid NOM fractions, while transphilic neutral NOM fractions contain a considerable proportion of proteins (i.e., in a wide biopolymer distribution) in their structure. Polysaccharides, amides, bases, and alkyl alcohols comprise strongly hydrophilic NOM species.^{8, 12-14}

Indeed, this rigorous and detailed characterization of NOM, as well as their fractions (i.e., relatively well-defined NOM sub-components), has played a central role in understanding NOM interaction with some other ubiquitous components in natural/engineered water systems (e.g., metal-binding/speciation, fate and transport of organic/inorganic pollutants and pathogens, colloidal stability, chlorination by-products, NOM membrane fouling, etc.).^{1, 8, 15-19} Interestingly, the fractionation of complex and heterogeneous NOM into more “homogeneous isolates” has

been a very practical and suitable approach that has assisted in better understanding those interactions.

Similarly, NOM interactions with viruses have been extensively studied in field, column, and batch experiments. For instance, several researchers have concluded that electrostatic forces dominate the interaction between viruses and mineral surfaces; nevertheless, natural organic matter has been widely suggested to hinder the deposition of viruses to mineral surfaces due to competition for adsorption sites.²⁰⁻²⁵ Conversely, other studies have proposed hydrophobicity to promote the interaction between viruses and NOM.^{26, 27} Recently, steric interactions arising due to the complex polymeric properties of NOM, have been also suggested to mediate between SRNOM and rotavirus or MS2 bacteriophage.^{17, 28} However, most of these studies have also reported different interacting behaviors in the presence of monovalent or divalent cations in solution.^{17, 29} This latter result indicates the importance of specific interactions probably occurring between divalent cations and deprotonated carboxylic groups on both NOM and viruses as also suggested elsewhere.^{30, 31} In addition, other investigation have shown that SRNOM or fulvic acid in solution have produced more negative zeta potentials on viruses, indicating some complexation degree between NOM and moieties on the outermost capsids of viruses.^{17, 32} From these studies it has been clearly observed that, along with solution chemistry, the interactions between NOM and viruses were highly dependent on the characteristics of NOM and viruses. However, to the best of our knowledge, there has been no research regarding direct measurement of intermolecular forces to elucidate the very specific dominant interacting mechanisms as a function (i.e., direct correlation) of physicochemical characteristics of NOM and outermost capsid of viruses.

Therefore, the main focus of this investigation was to study the interactions arising between viruses and two well-characterized NOM isolates of different physicochemical properties by atomic force microscopy (AFM). Suwanee River NOM was selected as a model humic NOM (also known as hydrophobic fraction) because of its weak anionic polyelectrolyte properties caused by the high presence of phenolic and carboxylic functional groups in its structure.^{33, 34} Conversely, Colorado River NOM was selected as a model non-humic NOM because of its lower aromatic and phenolic carbon content and presence of polysaccharide moieties and alcohol functional groups.^{10, 35} Rotavirus was selected as the model virus because it is the most common enteric virus causing severe gastrointestinal and acute dehydration among children worldwide and has been detected in almost every water environment.³⁶⁻⁴¹ Due to its sensitivity and non-destructive nature, atomic force microscopy was used in this investigation as a suitable tool to measure interaction forces at the sub-nano Newton resolution at different solution chemistries. The desired result from this investigation was to advance our fundamental understanding and predictive capabilities of the dominant interacting mechanisms between viruses and NOM as a function of the structural and chemical properties of NOM in specific natural ecosystems.

4.3 *Materials and Methods*

Solution chemistries and preparation of natural organic matter isolates. All the electrolyte solutions, natural organic matter and rotavirus stocks used in this investigation were prepared with ultrapure doubled-deionized water (DDI, 18 M Ω -cm resistivity, Millipore, USA) and analytical grade reagents. HEPES buffer was prepared with 10 mM N-(2-hydroxyethyl)piperazine-N'-2-ethanesulfonic acid and 100 mM NaCl at ambient pH (5-7-5.9), while PLL hydrobromide solution was prepared in HEPES buffer at a final concentration of 0.1

g/L. Before use, HEPES buffer and all the electrolyte solutions (with the exception of PLL hydrobromide solution) were sonicated, and subsequently filtered through a 0.22 μm cellulose acetate sterile membrane. Colorado River NOM (CRW) and Suwannee River NOM (SRNOM) were used as model dissolved organic matter isolates. SRNOM was obtained from International Humic Substances (IHSS, St. Paul, MN) while CRW was collected from the Colorado River in California LA Verne and isolated following the procedure described elsewhere.⁴² NOM stock solutions were prepared by dissolving every NOM isolate in a 1 mM NaHCO_3 solution to a final concentration of approximately 200 mg C/L, stirred overnight in the dark, and finally filtered through a 0.45 μm cellulose acetate sterile membrane.⁴³ NOM stocks were aliquoted, covered in aluminum foil, and stored at 4°C. A TOC-V CPH total organic carbon analyzer (Shimadzu, Japan) was used to measure total dissolved organic carbon (DOC) concentration of the NOM stocks.

Preparation of self-assembled monolayers (SAM) onto gold substrate and contact angle measurement. Self-assembled monolayers of 11-mercapto 1-undecanol and 11-mercaptopundecanoic acid were prepared on gold substrates following the next protocol.⁴⁴ Gold substrates mounted on glass slides were obtained from Asylum Research, USA (Cat. # 900.248). Prior to use, gold substrates were cleaned in piranha solutions (70% sulfuric acid, 30% hydrogen peroxide) for 3 minutes, rinse with DDI water, and finally dried with ultrapure N_2 gas. Solutions of 5 mM 11-mercapto 1-undecanol or 11-mercaptopundecanoic acid (Sigma Aldrich, USA) were prepared in ethanol. Approximately 200 μL of the 11-mercapto 1-undecanol or 11-mercaptopundecanoic acid solution was pipetted on top of the gold substrate and allowed to coat for 16 hours. Parafilm was used to prevent evaporation of the solution during coating. The solution was removed and the SAM substrate was carefully rinsed with ethanol and then DDI

water. The SAM substrate was immediately used for AFM experiments right after preparation. A second set of SAM substrates was prepared in parallel for contact angle measurements. Contact angles of 11-mercapto 1-undecanol SAM and 11-mercaptoundecanoic acid SAM were measured using a goniometer (KSV Instrument, CAM 200) by static sessile drop technique with water as a probe liquid. After 4 μ L of DDI water was dropped onto each surface, left and right contact angles were measured at least 10 times. The average contact angle was calculated for each side. The highest and lowest values were discarded.

Rotavirus stock production and purification, and infectivity assay. Replication of group A porcine OSU rotavirus (ATCC VR892) was performed in embryonic African green monkey kidney cells (MA-104) in the presence of trypsin as previously described.⁴⁵ Concentration and purification of rotavirus stock was conducted by centrifugation, filtration, and dialysis in a 1 mM NaCl and 0.1 mM CaCl₂ solution following the protocols described elsewhere.^{17, 46} The viral stock solution was aliquoted and stored at 4°C in the dark. Calcium concentration in the rotavirus stock was kept above the critical free calcium concentration to prevent solubilization of VP7 and VP4 proteins.⁴⁷ Rotavirus stock concentration was measured as $\sim 9 \times 10^6$ FFU/ml using focus forming unit (FFU) infectivity assay.⁴⁵ No aggregation (i.e., change in hydrodynamic diameter measured by dynamic light scattering technique) or significant variation in infectivity was detected in the rotavirus stock throughout the development of this study.

Measurement of electrophoretic mobility (EPM) for NOM isolates. EPM of bare silica particles (1.6 μ m in diameter, Polysciences, USA), PLL-coated silica particles, and SRNOM-coated or CRW-coated silica particles (i.e., used as surrogates for NOM-coated silica surfaces) was measured using a ZS90 Zetasizer equipment (Malvern, UK) under a wide range of

salt concentrations (1, 3, 10, 30, and 100 mM NaCl) and at ambient pH. A minimum of three measurements were performed for each electrolyte condition (i.e., data sets obtained were pooled and the mean results and standard deviations were presented) using clear disposable cells (Malvern, UK). NOM coating of the silica particles were conducted following the layer-by-layer protocol described elsewhere.¹⁶ Briefly, silica particles were rinsed in DDI water for 24 hours and separated by centrifugation (5000 RPM). PLL-coated silica particles were prepared by dispersing previously-cleaned silica particles in 1 mL of PLL hydrobromide solution for 24 hours. The PLL-coated silica particles were separated from the PLL hydrobromide solution by centrifugation (5000 RPM). The supernatant was removed and the PLL-coated silica particles were re-suspended in 1 mM NaCl solution for rinsing purposes. The PLL-coated silica particles were separated from the 1 mM NaCl rinsing solution by centrifugation (5000 RPM). The supernatant was removed and the PLL-coated silica particles were re-suspended in 1 mL of SRNOM or CRW solution at a final concentration of 50 mg C/L for 24 hours. The NOM-coated silica particles were separated from the NOM solution by centrifugation and re-suspended in 1 mM NaCl solution for rinsing purposes. Finally, the NOM-coated silica particles were separated from the 1 mM NaCl rinsing solution by centrifugation and re-suspended in 1 mM NaCl solution.

Interaction force measurement and data processing. A MFP-3D atomic force microscope (Asylum Research, USA) was used to measure interaction forces between rotavirus-coated silica probe and SRNOM-coated silica surface or CRW-coated silica surfaces. In addition, to elucidate the specific dominant interacting mechanisms between rotavirus and NOM isolates, interaction forces between rotavirus-coated probe and silica surface or mica surface; and between mica surface and SRNOM-coated probe or CRW-coated probe were also measured. Mica

surface was used as a control surface due to its molecularly-smoothed surface. A 1 μm silica sphere glued on a silicon nitride tip-less cantilever of a spring constant of ~ 0.06 N/m (Novascan Technologies, USA) was used as an AFM probe. Spherical colloidal probes have been widely used in interaction force studies.⁴⁸ The rotavirus and NOM coating protocol of the AFM probe, as well as the NOM coating protocol of the silica surfaces using PLL as an intermediate layer followed the layer-by-layer procedure described elsewhere^{16, 17} and were detailed in the next section. Similarly, control experiments for testing the NOM coating completeness of the silica surface were conducted and detailed in the next section.

Thermal tuning method was used to measure the spring constant of the cantilevers before every experiment, where deflection (V) was converted to force (nN) in accordance to Hooke's law.⁴⁹ Approaching and retracting force profiles were recorded at a 500 nm/s rate (i.e., rate consistent with previous studies)^{50, 51} using AR-MFP-3D v.101010 software (Asylum Research, USA). At least 25 force profile curves were recorded for every electrolyte condition at different locations of the surface of analysis. Force profiles with scatter larger than ± 0.05 nN in force were discarded.

During approaching, some interaction force profiles followed an exponential decay and were described by the following equation: $F = F_0 \exp(-\kappa h)$, where h is the separation distance, F is the interaction force, F_0 is a pre-exponential constant defined as force at contact in this study, and κ^{-1} is the interaction force decay length.^{48, 52} The value of κ^{-1} was calculated as the inverse of the slope of the linear region of a force profile as a function of separation distance in a semi-natural logarithm plot. The interaction force decay lengths of the next systems: a) SRNOM-mica, b) CRW-mica, c) rotavirus-mica, d) rotavirus-silica, e) rotavirus-SRNOM, f) rotavirus-CRW, g) rotavirus-11-mercapto 1-undecanol SAM, and h) rotavirus-11-mercaptoundecanoic acid SAM

were calculated for every solution condition and plotted as a function of ionic strength.^{53, 54} Experimental conditions a) and b), were conducted to elucidate the dominant interactions between the very hydrophilic/electronegative mica and the two NOM isolates of different physicochemical characteristics, while conditions c) and d), were conducted as control experiments¹⁷ for assessing the contribution of rotavirus to the overall interaction between rotavirus and SRNOM or CRW. Finally, conditions g) and h), were also performed as control experiments to measure the interacting forces between rotavirus and hydroxyl group-SAM or deprotonated carboxyl group-SAM (i.e., mimicking major functional groups on CRW and SRNOM, respectively).

Because of possible complex adhesion behavior due to the heterogeneous nature of NOM isolates, retracting force profiles were individually analyzed in terms of maximum adhesion force, maximum adhesion distance, and adhesion energy as described by previous studies.^{55, 56} For instance, maximum adhesion forces were determined based on the maximum force measured before total detachment of the rotavirus-coated probe from the NOM-coated surface. The adhesion distance was calculated as the maximum separation distance between the rotavirus-coated colloidal probe and NOM-coated surface during retraction, where the interaction ceases. Adhesion energies were directly calculated by integrating the pull-off forces by the separation distance using the trapezoidal rule.^{50, 55, 57} In addition, adhesion forces were further normalized by the silica probe radius as described in previous studies.⁴⁸ The probability of occurrence of adhesion distances, adhesion forces, and adhesion energies determined from the retracting force curves were described by Log-normal density function. The minimum detectable adhesion force included in this analysis was defined as 0.05 nN. Adhesion forces of lower magnitude were

taken into account for discussion but not quantified. The Log-normal distribution, mean, and variance, were determined from the measured adhesion forces.

Surfaces and probe preparation for Atomic Force Microscopy experiments. Silica surfaces were cleaned following the procedure previously described.¹⁷ Briefly, silica surfaces of approximately 0.7 cm² in area were first immersed in 2% hellmanex (Hellma Analytics, USA) solution for 30 minutes and subsequently rinsed in excess in DDI water. Then, 400 µL of 98% sulfuric acid with 30 g/L nochromix solution were pipetted on top of the silica surfaces and removed after 24 hours of exposure. The silica surfaces were then rinsed in excess in DDI water, dried with ultrapure N₂, and finally oxidized in an ozone/UV chamber for 30 minutes (BioForce Nano-sciences Inc., Ames, IA). The procedure for NOM-coating of silica surfaces was conducted following the layer-by-layer protocol.^{16, 17} First, 400 µL of PLL hydrobromide solution was pipetted on top of the silica surface and left undisturbed for 24 hours. The PLL hydrobromide solution was then removed and the PLL-coated silica surface was rinse with DDI water. Subsequently, 400 µL of approximately 200 mg C/L SRNOM or CRW solution was pipetted on top of the PLL-coated surface and left undisturbed for 24 hours. After the NOM solution was removed; the NOM-coated silica surface was rinsed with DDI water and immediately used in AFM experiments. Rotavirus-coated and CRW-coated and SRNOM-coated silica colloidal AFM probe were similarly prepared following the layer-by-layer procedure.^{16, 17} Briefly, a silica colloidal AFM probe was carefully immersed in 400 µL of PLL hydrobromide solution and allowed to coat for 24 hours. The PLL-coated silica colloidal probe was then removed from the PLL hydrobromide solution and rinsed in DDI water. Subsequently, the PLL-coated probe was immersed in 400 µL of $\sim 9 \times 10^6$ FFU/mL rotavirus solution or 400 µL of 50 mg C/L SRNOM solution or 400 µL of 50 mg C/L CRW solution and allowed to coat for 24 hours.

Finally, the probe was removed from the viral or NOM solution, rinsed in DDI water, and immediately used in AFM experiments. Moreover, the next set of experiments was conducted for testing the NOM-coating completeness of silica surfaces as described elsewhere.¹⁷ A silicon nitride (SiNi) AFM tip of 20 nm tip radius (0.24 N/m, NP series, Bruker, USA) was tested with the next surfaces: a) silica surface (0.7 cm²); b) PLL-coated silica surface; c) SRNOM-coated or CRW-coated silica surface. A minimum of 25 forces profile curves were recorded at different locations of the three tested surfaces in a 1 mM NaHCO₃ solution at a buffered pH of 8.3 and at ambient temperature.

4.4 Results and Discussion

Origin and characteristics of the NOM isolates. Both NOM isolates were originally obtained from surface waters of different characteristics and have been extensively studied in previous investigations.^{10, 34, 35, 58} Suwannee River has been described as black water with high humic content and high specific ultraviolet absorbance (SUVA). SRNOM has shown a high aromatic and phenolic carbon content with a predominance of tanning and lignin-derived fulvic acid structures where carboxyl group has been identified as a major functional group.³⁴ Colorado River has been described as non-humic water with low SUVA. Compared to SRNOM, this lower SUVA value indicates the more aliphatic character of CRW. There is a predominance of fulvic acid structures in CRW. Unlike SRNOM, these structures were originally derived from terpenoids (i.e., suggested as algal and bacterial-derived), where carboxyl groups are found distributed across aliphatic ring structures. The content of aromatic and phenolic carbon in CRW was low while methyl group content was found higher. Conversely, CRW was enriched in polysaccharide moieties and alcoholic functional groups.^{10, 35}

Electrophoretic mobility (EPM) analysis for NOM isolates. The EPM of silica particles

was negatively charged at the whole range of ionic strength tested (Figure 4.1), and became less negatively charged with increasing salt in solution (from -2.34 ± 0.26 to $-0.33 \pm 0.16 \mu\text{mcmV}^{-1}\text{s}^{-1}$ at 1 mM NaCl and 100 mM NaCl, respectively). As reported in previous investigations,¹⁶ PLL reversed the charge of silica particles. Similarly to silica, the charge of PLL-coated silica particles became less charged with increasing ionic strength (from 4.45 ± 0.14 to $2.20 \pm 0.11 \mu\text{mcmV}^{-1}\text{s}^{-1}$ at 1 mM NaCl and 100 mM NaCl, respectively). SRNOM or CRW adsorbed on PLL-coated silica particles caused another charge reversal. The mobility of both isolates was negative at the whole range tested and also decreased with increasing ionic strength (from -2.75 ± 0.30 at 1 mM NaCl to $-0.68 \pm 0.06 \mu\text{mcmV}^{-1}\text{s}^{-1}$ at 100 mM NaCl for SRNOM, and from -1.66 ± 0.14 at 1 mM NaCl to $-0.51 \pm 0.25 \mu\text{mcmV}^{-1}\text{s}^{-1}$ at 100 mM NaCl for CRW) as previously observed for other charged-colloids.^{46, 59, 60} This decrease in EPM was suggested to be caused due to compression of diffuse double layer associated with increased concentration of Na^+ ions in solution. Na^+ ions have been suggested to only weakly interact with NOM molecules via outer-sphere association.³¹ The different magnitudes of EPM obtained for both isolates were an indicative of their dissimilar surface characteristics. At the pH of the experiments, the charge displayed by both isolates would be a product of ionized carboxylate groups as a dominant acidic functional group as suggested elsewhere.³¹ However, the higher EPM exhibited by SRNOM would be the result of a larger presence of deprotonated carboxylate groups on its structure. Finally, the EPM of both isolates did not seem to reach a finite lower limit associated with limited charge screening at high salt concentration in solution as observed in previous studies.^{46,}

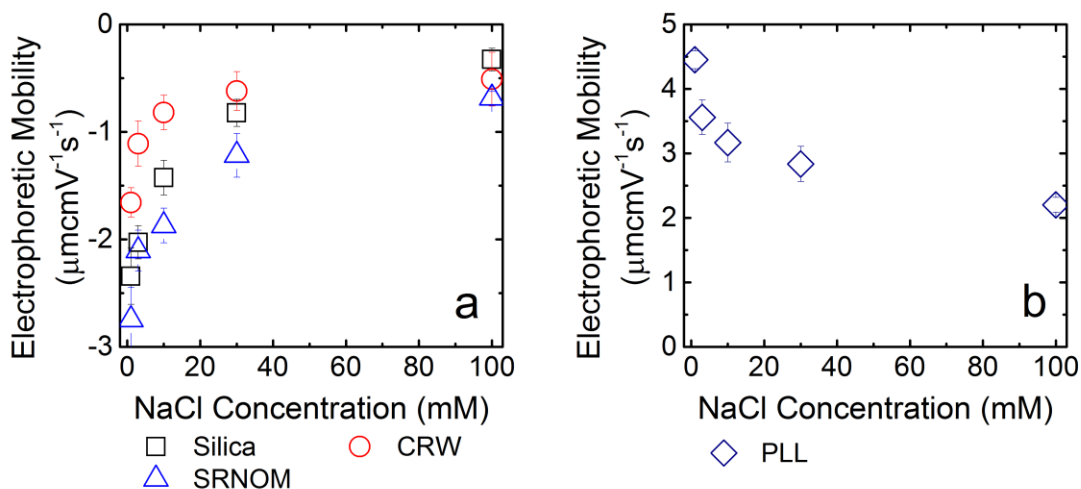


Figure 4.1 EPM of a) bared silica particles (1.6 μm), CRW-coated silica particles, SRNOM-coated silica particles, and b) PLL-coated silica particles as a function of ionic strength (ambient pH, 25°C). The different EPM magnitudes obtained for SRNOM and CRW were an indicative of their dissimilar surface characteristics.

NOM coating-completeness of silica surfaces. Control experiments were first conducted to assess NOM coating-completeness of the silica surfaces following protocols previously detailed.¹⁷ Repulsion forces were initially detected between the SiNi tip and silica surface during approach in 1 mM NaHCO_3 solution, indicating electrostatic repulsion originated by the negative charge of the tip and the silica surface at the pH of the experiment (8.3). Interaction force decay lengths calculated based on the approaching curves (i.e., 9.1 nm) closely followed theoretical Debye length at 1 mM ionic strength (i.e., 9.6 nm), suggesting DLVO forces as the exclusively interacting forces in this system as previously observed.⁵³ Conversely, attractive forces during approach and high adhesion during retraction were recorded between the negatively-charged SiNi tip and positively-charged PLL-coated silica surface, indicating that the silica surface was efficiently coated by PLL relative to the length-scale of the radius of curvature of the SiNi tip. Finally, repulsive forces were detected between SiNi tip and SRNOM-coated silica surfaces, indicating successful modification of the PLL-coated silica surface by the

adsorbed NOM isolate relative to the radius of curvature of the SiNi tip.

Interactions between mica surface and SRNOM-coated or CRW-coated silica colloidal probes. As described in the previous section, interaction force measurements between mica surface and SRNOM-coated or CRW-coated silica colloidal probes were first conducted to elucidate the dominant interaction mechanisms between the very hydrophilic/electronegative mica and the two NOM isolates of different physicochemical characteristics.

Approaching curves showed significantly different interacting behaviors between mica and the two isolates (Fig 4.2). Repulsion forces following an exponential decay were recorded between SRNOM and mica at 1, 10, and 100 mM NaCl solutions and at pH 5.7, and decreased with increasing ionic strength. Calculated interaction force decay lengths (8.21 ± 0.79 , 3.59 ± 0.46 , and 1.53 ± 0.53 nm at 1, 10, and 100 mM NaCl, respectively, $n=15$ per solution condition) closely followed theoretical Debye Length (9.61, 3.04, and 0.96 nm at 1, 10, and 100 mM NaCl, Figure 4.3), suggesting the solely influence of DLVO forces in this system. Ionized carboxyl groups (i.e., major functional group in SRNOM and humics/hydrophobic acid fractions in general) would be the main contributor to the negative charge of SRNOM at the pH of our experiments.³⁴ On the other hand, the high negative charge displayed by mica is attributed to sites of permanent and variable charge in solution.^{62, 63} The permanent charges are ascribed to isomorphic substitution in the crystal structure, while the variable (pH dependent) charge sites to aluminol and silanol functional groups. Interestingly, previous studies have shown that permanent charges contribute to more than 90% of the total surface charge of mica at neutral pH.⁶⁴ Therefore, strong electrostatic forces arising between ionized carboxylic groups on SRNOM and highly negatively charged mica would be a major contributor to the repulsive forces displayed at all ionic strength tested. In addition, the decrease in the negative charge on SRNOM with

increasing ionic strength (Figure 4.1) due to counter-ion charge screening would play a significant role in the decrease of repulsive forces.^{65, 66} However, in addition to strong electrostatics, other studies have suggested the presence of steric repulsive forces as another important mechanism during NOM interaction with surfaces. Depending on the NOM fraction and solution chemistry (e.g. pH or type and concentration of cations), adsorbed NOM has been long proposed to facilitate the stability and transport of colloids in natural water environments.^{5, 67, 68} Specifically, humic substances (e.g., SRNOM and its fractions) have been widely recognized for both steric and electrostatic stabilization in the presence of monovalent salts (i.e., not the case for multivalent cations), presumably because of its complex polymeric chains and ionized functional groups, respectively.^{5, 69-71} Indeed, previous studies have directly measured steric repulsive forces of surface-grafted polymers (polyethylene glycol, PEG).⁷² The steric interactions identified between PEG and a sharp tip produced long ranged-repulsive forces closely following exponential decays. In addition, conformational changes of the polymeric brush (i.e., compression/extension) due to solution conditions (poor or good solvents) were clearly observed.

Conversely, repulsive forces were not only absent between CRW-coated silica colloidal probe and mica, but jump-in to contact (i.e., unstable region where strong attractive forces cause considerable bending stresses to the cantilever, consequently exceeding its spring constant)⁴⁸ were recorded at every force profile and prevented the calculation of interaction force decay length. However, the magnitude of the jump-in to contact decreased with increasing ionic strength (i.e., 1.29 ± 0.04 , 0.69 ± 0.11 , and 0.41 ± 0.09 mN/m at 1, 10, and 100 mM NaCl solution, respectively, $n=15$ per solution condition), suggesting that this interacting mechanism is negatively influenced by the increase of ions in solution. These attractive forces were not

electrostatic in nature due to the negative charge of both mica and CRW (Figure 4.1), therefore an attractive acid-base component successfully overruling electrostatic repulsion would be involved in this system. These interactions could be explained by the characteristics of CRW isolate as follows. CRW can be defined as a transphilic acid NOM fraction (i.e., non-humic NOM with a considerable aliphatic character and intermediate hydrophilicity), where carboxyl groups play a major role in imparting a negative charge to the isolate and polysaccharide moieties, rich in alcohol groups, are incorporated in the structure of the NOM molecules. The jump-in to contact observed between mica and CRW would be caused by strong ionic hydrogen bonds between hydroxyl groups, present in abundance on CRW structure, and the very electronegative elements on the surface of mica at very short distances (i.e., ionic hydrogen bonds have been suggested as significantly stronger than neutral hydrogen bonds).^{73, 74} In addition, it has been previously suggested that hydrogen bonds in excess can overrule electrostatic repulsion forces.⁷⁵ In conclusion, two different interacting mechanisms were observed, during both approaching and retracting regimes, between mica and two NOM isolates of dissimilar physicochemical characteristics. For instance, high repulsion forces between SRNOM and mica during approach and lack of adhesion clearly differed from the strong attractive forces displayed between CRW and mica during approach and high adhesion during retraction. The aromatic/phenolic SRNOM with a high content of carboxyl groups (i.e., hydrophobic acid fraction/humic) markedly contrasted in characteristics with the less charged but more aliphatic in nature CRW (i.e., transphilic acid NOM with polysaccharides on its structure). Therefore, considering that mica was used as a control surface (i.e., very hydrophilic molecularly smooth phyllosilicate), it is reasonable to suggest that the characteristics of both isolates played a fundamental role in these dissimilar behaviors.

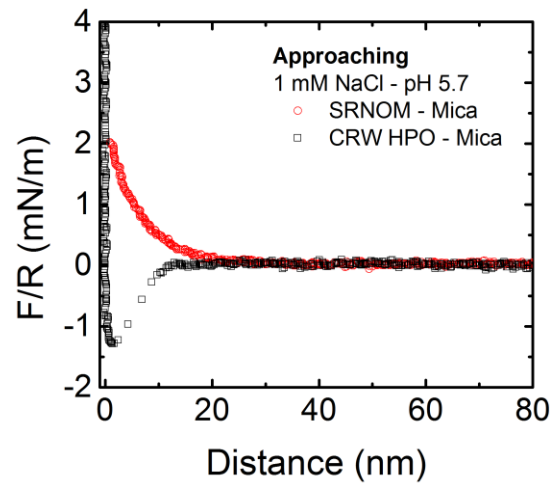


Figure 4.2 Approaching curves between mica surface and SRNOM-coated or CRW-coated silica colloidal probe (pH 5.7, 25°C). Significantly different force profiles were generated, indicating different dominant interacting mechanism arising due to the dissimilar surface characteristics of the two isolates.

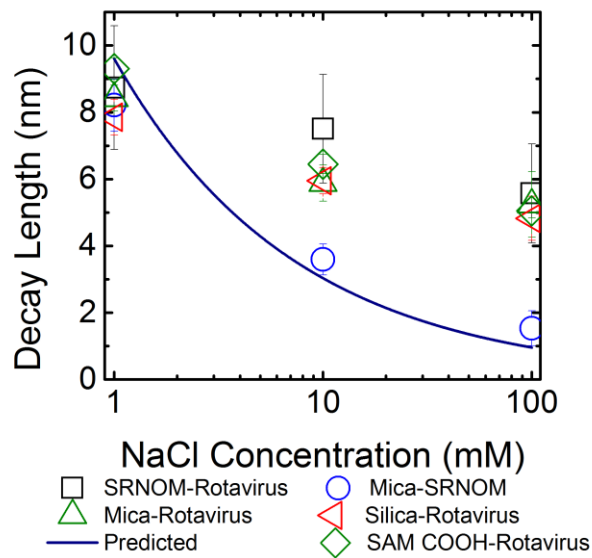


Figure 4.3 Interaction force decay length determined between rotavirus-coated silica colloidal probe and mica surface or silica surface or SRNOM-coated silica surface or SAM-COOH, and between mica surface and SRNOM-coated silica colloidal probe. Interaction force decay lengths between SRNOM and mica closely follow classic DLVO theory. Conversely, when rotavirus is present in the system, interaction force decay lengths suggest the presence of non-DLVO forces.

Interaction forces between rotavirus-coated silica colloidal probe and mica or silica surface during approaching. Interaction forces between rotavirus and mica or silica surface (i.e., selected as model hard surfaces) were first measured as a control experiment for assessing the contribution of rotavirus to the overall interaction between rotavirus and SRNOM or CRW.

The calculated interaction force decay lengths between rotavirus and mica or silica (fig. 4.3) showed no significant statistical difference (two-tailed t-test, $p=0.05$) at all the ionic strength tested (1, 10, and 100 mM NaCl, $n=20$ per solution condition). Although at 1 mM NaCl solution these decay lengths closely followed predicted Debye length (i.e., 8.42 ± 0.39 nm and 7.85 ± 0.54 nm for mica and silica surfaces, respectively, versus 9.6 nm for classic DLVO), a significant deviation was measured at 10 mM (i.e., 5.88 ± 0.54 nm and 5.95 ± 0.40 nm for mica and silica surfaces, respectively, versus 3.0 nm for classic DLVO) and 100 mM (i.e., 5.24 ± 0.98 nm and 4.82 ± 0.66 nm for mica and silica surfaces, respectively, versus 0.96 nm for classic DLVO) NaCl solutions. Similar interaction force decay length deviating from Debye length between rotavirus-coated AFM colloidal probe and silica surface has been reported previously.¹⁷ This deviation from theoretical Debye length, clearly originating from rotavirus, indicates little ionic strength dependence and the presence of an additional force interacting in this system besides classical DLVO forces (i.e., classic DLVO theory considers only Lifshitz-van der Waals forces and electrostatic double-layer interaction for perfectly smooth surfaces).^{76, 77} In an ideal DLVO system, increasing ionic strength is expected to compress the double layer, leading the interaction decay length to follow theoretical Debye length. In a previous study, three possible factors, or a combination of them, were suggested to cause this behavior on rotavirus particles: a) low Hamaker constant of viruses resulting in weak van der Waals forces, b) strong hydration forces, and c) steric interactions similarly observed in bacteria or oocysts.^{17, 24, 53, 78-81} However,

in order to understand rotavirus interactions with other surfaces, the dominant interacting mechanisms as a function of capsid characteristics and solution chemistry have to first be elucidated.

Rotavirus has been characterized as a non-enveloped (i.e., lacking a lipid bilayer membrane) enteric virus that infects both animals and man, comprising of three protein layers protecting its double stranded-RNA genome. The outer most protein layer consists of an outer glycoprotein capsid (VP7) with spike (nonglycosylated) proteins VP4 protruding from the core.^{37, 82} Intestinal trypsin causes proteolytic cleavage of VP4 into VP5 and terminal fragment VP8, the latter suggested as responsible of mediating attachment to cells and target of neutralizing antibodies.⁸³ The structure the outer most capsids of rotavirus and its fragments has been extensively studied at a high resolution (Å-level) and refined by multiple cycles of simulated annealing, energy minimization, and individual B-factor refinement.⁸³⁻⁸⁵ Recently, Aoki et. al, (2006) generated a surface representation in terms of electrostatic potential of a) the sialic acid-independent rotavirus (strain DS-1) VP8 core, and b) the sialic acid-binding VP8 core from simian (strain RRV) rotavirus (i.e., similar surface representations have been also generated for VP5 and VP7).^{82, 84, 85} The location of positive and negative charges was not homogeneously distributed on the surface of these viral proteins and, interestingly, these locations slightly differed in both DS-1 and RRV VP8 cores (i.e., however, these terminal fragments have been described as not hydrophobic at all). These results give us an insight of a) the heterogeneous charge distribution on the outer most capsids of rotavirus, and most importantly, b) the variability of these charges among different rotavirus strains. The latter statement is supported by studies of the variability of residues at specific locations of proteins between different rotavirus strains.^{83, 85} In addition, the amino acid sequence of the outer most capsids shows charged

moieties, hydrophobic, and hydrophilic neutral residues heterogeneously distributed all over the viral proteins.^{76, 78, 79} However, the location, accessibility (i.e., which is a direct result of protein conformation as a function of solution chemistry), and type/number of residues would play a fundamental role during the interaction with other surfaces (i.e., mica, silica), and of course colloids in solution, such as natural organic matter.

Interaction forces between rotavirus and SRNOM-coated silica surface. During approaching, repulsive forces following an exponential decay were solely recorded between rotavirus and SRNOM during the entire ionic strength range tested (i.e., 1, 10, and 100 mM NaCl solutions). Similarly to rotavirus and mica or silica, the interaction force decay length calculated between rotavirus and SRNOM-coated silica surfaces (Fig. 4.3) showed a considerable deviation from predicted Debye length at 10 and 100 mM NaCl solutions (i.e., 7.51 ± 1.63 nm and 5.57 ± 1.48 nm, respectively, $n=25$ for every solution condition), although it closely followed theoretical Debye length at 1 mM NaCl solutions (i.e., 8.74 ± 1.85 nm). There was no significant statistical difference (two-tailed t-test, $p < 0.05$) between rotavirus and silica or mica or SRNOM at 1 and 100 mM NaCl solutions, but at 10 mM NaCl solution. Considering the interaction decay lengths previously calculated for mica-SRNOM and mica-rotavirus systems (Fig. 4.3), it would be logical to suggest that the high deviation from theoretical Debye length for the rotavirus-SRNOM system was clearly originated from rotavirus and not from SRNOM. On the other hand, no adhesion forces between rotavirus and SRNOM were recorded during retraction even at high ionic strength (e.g., 100 mM NaCl solution) and the force versus distance profiles closely mirrored approaching force curves, as similarly reported elsewhere.¹⁷ Therefore, the strong repulsive forces observed during approaching and the absence of adhesion forces during retraction between SRNOM and rotavirus even at high salt concentration in solution, suggest that

the dominant interacting mechanisms are slightly sensitive to ionic strength. However, a deeper analysis regarding the high rejection exhibited between rotavirus and SRNOM and its correlation to their surface characteristics will be carried out in the next sections.

Interaction forces between rotavirus and CRW-coated silica surface. The interaction forces between rotavirus and CRW were significantly different from that exhibited between rotavirus and SRNOM. Similarly to CRW-mica interactions, at every ionic strength tested (e.g., 1, 10, and 100 mM NaCl solutions) not only repulsive forces were absent during approaching, but jump-in to contact were recorded in every generated curve (Figure 4.4a). As described in previous sections, jump-in instabilities are generated due to the gradient of strong attractive forces overcoming the spring constant of the cantilever. However, following this jump-in to contact, the presence of a non-linear region typically observed due to the compression of deformable materials was detected (i.e., probably originated from rotavirus/CRW system, and referenced in the literature as deformable materials with surface forces).⁴⁸ Due to the number of curves produced (n=20 at every solution condition) and a slight variability in the magnitudes of the interacting forces between CRW and rotavirus (i.e., measured from the end of the jump-in to contact to the end of the detected polymeric-like barrier), probability density functions were generated and fitted using Log-Normal distributions (Fig. 4.4b-d). The interacting forces decreased from a mean (μ) of 2.89 nN (variance: 0.30, R^2 : 0.75) at 1 mM NaCl solutions, to a μ of 1.48 nN (variance: 0.31, R^2 : 0.88) at 10 mM NaCl solutions. This decrease (more drastically observed during the jump-in to contact) suggests that the dominant mechanism is inversely affected by ionic strength. Nevertheless, the interacting forces at 100 mM NaCl were similar in magnitude to those at 10 mM NaCl (μ : 1.32 nN, variance: 0.30, R^2 : 0.94), indicating that the

dominant interacting mechanism has not experience a significant change during this increase in ionic strength.

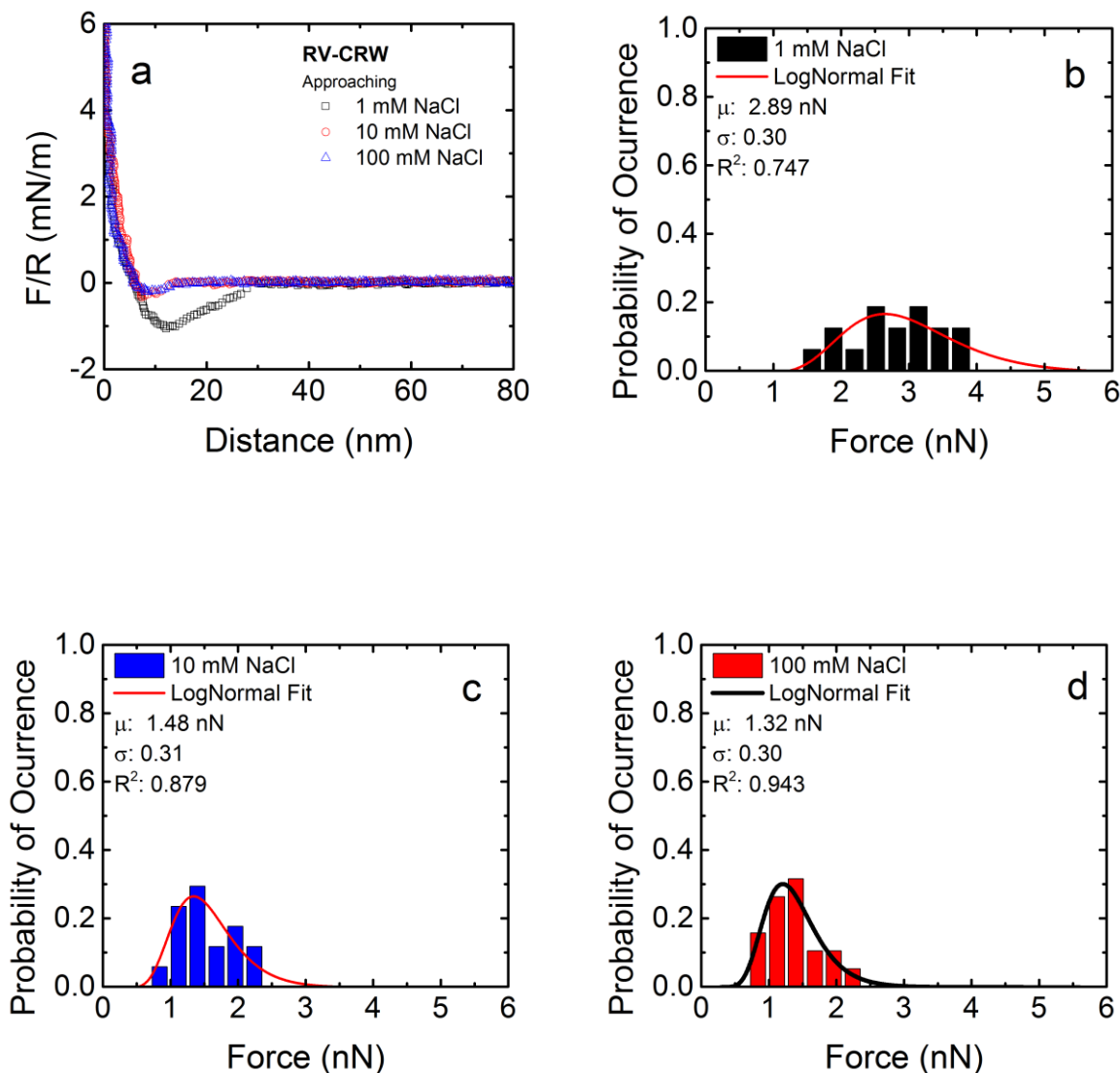


Figure 4.4 a) Model approaching curves between rotavirus-coated silica colloidal probe and CRW-coated silica surface measured at 1, 10, and 100 mM NaCl solutions and at pH 5.7 and 25°C. Jump-in to contact was present at every generated curve. Probability density functions (Log-Normal fit) describing the interacting force distributions between rotavirus and CRW during approaching at b) 1 mM NaCl, c) 10 mM NaCl, and d) 100 mM NaCl solutions.

On the other hand, considerable adhesion (totally absent between SRNOM and rotavirus) were recorded during retracting at every ionic strength tested (Fig. 4.5). Once again, due to the amount of curves produced and a slight variability in the magnitudes of the maximum adhesion forces between CRW and rotavirus (i.e., maximum adhesion forces were determined based on the maximum force measured before total detachment between the rotavirus-coated probe and the CRW-coated silica surface), probability density functions were generated and fitted using Log-Normal distributions (Fig. 4.6a-c). A similar statistical analysis was conducted for maximum adhesion distances (i.e., maximum adhesion distance was calculated as the maximum separation distance between the rotavirus coated-colloidal probe and CRW-coated silica surface during retraction, where the interaction ceases, figure 4.7a-c), and for adhesion energies (i.e., adhesion energies were directly calculated by integrating the pull-off forces by the separation distance using the trapezoidal rule, as described in the materials and method section, figure 4.8a-c). A decrease in maximum adhesion forces (μ : 3.3 nN, variance: 0.21, R^2 : 0.88; μ : 2.2 nN, variance: 0.14, R^2 : 1.0; μ : 1.3 nN, variance: 0.29, R^2 : 1.0; at 1, 10, and 100 mM NaCl solutions, respectively) was clearly observed with increasing ionic strength (Figure 4.6a-c). Similarly, long adhesion distances were recorded at every single retracting curve generated, and they also decreased with increasing ionic strength (μ : 209 nN, variance: 0.33, R^2 : 0.99; μ : 148 nN, variance: 0.79, R^2 : 0.98; μ : 142 nN, variance: 0.63, R^2 : 0.94; at 1, 10, and 100 mM NaCl solutions, respectively, Figure 4.7a-c). Interestingly, these distances (longer than the diameter of a rotavirus particle or a CRW molecule) suggest a possible detachment (pull-off) occurring at the substrate or AFM probe, as suggested in previous studies.^{17, 86, 87} In addition, multiple detachments were also observed (i.e., more clearly at low ionic strength), indicating multiple

discrete adsorption sites occurring between CRW-coated surface and rotavirus-coated colloidal probe.^{88, 89}

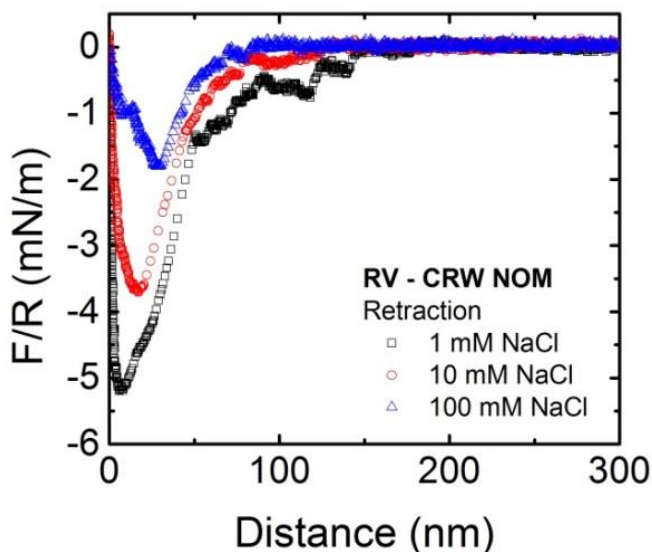


Figure 4.5 Model retracting curves between rotavirus-coated silica colloidal probe and CRW-coated silica surface measured at 1, 10, and 100 mM NaCl solutions and at pH 5.7. Maximum adhesion forces and maximum adhesion distances clearly decreased with increasing ionic strength, suggesting that the dominant interacting mechanism is negatively affected by ionic strength.

| Sample | $\theta_{\text{H}_2\text{O}}$ |
|----------------------------|-------------------------------|
| Au: Gold surface (cleaned) | 63.2±2.5 |
| Au / SAM-OH | 13.4±1.8 |
| Au / SAM-COOH | 14.1±2.1 |

Table 4.1 Contact angles (deg) measured by static sessile drop technique using water as a probe liquid. Surfaces probed included: gold surfaces previously cleaned with piranha solution (control), SAM-OH deposited on gold surface, and SAM-COOH deposited on gold surface.

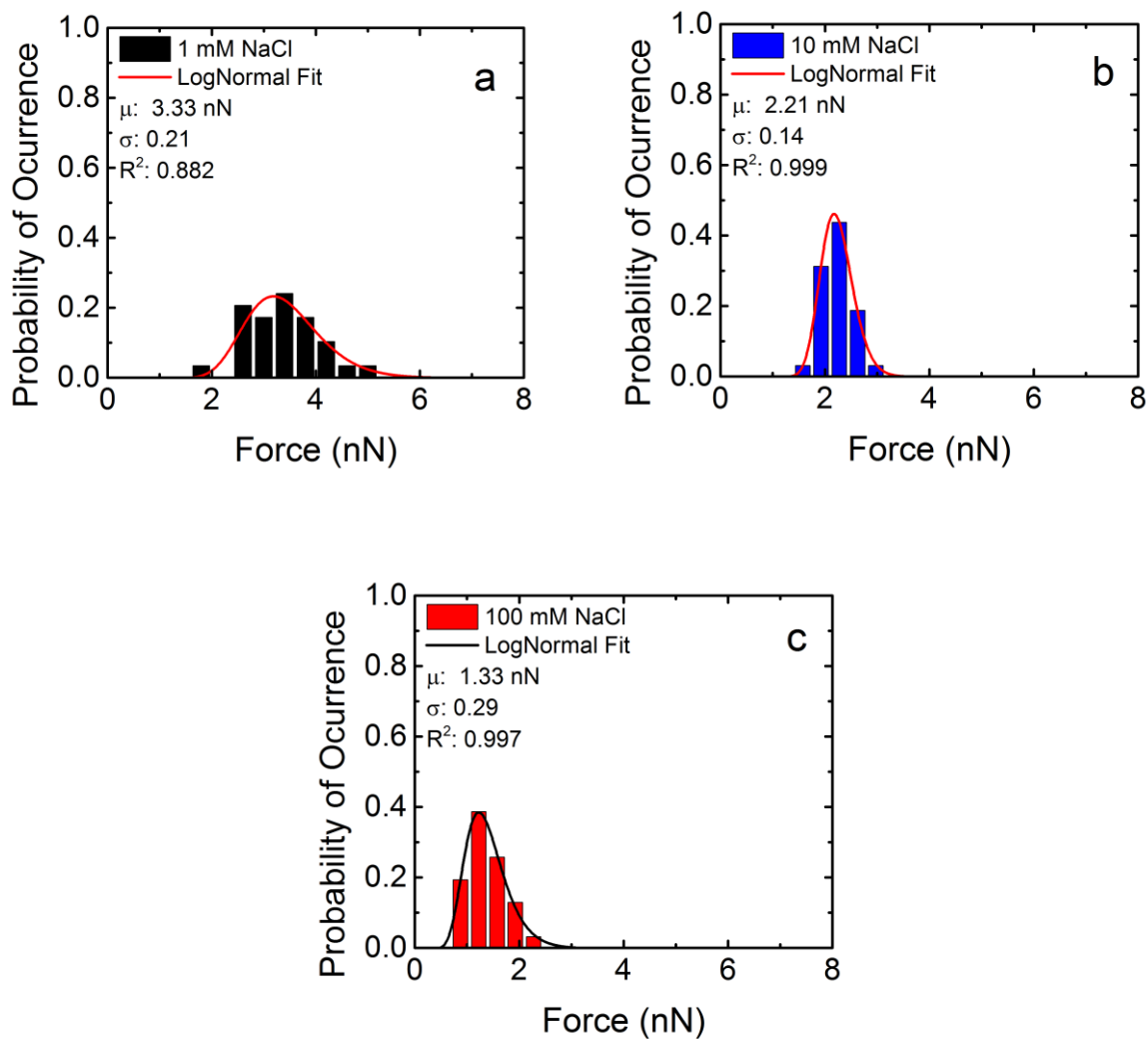


Figure 4.6 Probability density functions (Log-Normal fit) describing maximum adhesion force distributions between rotavirus and CRW during retracting at a) 1 mM NaCl, b) 10 mM NaCl, and c) 100 mM NaCl solutions. Adhesion forces clearly decrease with increasing ionic strength.

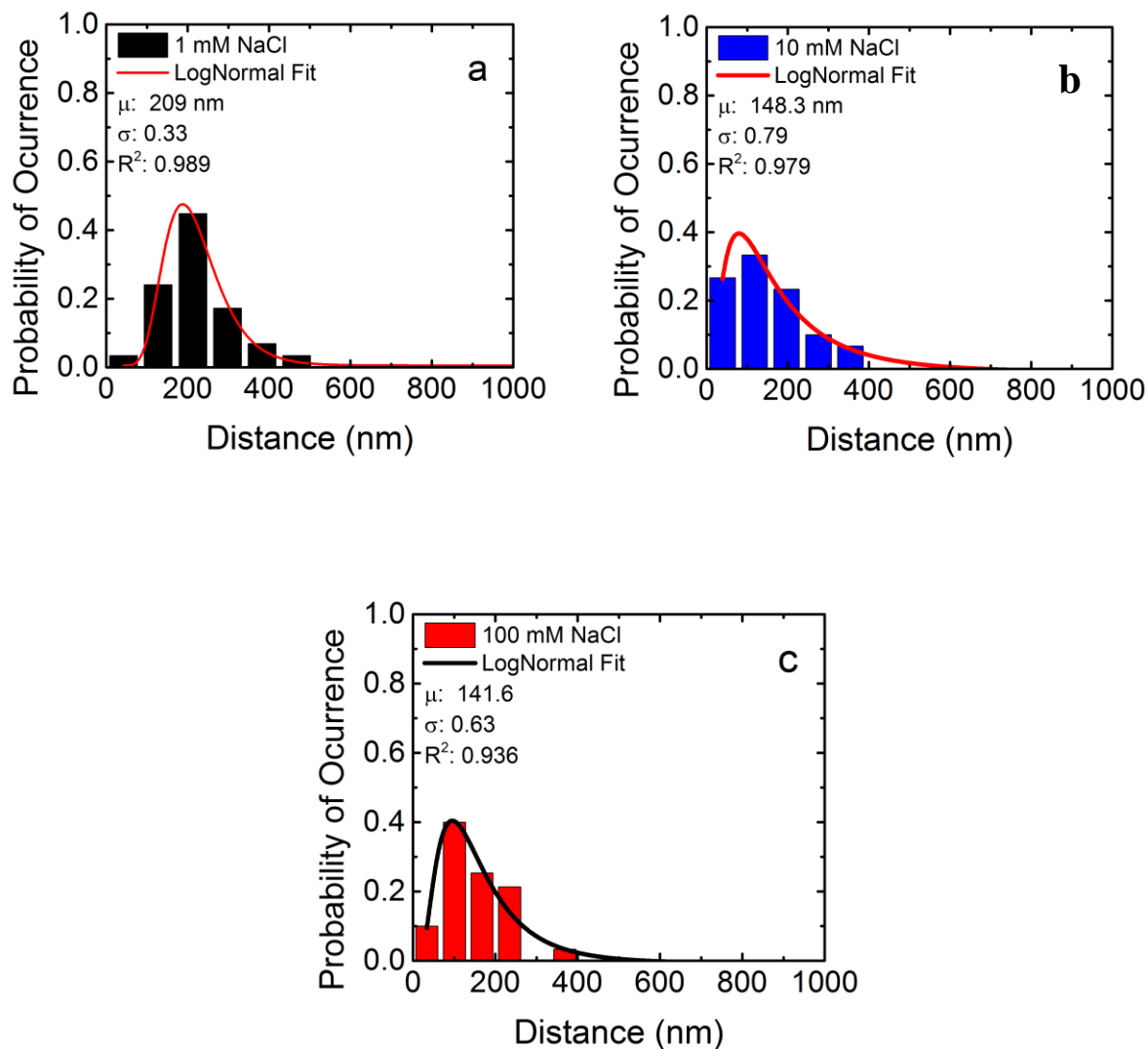


Figure 4.7 Probability density functions (Log-Normal fit) describing maximum adhesion distance distributions between rotavirus and CRW during retracting at a) 1 mM NaCl, b) 10 mM NaCl, and c) 100 mM NaCl solutions. Similarly to adhesion forces, maximum adhesion distances clearly decrease with increasing ionic strength. However, these long distances suggest possible CRW or rotavirus pull-off from substrate.

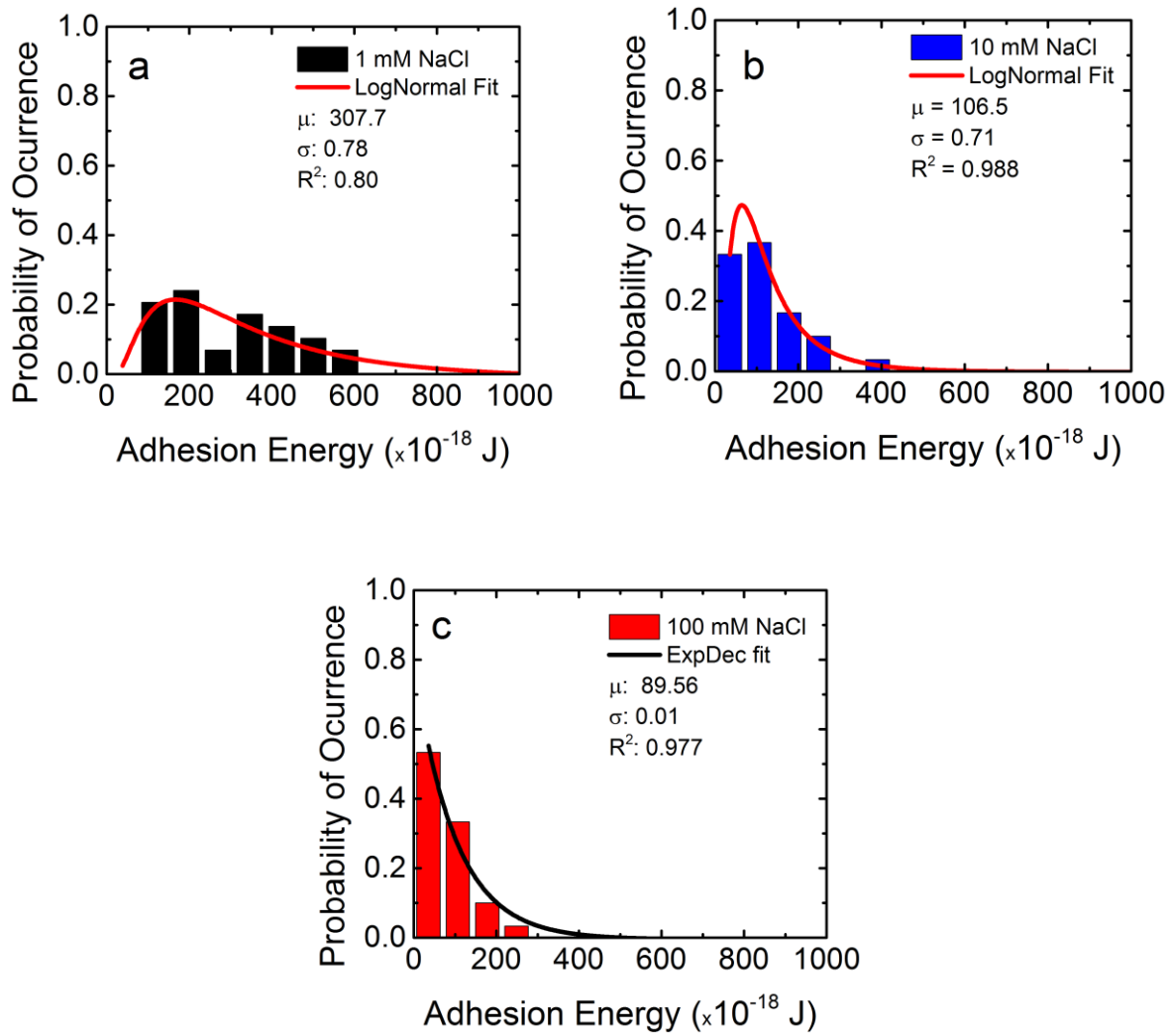


Figure 4.8 Probability density functions describing adhesion energy distributions between rotavirus and CRW during retracting at a) 1 mM NaCl, b) 10 mM NaCl, and c) 100 mM NaCl solutions. Adhesion energies were calculated by integrating the pull-off forces by the separation distance using the trapezoidal rule.

Similarly to the decrease of maximum adhesion forces and maximum adhesion distances with increasing ionic strength, calculated adhesion energies between CRW and rotavirus consequently decreased with increasing ion concentration in solution ($\mu: 308 \times 10^{-18}$ J, variance: 0.78, $R^2: 0.80$; $\mu: 107 \times 10^{-18}$ J, variance: 0.71, $R^2: 0.99$; $\mu: 89 \times 10^{-18}$ J, variance: 0.01, $R^2: 0.98$; at 1, 10, and 100 mM NaCl solutions, respectively, Figure 4.8a-c). Evidently, the dominant

interacting mechanism between CRW and rotavirus in NaCl solutions was inversely correlated to the addition of anions in solution, and this high affinity was clearly observed not only during approaching (i.e., attractive forces causing jump-in effects), but during retracting as well (i.e., high adhesion). Furthermore, this mechanism can be described as fundamentally different from that between SRNOM and rotavirus. Nevertheless, the interacting behaviors between rotavirus and CRW or SRNOM would also be explained in terms of the characteristics of rotavirus and both isolates as follows.

Interactions between rotavirus and 11-mercapto 1-undecanol (SAM-OH) or 11-mercaptoundecanoic acid (SAM-COOH) self-assembled monolayers. As described in previous sections, these experimental conditions were performed as a control to measure the interacting forces between rotavirus and hydroxyl group-SAM or carboxyl group-SAM. These two SAMs mimic the major functional groups identified on CRW and SRNOM, respectively. Contact angles measured between water (probe solution) and previously-cleaned gold (Au) surface, Au SAM-OH, and Au SAM-COOH, indicates a modification of the originally hydrophobic gold surface (Table 1). During approach, repulsion forces following an exponential decay were observed between rotavirus-coated colloidal probe and SAM-COOH (Figure 4.9a). These repulsive forces increased with decreasing distance and were evident even at high ionic strength (100 mM NaCl solutions). The carboxyl group on SAM-COOH is expected to be deprotonated at the ambient pH of the experiments (5.7-5.9). Likewise, rotavirus was negatively charged under the same conditions. Therefore, electrostatics would be expected to influence the interactions between rotavirus and SAM-COOH. Nevertheless, interaction force decay lengths clearly deviated from theoretical Debye length (Figure 4.3). Similarly to the experimental conditions described in previous sections (rotavirus/SRNOM, rotavirus/mica, rotavirus/silica),

the presence of rotavirus was influential during the interaction with SAM-COOH. Conversely, during retraction no significant adhesion was observed (Figure 4.9b). The interaction between rotavirus and SAM-OH significantly differed from SAM-COOH (Figure 4.9a), but closely resembled that of rotavirus-CRW (Figure 4.4a). A jump-in to contact was observed during approach at every curve generated. Following the jump-in to contact, a non-linear region resembling compression of structures was clearly observed. This compression might be originated from rotavirus and CRW. During retraction high adhesion forces were recorded at 1 mM NaCl, and decreased with increasing ionic strength (i.e., as observed during rotavirus-CRW). The dissimilar interactions shown by rotavirus with the two SAMs tested leads to conclude that: 1) rotavirus exerts an important influence in the interactions with silica, mica, and SRNOM which causes deviation from the measured interaction decay lengths, and 2) the major functional group on both SRNOM and CRW (mimicked by SAM-COOH and SAM-OH, respectively) are fundamental during interactions with rotavirus.

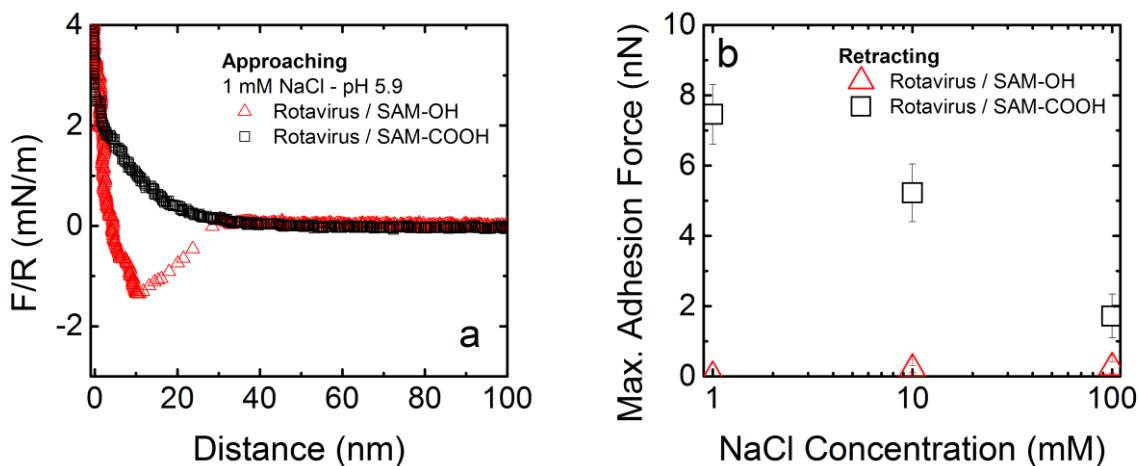


Figure 4.9 a) Model approaching curves for rotavirus-coated colloidal probe and 11-mercapto 1-undecanol SAM (SAM-OH) or 11-mercaptoundecanoic acid SAM (SAM-COOH), and b) Maximum adhesion forces measured during retracting between rotavirus-coated colloidal probe and SAM-OH or SAM-COOH.

Possible interacting mechanisms between rotavirus and SRNOM or CRW. As described in previous sections, carboxyl have been suggested as a major functional group responsible of imparting a negative charge to SRNOM.³⁴ In addition to carboxyl groups, phenols are also present in hydrophobic acid NOM fractions (i.e., also typically defined as humic NOM). Phenols (i.e., hydroxyl group bonded to a phenyl/benzene ring) are weak acids with a pK_a of ~ 10 , consequently acting as protic solvents. The hydroxyl group is bonded to an unsaturated (sp^2) carbon with a tight coupling with oxygen and a relative loose bond between oxygen and hydrogen. Conversely, polysaccharide moieties rich in alcohol groups are incorporated in the structure of transphilic acid CRW molecules (i.e., CRW has been characterized as considerably aliphatic nature, and EPM results suggest a lower presence of carboxyl groups compared to SRNOM). In alcohols, the hydroxyl group is bonded to a saturated carbon (sp^3 hybridized) with therefore no multiple bonds. The pK_a of this group is ~ 16 to 18 , which makes it at least 10^6 times less acidic than phenols.⁹⁰ In general, hydroxyl groups are polar functional groups which interact with other molecules (e.g., water molecules) or compounds by forming neutral or ionic hydrogen bonds (i.e., except when the hydroxyl groups are “hidden/buried” by other functional groups by means of steric hindrance).⁹¹ In phenols and aliphatic alcohols, hydroxyl groups improve the solubility of these molecules in water, while carbon tends to resist to it. For instance, the solubility of molecules containing hydroxyl groups and long hydrocarbon chains is usually lower than those containing short hydrocarbon chains (e.g., butanol vs. ethanol, respectively).^{90, 92} Basically, the difference in NOM structures abovementioned would play a significant role in their interactions with other surfaces. However, recent studies have also indicated the importance of specific interactions between different functional groups, which would also highly impact rotavirus-CRW and rotavirus-SRNOM interactions, as follows.

Briefly, the interactions between different functional groups in solution using self-assembled monolayers (SAMs) have been previously documented in the literature. The advantage of SAMs is their well-defined surface chemistry and homogeneity at the molecular level. For instance, a comprehensive study by Azmi et.al, (2013) used ortho- and meta-hydroxyphenol, and mono-protic phosphate alkanethiol self-assembled monolayers (SAM) to measure the competitive adsorption (i.e., forces of adhesion) of phenol/phenol, phenol/phosphate, and phosphate/phosphate species at a wide range of pH by chemical force spectrometry.⁴⁴ Maximum adhesion forces between o-hydroxyphenol SAMs or between m-hydroxyphenol SAMs were measured at pH 9 to 9.5 (i.e., $pK_{1/2}$ of hydroxyl groups); indicating ionic hydrogen bonds (suggested as significantly stronger than neutral hydrogen bonds)^{73, 74} as the dominant mechanism in this system. Conversely, at environmentally relevant pH 6 to 8 (i.e., pH at which hydroxyl groups are fully protonated and only neutral hydrogen bonding interactions are expected) as well as $pH > 11$ (i.e., pH at which hydroxyl groups are ionized and only electrostatic repulsion forces are expected) the lowest adhesion forces were recorded. On the other hand, maximum adhesion forces between mono-protic phosphate SAMs were observed at $pH \sim 4$, which similarly to the case of o-hydroxyphenol or m-hydroxyphenol SAMs, indicated high degree of hydrogen bonding due to partial deprotonation of phosphate species. Above pH 6 strong electrostatic repulsion forces due to ionized phosphate species arose between SAMs and caused the lowest adhesion forces. Interestingly, maximum adhesion forces between two mono-protic phosphate surfaces and between two ortho- or meta-hydroxyphenol surfaces occurred at environmental pH of 6 to 8. This strong interaction was suggested to be caused by ionic hydrogen bonds between ionized mono-protic phosphate and protonated hydroxyl groups on o-hydroxyphenol and m-hydroxyphenol. However, the magnitude of adhesion forces was higher

for o-hydroxyphenol, suggesting the importance of the location of the hydroxyl group. In another comprehensive study using atomic force microscopy, negligible adhesion forces were measured at pH 7.4 (PBS-buffered) between two alkanethiol SAM-COO⁻ surfaces, while slightly higher adhesion force was recorded between two SAM-OH surfaces.⁹³ These investigations remark the extremely low affinity between -COO⁻/-COO⁻, and the slightly higher adhesion between -OH/-OH by means of neutral hydrogen bonding. Results from this investigation clearly indicated that: a) the location and orientation of phenol species affect hydrogen bonding, and b) electrostatics and ionic hydrogen bonds were two major interacting mechanisms to be considered between strong and weak acids at environmentally relevant pH.

A similar interpretation can be conducted to explain the results obtained in the present investigation as follows. The high negative charge shown by both rotavirus⁴⁶ and SRNOM and the low negative charge exhibited by CRW at the pH in the current study (pH ~6) would be a result of deprotonated carboxyl groups. Conversely, their hydroxyl groups are expected to be fully protonated. The low affinity between SRNOM and electronegative/hydrophilic mica suggest a dominant mechanism driven by long range electrostatic interactions probably due to deprotonated carboxyl groups as a dominant functional group. Conversely, the high affinity between CRW and mica (i.e., the former with a considerable presence of polysaccharide moieties in its structure) suggest a dissimilar dominant mechanism, possibly related to different dominant functional groups. Furthermore, interactions between rotavirus and SRNOM also showed low affinities as opposed to CRW. Considering the high negative charge of rotavirus in solution, carboxyl groups would be an important contributor to the high rejection displayed to SRNOM. Contrariwise, these deprotonated carboxyl groups can also potentially show affinity to alcohol groups on CRW and be responsible of the high adhesion observed.

The hydrogen bond-based mechanism suggested in this study has been tested in a previous study. Briefly, the interaction forces due to hydrogen bonding between carboxyl group-terminated SAM and phenylurea groups in ethanol solutions by atomic force microscopy were studied (i.e., urea is commonly used as a protein denaturant due to its extraordinary affinity for hydrogen bonding caused its by proton-accepting group C=O and two proton-donating groups N-H).^{94,95} These very controlled conditions (e.g., SAMs, ethanol solution, urea groups) allowed the direct measurement of hydrogen bonding between these two species. However, the addition of 1 mM H_2PO_4^- to the ethanol solution decreased the adhesion forces between carboxyl groups and phenylurea groups. H_2PO_4^- ions were suggested to highly interact with phenylurea groups, acting as a blocking agent. The decrease in the strength of hydrogen bonding-based interactions has been previously suggested as caused by increasing ionic strength in solution.⁹⁶ Similar decrease in adhesion was observed between CRW and rotavirus or mica with increasing anions in solution. Therefore, the investigation described above provides supporting evidence of ionic hydrogen bonding as a dominant interacting mechanism between CRW and rotavirus.

As a final remark, the same study by Sethuraman et. al (2004) also investigated interactions between SAM-OH or SAM-COO⁻ and various proteins of different molecular weights, isoelectric points, and structures.⁹³ Although higher adhesion forces were measured between SAM-OH and IgG or BGG or Pyr; RNase A and Lys showed similar adhesion behavior to both SAM-OH and SAM-COO⁻. Therefore, although the capsids of non-enveloped viruses (i.e., including rotavirus) are made of proteins, we must be careful in analyzing every case since the characteristics of proteins can extremely differ from each other due to their inherent structural complexity and conformation. Therefore, we believe this current study gives us a fundamental insight of the importance of repulsive electrostatic interactions and the strength of

ionic hydrogen bonding occurring between ionized species and hydroxyl groups as a function of solution pH, where the reactivity of rotavirus and NOM isolates would be highly dependent on their surface characteristics.

Acknowledgements. This work was partially supported by Safe Global Water Institute, the Academic Excellence Alliance program at King Abdullah University of Science and Technology. We also acknowledge Dr. Jean-Philippe Croue, Dr. Scott McLaren, Dr. Rick Haasch, and the Frederick Seitz Materials Research Laboratory. We would also like to thank Dr. Howard Fairbrother from Johns Hopkins University.

4.5 References

1. Cabaniss, S. E.; Shuman, M. S., COPPER-BINDING BY DISSOLVED ORGANIC-MATTER .1. SUWANNEE RIVER FULVIC-ACID EQUILIBRIA. *Geochimica Et Cosmochimica Acta* **1988**, 52, (1), 185-193.
2. Cabaniss, S. E.; Shuman, M. S., COPPER-BINDING BY DISSOLVED ORGANIC-MATTER .2. VARIATION IN TYPE AND SOURCE OF ORGANIC-MATTER. *Geochimica Et Cosmochimica Acta* **1988**, 52, (1), 195-200.
3. Ma, H. Z.; Allen, H. E.; Yin, Y. J., Characterization of isolated fractions of dissolved organic matter from natural waters and a wastewater effluent. *Water Research* **2001**, 35, (4), 985-996.
4. Thurman, E. M., *Organic geochemistry of natural waters*. Martinus Nijhoff/Dr. W. Junk Publishers: The Netherlands, 1985.
5. Gu, B.; Schmitt, J.; Chen, Z.; Liang, L.; McCarthy, J. F., Adsorption and desorption of different organic matter fractions on iron oxide. *Geochimica Et Cosmochimica Acta* **1995**, 59, (2), 219-229.

6. Aiken, G. R., *Humic substances in soil, sediment, and water: geochemistry, isolation, and characterization*. Wiley: 1985.
7. Imai, A.; Fukushima, T.; Matsushige, K.; Kim, Y. H., Fractionation and characterization of dissolved organic matter in a shallow eutrophic lake, its inflowing rivers, and other organic matter sources. *Water Research* **2001**, 35, (17), 4019-4028.
8. Croue, J. P.; Benedetti, M. F.; Violleau, D.; Leenheer, J. A., Characterization and copper binding of humic and nonhumic organic matter isolated from the South Platte River: Evidence for the presence of nitrogenous binding site. *Environmental Science & Technology* **2003**, 37, (2), 328-336.
9. Ma, H.; Allen, H. E.; Yin, Y., Characterization of isolated fractions of dissolved organic matter from natural waters and a wastewater effluent. *Water Research* **2001**, 35, (4), 985-996.
10. Hwang Cordelia, J.; Kranser, S. W.; Amy, G.; Bruchet, A.; Croue, J. P.; Leenheer Jerry, A., *Polar NOM: Characterization, DBPs, Treatment*. AWWA Research Foundation: 2001.
11. Leenheer, J. A., COMPREHENSIVE APPROACH TO PREPARATIVE ISOLATION AND FRACTIONATION OF DISSOLVED ORGANIC-CARBON FROM NATURAL-WATERS AND WASTEWATERS. *Environmental Science & Technology* **1981**, 15, (5), 578-587.
12. Singer, P. C., *Formation and control of disinfection by-products in drinking water*. American Water Works Association: 1999.
13. Aiken, G. R.; McKnight, D. M.; Thorn, K. A.; Thurman, E. M., ISOLATION OF HYDROPHILIC ORGANIC-ACIDS FROM WATER USING NONIONIC MACROPOROUS RESINS. *Organic Geochemistry* **1992**, 18, (4), 567-573.

14. Amy, G.; Cho, J., Interactions between natural organic matter (NOM) and membranes: Rejection and fouling. *Water Science and Technology* **1999**, 40, (9), 131-139.
15. Leboeuf, E. J.; Weber, W. J., Macromolecular characteristics of natural organic matter. 2. Sorption and desorption behavior. *Environmental Science & Technology* **2000**, 34, (17), 3632-3640.
16. Liu, Y.; Janjaroen, D.; Kuhlenschmidt, M. S.; Kuhlenschmidt, T. B.; Nguyen, T. H., Deposition of cryptosporidium parvum oocysts on natural organic matter surfaces: Microscopic evidence for secondary minimum deposition in a radial stagnation point flow cell. *Langmuir* **2009**, 25, (3), 1594-1605.
17. Gutierrez, L.; Nguyen, T. H., Interactions between Rotavirus and Suwannee River Organic Matter: Aggregation, Deposition, and Adhesion Force Measurement. *Environmental Science & Technology* **2012**, 46, (16), 8705-8713.
18. Fan, L. H.; Harris, J. L.; Roddick, F. A.; Booker, N. A., Influence of the characteristics of natural organic matter on the fouling of microfiltration membranes. *Water Research* **2001**, 35, (18), 4455-4463.
19. Minear, R. A.; Amy, G. L., *Disinfection By-Products in Water Treatment: The Chemistry of Their Formation and Control*. Lewis Publishers: 1996.
20. Ryan, J. N.; Elimelech, M.; Ard, R. A.; Harvey, R. W.; Johnson, P. R., Bacteriophage PRD1 and silica colloid transport and recovery in an iron oxide-coated sand aquifer. *Environmental Science & Technology* **1999**, 33, (1), 63-73.
21. Gutierrez, L.; Li, X.; Wang, J. W.; Nangmenyi, G.; Economy, J.; Kuhlenschmidt, T. B.; Kuhlenschmidt, M. S.; Nguyen, T. H., Adsorption of rotavirus and bacteriophage MS2 using glass fiber coated with hematite nanoparticles. *Water Research* **2009**, 43, (20), 5198-5208.

22. Gerbo, C. P.; Goyal, S. M.; Cech, I.; Bogdan, G. F., Quantitative Assessment of the Adsorptive Behavior of Viruses to Soils. *Environmental Science & Technology* **1981**, 15, (8), 940-944.
23. Gerba, C. P., Applied and theoretical aspects of virus adsorption to surfaces. *Advances in Applied Microbiology* **1984**, 30, 133-168.
24. Penrod, S. L.; Olson, T. M.; Grant, S. B., Deposition kinetics of two viruses in packed beds of quartz granular media. *Langmuir* **1996**, 12, (23), 5576-5587.
25. Zhuang, J.; Jin, Y., Virus retention and transport as influenced by different forms of soil organic matter. *Journal of Environmental Quality* **2003**, 32, (3), 816-823.
26. Kinoshita, T.; Bales, R. C.; Maguire, K. M.; Gerba, C. P., Effect of pH on bacteriophage transport through sandy soils. *Journal of Contaminant Hydrology* **1993**, 14, (1), 55-70.
27. Bales, R. C.; Hinkle, S. R.; Kroeger, T. W.; Stocking, K.; Gerba, C. P., Bacteriophage adsorption during transport through porous media: chemical perturbations and reversibility. *Environmental Science & Technology* **1991**, 25, (12), 2088-2095.
28. Yuan, B. L.; Pham, M.; Nguyen, T. H., Deposition Kinetics of Bacteriophage MS2 on a Silica Surface Coated with Natural Organic Matter in a Radial Stagnation Point Flow Cell. *Environmental Science & Technology* **2008**, 42, (20), 7628-7633.
29. Pham, M.; Mintz, E. A.; Nguyen, T. H., Deposition kinetics of bacteriophage MS2 to natural organic matter: Role of divalent cations. *Journal of Colloid and Interface Science* **2009**, 338, (1), 1-9.
30. Kalinichev, A. G.; Iskrenova-Tchoukova, E.; Ahn, W.-Y.; Clark, M. M.; Kirkpatrick, R. J., Effects of Ca²⁺ on supramolecular aggregation of natural organic matter in aqueous solutions: A comparison of molecular modeling approaches. *Geoderma* **2011**, 169, (0), 27-32.

31. Kalinichev, A. G.; Kirkpatrick, R. J., Molecular dynamics simulation of cationic complexation with natural organic matter. *European Journal of Soil Science* **2007**, 58, (4), 909-917.
32. Bixby, R. L.; Obrien, D. J., INFLUENCE OF FULVIC-ACID ON BACTERIOPHAGE ADSORPTION AND COMPLEXATION IN SOIL. *Applied and Environmental Microbiology* **1979**, 38, (5), 840-845.
33. O'Melia, C. R.; Becker, W. C.; Au, K. K., Removal of humic substances by coagulation. In 1999; Vol. 40, pp 47-54.
34. Averett, R. C.; Leenheer, J. A.; McKnight, D. M.; Thorn, K. A., Humic substances in the Suwannee River, Georgia: interactions, properties, and proposed structures. *US Geological Survey Water-Supply Paper* **1994**, 2373.
35. Leenheer, J. A.; Nanny, M. A.; McIntyre, C., Terpenoids as Major Precursors of Dissolved Organic Matter in Landfill Leachates, Surface Water, and Groundwater. *Environmental Science & Technology* **2003**, 37, (11), 2323-2331.
36. Wyn-Jones, A. P.; Sellwood, J., Enteric viruses in the aquatic environment. *Journal of Applied Microbiology* **2001**, 91, (6), 945-962.
37. Gerba, C. P.; Rose, J. B.; Haas, C. N.; Crabtree, K. D., Waterborne rotavirus: A risk assessment. *Water Research* **1996**, 30, (12), 2929-2940.
38. Villena, C.; El-Senousy, W. M.; Abad, F. X.; Pinto, R. M.; Bosch, A., Group a rotavirus in sewage samples from Barcelona and Cairo: Emergence of unusual genotypes. *Applied and Environmental Microbiology* **2003**, 69, (7), 3919-3923.

39. Borchardt, M. A.; Haas, N. L.; Hunt, R. J., Vulnerability of drinking-water wells in La Crosse, Wisconsin, to enteric-virus contamination from surface water contributions. *Applied and Environmental Microbiology* **2004**, 70, (10), 5937-5946.
40. Gutierrez, M. F.; Alvarado, M. V.; Martinez, E.; Ajami, N. J., Presence of viral proteins in drinkable water - Sufficient condition to consider water a vector of viral transmission? *Water Research* **2007**, 41, (2), 373-378.
41. Espinosa, A. C.; Mazari-Hiriart, M.; Espinosa, R.; Maruri-Avidal, L.; Mendez, E.; Arias, C. F., Infectivity and genome persistence of rotavirus and astrovirus in groundwater and surface water. *Water Research* **2008**, 42, (10-11), 2618-2628.
42. Leenheer Jerry, A.; Croué, J.-P.; Benjamin, M.; Korshin Gregory, V.; Hwang Cordelia, J.; Bruchet, A.; Aiken George, R., Comprehensive Isolation of Natural Organic Matter from Water for Spectral Characterizations and Reactivity Testing. In *Natural Organic Matter and Disinfection By-Products*, American Chemical Society: 2000; Vol. 761, pp 68-83.
43. Nguyen, T. H.; Elimelech, M., Adsorption of plasmid DNA to a natural organic matter-coated silica surface: Kinetics, conformation, and reversibility. *Langmuir* **2007**, 23, (6), 3273-3279.
44. Azmi, A. A.; Ebralidze, I. I.; Dickson, S. E.; Horton, J. H., Characterization of hydroxyphenol-terminated alkanethiol self-assembled monolayers: Interactions with phosphates by chemical force spectrometry. *Journal of Colloid And Interface Science* **2013**, 393, 352-360.
45. Rolsma, M. D.; Gelberg, H. B.; Kuhlenschmidt, M. S., Assay for Evaluation of Rotavirus-Cell Interactions - Identification of an Enterocyte Ganglioside Fraction That Mediates Group-a Porcine Rotavirus Recognition. *Journal of Virology* **1994**, 68, (1), 258-268.

46. Gutierrez, L.; Mylon, S. E.; Nash, B.; Nguyen, T. H., Deposition and Aggregation Kinetics of Rotavirus in Divalent Cation Solutions. *Environmental Science & Technology* **2010**, 44, (12), 4552-4557.
47. Ruiz, M. C.; Charpilienne, A.; Liprandi, F.; Gajardo, R.; Michelangeli, F.; Cohen, J., The concentration of Ca^{2+} that solubilizes outer capsid proteins from rotavirus particles is dependent on the strain. *Journal of Virology* **1996**, 70, (8), 4877-4883.
48. Butt, H. J.; Cappella, B.; Kappl, M., Force measurements with the atomic force microscope: Technique, interpretation and applications. *Surface Science Reports* **2005**, 59, (1-6), 1-152.
49. Gaboriaud, F.; Dufrêne, Y. F., Atomic force microscopy of microbial cells: Application to nanomechanical properties, surface forces and molecular recognition forces. *Colloids and Surfaces B: Biointerfaces* **2007**, 54, (1), 10-19.
50. Cail, T. L.; Hochella, M. F., The effects of solution chemistry on the sticking efficiencies of viable *Enterococcus faecalis*: An atomic force microscopy and modeling study. *Geochimica Et Cosmochimica Acta* **2005**, 69, (12), 2959-2969.
51. Lower, S. K.; Tadanier, C. J.; Hochella, M. F., Measuring interfacial and adhesion forces between bacteria and mineral surfaces with biological force microscopy. *Geochimica Et Cosmochimica Acta* **2000**, 64, (18), 3133-3139.
52. Byrd, T. L.; Walz, J. Y., Investigation of the interaction force between *Cryptosporidium parvum* oocysts and solid surfaces. *Langmuir* **2007**, 23, (14), 7475-7483.
53. Byrd, T. L.; Walz, J. Y., Interaction force profiles between *Cryptosporidium parvum* oocysts and silica surfaces. *Environmental Science & Technology* **2005**, 39, (24), 9574-9582.

54. Asatekin, A.; Menniti, A.; Kang, S. T.; Elimelech, M.; Morgenroth, E.; Mayes, A. M., Antifouling nanofiltration membranes for membrane bioreactors from self-assembling graft copolymers. *Journal of Membrane Science* **2006**, 285, (1-2), 81-89.
55. Gordesli, F. P.; Abu-Lail, N. I., The Role of Growth Temperature in the Adhesion and Mechanics of Pathogenic *L. monocytogenes*: An AFM Study. *Langmuir* **2012**, 28, (2), 1360-1373.
56. Chen, K. L.; Mylon, S. E.; Elimelech, M., Enhanced aggregation of alginate-coated iron oxide (hematite) nanoparticles in the presence of calcium, strontium, and barium cations. *Langmuir* **2007**, 23, (11), 5920-5928.
57. Cox, M. G., The area under a curve specified by measured values. *Metrologia* **2007**, 44, (5), 365-378.
58. Croue, J. P.; Korshin Gregory, V.; Benjamin, M. M., *Isolation, Fractionation and Characterization of Natural Organic Matter in Drinking Water*. AWWA Research Foundation and American Water Works Association: USA, 1999.
59. Brady-Estevéz, A. S.; Nguyen, T. H.; Gutierrez, L.; Elimelech, M., Impact of solution chemistry on viral removal by a single-walled carbon nanotube filter. *Water Research* **2010**, 44, (13), 3773-3780.
60. de Kerchove, A. J.; Elimelech, M., Relevance of electrokinetic theory for "soft" particles to bacterial cells: Implications for bacterial adhesion. *Langmuir* **2005**, 21, (14), 6462-6472.
61. Mylon, S. E.; Rinciog, C. I.; Schmidt, N.; Gutierrez, L.; Wong, G. C. L.; Nguyen, T. H., Influence of Salts and Natural Organic Matter on the Stability of Bacteriophage MS2. *Langmuir* **2010**, 26, (2), 1035-1042.

62. Nishimura, S.; Tateyama, H.; Tsunematsu, K.; Jinnai, K., Zeta potential measurement of muscovite mica basal plane-aqueous solution interface by means of plane interface technique. *Journal of Colloid And Interface Science* **1992**, 152, (2), 359-367.
63. Scales, P. J.; Grieser, F.; Healy, T. W., Electrokinetics of the muscovite mica-aqueous solution interface. *Langmuir* **1990**, 6, (3), 582-589.
64. Maslova, M. V.; Gerasimova, L. G.; Forsling, W., Surface Properties of Cleaved Mica. *Colloid Journal* **2004**, 66, (3), 322-328.
65. Mosley, L. M.; Hunter, K. A.; Ducker, W. A., Forces between Colloid Particles in Natural Waters. *Environmental Science & Technology* **2003**, 37, (15), 3303-3308.
66. Sander, S.; Mosley, L. M.; Hunter, K. A., Investigation of Interparticle Forces in Natural Waters: Effects of Adsorbed Humic Acids on Iron Oxide and Alumina Surface Properties. *Environmental Science & Technology* **2004**, 38, (18), 4791-4796.
67. Gu, B.; Doner, H. E., Dispersion and Aggregation of Soils as Influenced by Organic and Inorganic Polymers and Inorganic Polymers. *Soil Sci. Soc. Am. J.* **1993**, 57, (3), 709-716.
68. Liang, L.; Morgan, J., Chemical aspects of iron oxide coagulation in water: Laboratory studies and implications for natural systems. *Aquatic Sciences* **1990**, 52, (1), 32-55.
69. Ghosh, S.; Jiang, W.; McClements, J. D.; Xing, B., Colloidal Stability of Magnetic Iron Oxide Nanoparticles: Influence of Natural Organic Matter and Synthetic Polyelectrolytes. *Langmuir* **2011**, 27, (13), 8036-8043.
70. Mylon, S. E.; Chen, K. L.; Elimelech, M., Influence of natural organic matter and ionic composition on the kinetics and structure of hematite colloid aggregation: Implications to iron depletion in estuaries. *Langmuir* **2004**, 20, (21), 9000-9006.

71. Domingos, R. F.; Tufenkji, N.; Wilkinson, K. J., Aggregation of Titanium Dioxide Nanoparticles: Role of a Fulvic Acid. *Environmental Science & Technology* **2009**, 43, (5), 1282-1286.
72. Lim, R. Y. H.; Deng, J., Interaction Forces and Reversible Collapse of a Polymer Brush-Gated Nanopore. *ACS Nano* **2009**, 3, (10), 2911-2918.
73. Smith, D. A.; Connell, S. D.; Robinson, C.; Kirkham, J., Chemical force microscopy: applications in surface characterisation of natural hydroxyapatite. *Analytica Chimica Acta* **2003**, 479, (1), 39-57.
74. Meotner, M.; Sieck, L. W., THE IONIC HYDROGEN-BOND AND ION SOLVATION .5. OH...O- BONDS - GAS-PHASE SOLVATION AND CLUSTERING OF ALKOXIDE AND CARBOXYLATE ANIONS. *Journal of the American Chemical Society* **1986**, 108, (24), 7525-7529.
75. Rath, R. K.; Subramanian, S., Studies on adsorption of guar gum onto biotite mica. *Minerals Engineering* **1997**, 10, (12), 1405-1420.
76. Derjaguin, B., Untersuchungen über die Reibung und Adhäsion, IV. *Colloid & Polymer Science* **1934**, 69, (2), 155-164.
77. Verwey, E. J. W.; Overbeek, J. T. G., *Theory of the Stability of Lyophobic colloids*. Elsevier: Amsterdam, 1948.
78. Butt, H. J.; Kappl, M.; Mueller, H.; Raiteri, R.; Meyer, W.; Rühle, J., Steric forces measured with the atomic force microscope at various temperatures. *Langmuir* **1999**, 15, (7), 2559-2565.
79. Behrens, S. H.; Borkovec, M.; Schurtenberger, P., Aggregation in Charge-Stabilized Colloidal Suspensions Revisited. *Langmuir* **1998**, 14, (8), 1951-1954.

80. Behrens, S. H.; Christl, D. I.; Emmerzael, R.; Schurtenberger, P.; Borkovec, M., Charging and aggregation properties of carboxyl latex particles: Experiments versus DLVO theory. *Langmuir* **2000**, 16, (6), 2566-2575.
81. Nir, S., Van der Waals interactions between surfaces of biological interest. *Progress in Surface Science* **1977**, 8, (1), 1-58.
82. Aoki, S. T.; Settembre, E. C.; Trask, S. D.; Greenberg, H. B.; Harrison, S. C.; Dormitzer, P. R., Structure of Rotavirus Outer-Layer Protein VP7 Bound with a Neutralizing Fab. *Science* **2009**, 324, (5933), 1444-1447.
83. Monnier, N.; Higo-Moriguchi, K.; Sun, Z. Y. J.; Prasad, B. V. V.; Taniguchi, K.; Dormitzer, P. R., High-resolution molecular and antigen structure of the VP8*core of a sialic acid-independent human rotavirus strain. *Journal of Virology* **2006**, 80, (3), 1513-1523.
84. Dormitzer, P. R.; Nason, E. B.; Prasad, B. V. V.; Harrison, S. C., Structural rearrangements in the membrane penetration protein of a non-enveloped virus. *Nature* **2004**, 430, (7003), 1053-1058.
85. Dormitzer, P. R.; Sun, Z. Y. J.; Wagner, G.; Harrison, S. C., The rhesus rotavirus VP4 sialic acid binding domain has a galectin fold with a novel carbohydrate binding site. *Embo Journal* **2002**, 21, (5), 885-897.
86. Mi, B. X.; Elimelech, M., Organic fouling of forward osmosis membranes: Fouling reversibility and cleaning without chemical reagents. *Journal of Membrane Science* **2010**, 348, (1-2), 337-345.
87. de Kerchove, A. J.; Elimelech, M., Formation of polysaccharide gel layers in the presence of Ca²⁺ and K⁺ ions: Measurements and mechanisms. *Biomacromolecules* **2007**, 8, (1), 113-121.

88. Considine, R. F.; Dixon, D. R.; Drummond, C. J., Oocysts of *Cryptosporidium parvum* and model sand surfaces in aqueous solutions: an atomic force microscope (AFM) study. *Water Research* **2002**, 36, (14), 3421-3428.
89. Kang, S.; Elimelech, M., Bioinspired Single Bacterial Cell Force Spectroscopy. *Langmuir* **2009**, 25, (17), 9656-9659.
90. Vollhardt, K. P. C.; Schore, N. E., *Organic Chemistry, Fourth Edition: Structure and Function*. W. H. Freeman: 2003.
91. Grabowski, S. J., *Hydrogen Bonding: New Insights*. Springer London, Limited: 2006.
92. Israelachvili, J. N., *Intermolecular and Surface Forces: Revised Third Edition*. Elsevier Science: 2011.
93. Sethuraman, A.; Han, M.; Kane, R. S.; Belfort, G., Effect of surface wettability on the adhesion of proteins. *Langmuir* **2004**, 20, (18), 7779-7788.
94. Zhang, Y.; Cremer, P. S., Interactions between macromolecules and ions: the Hofmeister series. *Current Opinion in Chemical Biology* **2006**, 10, (6), 658-663.
95. Kado, S.; Murakami, T.; Kimura, K., Effect of intramonolayer hydrogen bonding of carboxyl groups in self-assembled monolayers on a single force with phenylurea on an AFM probe tip. *Analytical Sciences* **2006**, 22, (4), 521-527.
96. Oh, H. I.; Hoff, J. E.; Armstrong, G. S.; Haff, L. A., Hydrophobic interaction in tannin-protein complexes. *Journal of Agricultural and Food Chemistry* **1980**, 28, (2), 394-398.

CHAPTER 5

CONCLUSIONS

Rotavirus particles showed high stability in NaCl solutions of up to 600 mM. Clearly, DLVO forces were not the solely mechanisms governing rotavirus particles interactions. Conversely, divalent cations in solution (Mg^{2+} and Ca^{2+}) caused a profound effect in rotavirus stability. Cation bridging between deprotonated carboxylic groups on rotavirus surface was suggested as the main mechanism disrupting rotavirus stability. Interestingly, rotavirus aggregation was not measurable under typical groundwater hardness values found in USA (Yates et al., 1985). Viruses are present in the environment at diluted concentrations; consequently, aggregation would not be expected as a fate. However, the relevance of these results is based on accurate measurement of rotavirus surface moieties reactivity for mono and divalent cations; results particularly important when other component is added to the system, such as NOM. Rotavirus did not aggregate in NaCl and SRNOM-containing solutions even at high ionic strength, suggesting the presence of non-DLVO forces. Divalent cations broke the stability of SRNOM and rotavirus, and aggregation occurred faster than in the absence of SRNOM. Cation bridging was suggested as the main mechanism between carboxyl groups on SRNOM and rotavirus. However, aggregation was measurable at hardness values found in groundwater. This result is particularly significant because it shows rotavirus affinity for a typical humic (SRNOM) in divalent cation solutions (i.e., plausible scenario in certain water systems). On the other hand, no rotavirus deposition was observed on silica and SRNOM-coated surfaces in NaCl solutions. Rotavirus deposition was observed in typical values of hardness found in groundwater, and was higher on SRNOM-coated surfaces. This result was in good agreement to aggregation experiments, and suggests divalent cation bridging as an important mechanism that may control

deposition of viruses on humic-like materials in water systems. However, rotavirus interactions with NOM were found to be highly dependent on NOM characteristics. Interaction forces measured at the nano-scaled showed dissimilar interacting mechanism between rotavirus and a model humic (SRNOM) or a model non-humic NOM (CRW) in NaCl solutions. Strong repulsive forces during approaching and no adhesion during retraction were recorded between rotavirus and SRNOM even at high ionic strength (i.e., in good agreement with deposition and aggregation experiments previously described). However, attractive forces during approach and high adhesion were observed between rotavirus and CRW at low ionic strength commonly found in aquatic environments. These results indicate that the properties of NOM would have a profound influence in the interaction with viruses that might affect their transport and fate in natural water systems.

In addition to the above suggested environmental implications, the contribution of this work can be measured in terms of the development of protocols that can be extended to other applications. A dialysis-concentration rotavirus purification method was optimized to obtain a highly pure stock without significantly affecting its infectivity. Complementary techniques (e.g., TR-DLS, EPM) were used to assess the quality of the final viral stock. A direct comparison with CsCl-purified rotavirus stock indicates that the dialysis/concentration protocol produces viral stocks suitable for high quality research, and can be extended to purify other viral solutions. A protocol for bio-modification of AFM colloidal probes and surfaces with rotavirus was introduced. Systematic control experiments (i.e., based on force measurements with sharp AFM tips in contact mode) were designed to assess the coating-completeness of NOM-coated and rotavirus-coated silica surfaces. The procedures developed in this work are promising tools to study surface interactions between viruses and organic material of diverse characteristics.

CHAPTER 6

FUTURE RESEARCH

Bio-modification of AFM probes is a powerful tool to study surface interactions at the nano-scale. The current investigation introduced a protocol for virus-coating of AFM colloidal probes to study interactions with environmentally relevant surfaces at a wide range of solution ionic composition. Nevertheless, several key environmental parameters not covered in this study, remained a challenge for future research.

- Dissimilar pH conditions are expected at different water systems. For instance, in a previous study, pH fluctuations ranging from 6 to 8.3 were observed in groundwater samples collected at different location in USA (Yates et al., 1985). pH conditions have been extensively described to cause a deep effect on not only functional groups but also on the properties of proteins (e.g., conformation). The influence of pH on the dominant mechanisms between rotavirus and MOM remains unknown; consequently, a comprehensive study including this key parameter is required.
- This study was entirely conducted at ambient room temperature (25°C). However, an investigation of the role of temperature on the interactions between rotavirus and surfaces is essential. Natural ecosystems are typically characterized by their temperature fluctuations on a diurnal and seasonal basis. These fluctuations are highly variable among different ecosystems. Therefore, temperature might potentially cause a profound effect on the surface characteristics of both NOM and viruses (e.g., conformation of the polymeric chains of NOM and proteins in viral capsids, etc.), influencing their interaction with other surfaces.
- As described in chapter 4, previous investigations have characterized several strains of rotavirus at high resolution. Generated surface representations in terms of electrostatic

potential have shown a heterogeneous charge distribution on the surface of outer viral proteins. But more importantly, these studies have also observed a variability of these residues (e.g., hydrophobic, neutral hydrophilic, charged) among different strains. The impact of this variability of residues among strains on their interaction with surfaces is currently unknown. Therefore, a comparative study including a human rotavirus would be essential to understand this phenomenon.

APPENDIX

PROTOCOLS FOLLOWED

1 Rotavirus propagation on MA-104 cells^{1, 2}

- 1.1 Unless indicated, all the following steps must be conducted in a certified bio-safety level 2 laboratory and in a laminar flow hood under strict sterile conditions.
- 1.2 Purchase MA-104 Clone 1 cells (ATCC CRL-2378.1). Although originally cryopreserve in liquid nitrogen vapor phase (below -130°C, Eagle's Minimum Essential Medium, 85%; fetal bovine serum 10%; DMSO, 5%), MA-104 cells will be delivered on dry ice which maintains a temperature between -70°C to -80°C and do not affect the viability of the cell cultures.
- 1.3 The next materials and solutions must be prepared before receiving/thawing the cell culture.
- 1.4 Prepared 10 L of Eagle's Minimum Essential Medium (MEM) by diluting Eagle's MEM powder (Gibco #41500-018), 22 g NaHCO₃ (Sigma Aldrich #S5761-500g), and 23.8 g HEPES (Sigma Aldrich #H3784-25g) in 10 liters of dionized water (DI, resistivity 18 MΩ-cm, Millipore, USA). Filter these 10 liters through a disposable sterile 45 mm diameter bottle-top 0.22 µm cellulose acetate (CA) membrane filter (Corning) and dispense into ten 500 mL 45 mm diameter neck sterile Pyrex media bottle (500 mL of MEM in each 500 mL sterile Pyrex bottle). Store the MEM at -4°C.
- 1.5 Prepare 10 L of CELL MEM by diluting Eagle's MEM powder, 22 g NaHCO₃, and 23.8 g HEPES in 10 liters of DI water. Filter these 10 liters through a disposable sterile 45 mm diameter bottle-top 0.22 µm CA membrane filter and dispense into twelve 500 mL 45 mm diameter neck sterile Pyrex media bottle (450 mL of MEM in each 500 mL sterile

- Pyrex bottle). Add 50 mL of fetal bovine serum (FBS) (Gibco # 10438-026) and 0.5 mL of 100X antibiotic/antimycotic (Gibco # 15240-062) to every bottle of 450 mL MEM solution. Store the CELL MEM at -4°C.
- 1.6 Prepare Phosphate Buffer solution (PBS) by adding 8 g of NaCl (Fisher # S640-3), 0.2 g of KCl (Fisher # BP366-500), 2.06 g of Na₂HPO₃·7H₂O (Fisher #S373-500), and 0.2 g of KH₂PO₄ (Fisher # P380-500) to 1 L of DI water. Dispense in 500 mL Pyrex bottles and autoclave in a 30 minutes liquid process with the cap of the bottle slightly loose. Store at -4°C.
 - 1.7 Autoclave 1 L of DI water (1 L Pyrex bottle) in 30 minutes liquid process. Wait until the autoclaved-DI water reaches ambient temperature. Prepare Trypsin/EDTA solution by adding 10 mL of 0.5% Trypsin-EDTA 10X (Sigma-Aldrich #T0303) in 90 mL of pre-autoclaved DI water (use a sterile 250 mL Pyrex bottle). Store at -20°C.
 - 1.8 Add 25 mL of CELL MEM to a 150 cm² culture flask (Corning # 430823) by pipetting with a 25 mL sterile polystyrene disposable serological pipette with magnifier stripe (Fisherbrand) using a Drummond 4-000-100 portable Pipet-Aid. Incubate the flask at 37°C and in a 5% CO₂ environment for approximately 2 hours, along with 1 Pyrex bottle containing 500 mL of CELL MEM.
 - 1.9 This only step is not conducted in a laminar flow hood. Immediately upon receiving the cell culture, initiate the next thawing process. Place the received vial in a water bath at 37°C (to reduce risk of contamination, do not completely immerse the vial in the warm water, keep the oring and cap out of the water). Carefully monitor the vial until the thawing is complete (consider applying gentle agitation). Remove the vial from the water

bath, dry it with kimwipes, and spray/wipe it in excess with 70% ethanol solution (disinfection/cleaning purposes).

- 1.10 It is extremely important that during growth, the temperature of the cells must be kept at 37°C. However, during handling of cells, sudden or significant changes in temperature must be avoided. Therefore, whenever cells are removed from incubation, any protocol must be followed rapidly and efficiently, and any necessary material and reagent must be prepared in advance.
- 1.11 The next steps are again conducted in a laminar flow hood. Open the vial and transfer the recently-thawed MA-104 cells to the 150 cm² culture flask containing 25 mL of CELL MEM by pipetting with a new 5 mL sterile polystyrene disposable serological pipette with magnifier stripe (Fisherbrand) using a Drummond portable Pipet-Aid. Incubate for 1 hour at 37°C and in a 5% CO₂ environment. After the 1 hour, carefully monitor under a microscope (10X magnification) if the cells are attached to the substrate of the flask. If the attachment of the majority of the cells is successful (cells should look as perfect dark orange-colored spheres and mono-attached all over the substrate), remove CELL MEM from the flask (this step is conducted to remove cryo-protective DMSO) by pipetting with a new 25 mL sterile disposable serological pipette. Pour this CELL MEM in a properly-labeled “MEM WASTE” container for further 30 minutes liquid autoclave process. Immediately pipette 25 mL of CELL MEM (already kept at 37°C to avoid shocking the cells with sudden temperature change) to the 150 cm² flask containing the MA-104 cells. Incubate the flask at 37°C and in a 5% CO₂ environment for 48 hours. Place the CELL MEM Pyrex bottle, which was in the incubator, back in -4°C.

- 1.12 Discard all the used disposable serological pipettes in biohazard bags for further 30 minutes gravity autoclave process.
- 1.13 After 48 hours, place a CELL MEM bottle at 37°C for 2 hours. When the temperature of the CELL MEM in the Pyrex bottle has reached 37°C, monitor the growing process of the MA-104 cells under a microscope (10X). By now, the cells should not look spherical in shape and mono-attached anymore but rather flat, polymorphic, light orange-colored, and visibly dividing as a monolayer. The recommended medium renewal for MA-104 cells is 2 to 3 days, therefore, remove the CELL MEM from the 150 cm² flask by pipetting with a new 25 mL sterile polystyrene disposable serological pipette using a Drummond portable Pipet-Aid. Dispose this used CELL MEM in the MEM WASTE container. Immediately pipette 25 mL of CELL MEM (already kept at 37°C) to the 150 cm² flask containing the MA-104 cells. Incubate the flask at 37°C and in a 5% CO₂ environment for 48 hours. Place the CELL MEM Pyrex bottle, which was in the incubator, back in -4°C.
- 1.14 Repeat the step above (medium renewal every 2 days) until reaching cell confluence. Confluence for a new line of cells (first generation) takes between 6 to 10 days. Therefore this process would be repeated 3 to 5 times.
- 1.15 After confirmation of cell confluence, start the process of splitting cells as follows: place a CELL MEM bottle and a PBS bottle at 37°C for 2 hours.
- 1.16 Thaw a bottle of Trypsin/EDTA solution (originally at -20°C) at 37°C in a water bath.
- 1.17 Remove the CELL MEM solution from the confluent MA-104 cells in the 150 cm² flask by pipetting with a new 25 mL sterile polystyrene disposable serological pipette using a Drummond portable Pipet-Aid. Dispose this used CELL MEM in the MEM WASTE

container. Immediately rinse the MA-104 cells twice with 7 mL of PBS by pipetting with a new 10 mL sterile polystyrene disposable serological pipette using a Drummond portable Pipet-Aid. Dispose this used PBS in the MEM WASTE container.

- 1.18 Add 3 ml of the Trypsin/EDTA solution to the monolayer of MA-104 cells and rock the flask to evenly coat the cells with the Trypsin/EDTA solution.
- 1.19 Incubate the flask at 37°C and in a 5% CO₂ environment for approximately 5 minutes.
- 1.20 While incubation of the MA-104 cells, pipette 25 mL of CELL MEM (already kept at 37°C) to nine 150 cm² flasks. Eight of these flasks will be used for roller bottle cell production while the remaining one flask will be used for rotavirus infectivity assay described in the next section (focus forming unit assay, FFU).
- 1.21 After the 5 minutes, gently hit the flask with the palm of the hand to detach cells from the flask. Then, carefully monitor under the microscope (10X) the dissociation of cells from the substrate of the flask. If a considerable fraction of the cells are still attached to the substrate, place again the flask into incubation for additional 2 minutes, and constantly monitor the progress of detachment of cells. If over-exposure to Trypsin/EDTA, cells may not be able to attach to a new substrate again.
- 1.22 Once confirmed the detachment of the majority of cells, add 25 mL of MEM CELL by pipetting with a new 25 mL sterile polystyrene disposable serological pipette using a Drummond portable Pipet-Aid. Titurate the cell-solution with the pipette to avoid fast sedimentation of cells due to their large size.
- 1.23 Pipette 3 mL of the cell-solution to every of the nine 150 cm² flasks containing 25 mL of CELL MEM (already kept at 37°C). Remember, eight flasks will be destined for roller

bottle cell production and the remaining one flask will be destined for rotavirus infectivity assays (focus forming unit assay, FFU).

- 1.24 Return the CELL MEM bottle to -4°C and the Trypsin/EDTA bottle to -20°C.
- 1.25 Incubate the eight 150 cm² flasks at 37°C and in a 5% CO₂ environment for 48 hours. Repeat the procedures described above for media renewal of the eight 150 cm² flasks and periodically monitor the growth of cells under a microscope (10X) until confluence.
- 1.26 When cells in the flask are confluent, follow the next protocol for Roller Bottle cell production.
- 1.27 Place a CELL MEM bottle (originally at -4°C) at 37°C for 2 hours and thaw a bottle of Trypsin/EDTA solution (originally at -20°C) at 37°C in a water bath.
- 1.28 Add 50 mL of CELL MEM to an 850 cm² roller bottle (Corning #430849) and incubate for 2 hours at 37°C and in a 5% CO₂ environment by rotation at 0.75 rpm using a Wheaton Compact Roller System for Small Bottles (Fisher #22-288-525). Keep the cap slightly open to allow CO₂ to enter the roller bottle (for the rest of this study, the roller bottles will be placed inside the incubator with the cap slightly opened).
- 1.29 Remove one 150 cm² flask from incubation and start the process of cell detachment from the substrate as previously described above.
- 1.30 Once confirmed the detachment of the majority of cells, add 10 mL of MEM CELL by pipetting with a new 10 mL sterile polystyrene disposable serological pipette using a Drummond portable Pipet-Aid. Titrate the cell-solution with the pipette to avoid fast sedimentation of cells due to their large size.

- 1.31 Pipette the 10 mL of the cell-solution to an 850 cm² roller bottle containing 50 mL of CELL MEM (already kept at 37°C) and incubate for 48 hours at 37°C and in a 5% CO₂ environment by rotation at 0.75 rpm.
- 1.32 Repeat the Roller Bottle cell production for each of the remaining seven 150 cm² flask containing MA-104 cells, one at a time.
- 1.33 Return the CELL MEM bottle to -4°C and the Trypsin/EDTA bottle to -20°C.
- 1.34 Repeat the procedures described above for media renewal of the eight 850 cm² roller bottles and periodically monitor the growth of cells under a microscope (10X) until confluence. Confluence for a new line of cells (now second generation) on roller bottles takes between 8 to 12 days.
- 1.35 Start the rotavirus stock production as follows.
- 1.36 Obtain Group A porcine rotavirus OSU strain stock (ATCC-VR892, originally stored at -70°C in MEM solution). Similarly to MA-104 cells, the virus stock should be shipped in dry ice.
- 1.37 Prepare trypsin solution by diluting 0.01 g Trypsin (Sigma Aldrich #T0303) in 10 mL MEM solution (dose: 1 mg Trypsin/mL MEM). To prevent contamination, aliquot in Eppendorf Snap-Cap 2 mL Microcentrifuge Safe-Lock Tubes.
- 1.38 Place a PBS bottle and a MEM bottle (originally at -4°C) at 37°C for 2 hours. Do not confuse MEM with CELL MEM. AT this stage of the process we will no longer use CELL MEM. The FBS (serum) contained in the CELL MEM inhibits RV attachment to cells and therefore negatively impacts the rotavirus stock production.
- 1.39 Thaw the virus stock in a water bath at 37°C but carefully leaving the cap and oring out of the water. After thawed, spray the vial with 70% ethanol in excess.

- 1.40 Add the virus solution, 192 μ L of Trypsin (dose: 8 μ L Trypsin/ml virus solution), and 24 mL of MEM (already kept at 37°C) to a 33 mm polyethylene flat-top screw cap sterile 50 mL conical centrifuge tubes (BD Falcon). Incubate at 37°C for 30 minutes. By exposing rotavirus to trypsin, the infectivity of viral particles increases significantly. Right after use, the trypsin solution must be stored at -70°C.
- 1.41 Remove the CELL MEM solution from the confluent MA-104 cells in the 850 cm² roller bottle by pipetting with a new 25 mL sterile polystyrene disposable serological pipette using a Drummond portable Pipet-Aid. Dispose this used CELL MEM in the MEM WASTE container. Immediately rinse the MA-104 cells twice with 15 mL of PBS by pipetting with a new 25 mL sterile polystyrene disposable serological pipette using a Drummond portable Pipet-Aid. Dispose this used PBS in the MEM WASTE container.
- 1.42 Add 3 mL of the recently-trypsinised rotavirus solution and 12 mL of MEM to the 850 cm² roller bottle and incubate for 90 minutes at 37°C and in a 5% CO₂ environment by rotation at 0.75 rpm.
- 1.43 Remove the viral solution by pipetting with a new 25 mL sterile polystyrene disposable serological pipette using a Drummond portable Pipet-Aid, and subsequently rinse the cells with 15 mL PBS. Discard the viral solution and rinsing PBS solution in the MEM WASTE container.
- 1.44 Add 15 mL of MEM (Already kept at 37°C) to the 850 cm² roller bottle by pipetting with a new 25 mL sterile polystyrene disposable serological pipette using a Drummond portable Pipet-Aid and incubate at 37°C and in a 5% CO₂ environment by rotation at 0.75 rpm.

- 1.45 Conduct this process of rotavirus infection on MA-104 cells for the rest of the seven roller bottles, one at a time.
- 1.46 Incubate the 8 roller bottles until cytopathic effects are evident (some rounding, cell degeneration, and sloughing), and must be monitored under a microscope (10X). When at least approximately 90% of the cells are detached (usually below 24 hours), remove the cell/viral solution by pipetting with a new 25 mL sterile polystyrene disposable serological pipette using a Drummond portable Pipet-Aid and store in 4 sterile 50 mL conical centrifuge tubes (30 ml of viral/cell solution per centrifuge tube).
- 1.47 Properly discard every disposable material that has been in contact with MA-104 cells (e.g., flasks, roller bottles, pipettes) or rotavirus in biohazard bags for further 30 minutes gravity autoclave process. Autoclave the effluents produced from this rotavirus production process (e.g., MEM and PBS) along with every non-disposable material that has been in contact with MA-104 cells or rotavirus in 30 minutes liquid process.
- 1.48 Store the four 50 ml centrifuge tubes at -70°C for 24 hours and then thaw them in a water bath at 37°C. This sudden change in temperature causes the MA-104 cells to break apart and to liberate rotavirus particles that might still be inside partially-lysed cells. Repeat this process a total of 3 times.

2 Rotavirus stock concentration and purification^{3, 4}

- 2.1 The next centrifugation and sequential filtration steps are conducted to remove relatively large cell fragments and are optimized to minimize the loss of rotavirus particles during the process.
- 2.2 Aliquot the viral solution (ca. 200 mL) in four 33 mm polyethylene flat-top screw cap sterile 50 mL conical centrifuge tubes (BD Falcon). The caps must be screwed with

sterile 33x1.5 mm (internal diameter x cross section) nitrile orings to prevent biohazard spills during the next centrifugation step.

- 2.3 Centrifuge the four 50 mL conical tubes at 5000 rpm in a Eppendorf centrifuge 5416 for 15 minutes. A whitish pellet made of lysed cells and a red and clear supernatant (i.e., containing rotavirus particles in MEM solution) with no apparent suspended solids is produced after the centrifugation process. Carefully remove the supernatant without re-suspending the pellet by pipetting with a 25 mL sterile polystyrene disposable serological pipette with magnifier stripe (Fisherbrand) using a Drummond 4-000-100 portable Pipet-Aid. Pour the supernatant in a 500 mL 45 mm diameter neck sterile Pyrex media bottle. Take a 0.5 mL sample in an Eppendorf Snap-Cap 2 mL Microcentrifuge Safe-Lock Tubes (label properly) for further infectivity assay.
- 2.4 Vacuum-filter the viral solution (ca. 200 mL) through a disposable sterile 45 mm diameter bottle-top 0.45 µm cellulose acetate (CA) membrane filter (Corning) into a 500 mL 45 mm diameter neck sterile Pyrex media bottle. Large cell fragments that were not separated during the previous centrifugation step are removed. Take a 0.5 mL sample for further infectivity assay.
- 2.5 Similarly to the previous step, vacuum-filter the viral solution (ca. 200 mL) through a disposable sterile 45 mm diameter bottle-top 0.22 µm cellulose acetate (CA) membrane filter (Corning) into a 500 mL 45 mm diameter neck sterile Pyrex media bottle. Small cell fragments that were not separated during the previous filtration step are removed. Take a 0.5 mL sample for further infectivity assay.
- 2.6 The next dialysis/concentration step is conducted to remove small cell debris and MEM, delivering a pure and concentrated rotavirus stock solution.

- 2.7 Prepare 2x1 L of 1 mM NaCl and 0.1 mM CaCl₂ solution by adding 0.058 g of NaCl and 0.011 g of CaCl₂ in 1 liter of ultrapure double-deionized water (18 MΩ-cm resistivity). Filter this solution through a disposable sterile 45 mm diameter bottle-top 0.22 μm cellulose acetate (CA) membrane filter (Corning) into a 1 L 45 mm diameter neck sterile Pyrex media bottle.
- 2.8 Place a 63.5 mm diameter 100 kDa polyvinylidene difluoride (PVDF) sterile membrane (HFM-180, Koch membranes) in a 200 mL Millipore Amicon Bioseparations Stirred Cell (model 8200). Pour the viral solution (ca. 200 mL) in the Amicon cell and connect it directly to a pressure valve-regulated ultrapure Nitrogen gas (N₂) tank. By directly applying N₂ gas at 40 psi pressure and a stirring velocity of approximately 60 rpm, small debris and MEM will be removed through the ultrafiltration PVDF membrane while the rotavirus particles will be kept in the Amicon cell. Collect the effluents in a 1 L 45 mm diameter neck Pyrex media bottle. Stop the process by closing the pressure valve when the viral solution inside the Amicon cell reaches approximately 20 mL. Add 180 mL of the previously prepared 1 mM NaCl and 0.1 mM CaCl₂ solution in the Amicon cell, close the cap, and apply direct N₂ gas pressure until the viral solution reaches approximately 20 mL. Repeat this process a total of 11 times, until finishing the 2 L of previously prepared 1 mM NaCl and 0.1 mM CaCl₂ solution. Remove the remaining 20 mL of purified rotavirus solution and aliquot in ten Eppendorf Snap-Cap 2 mL Microcentrifuge Safe-Lock Tubes (label properly). Store this rotavirus stock at 4°C in the dark. Take a 0.2 mL sample for further infectivity assay.
- 2.9 Measure the hydrodynamic diameter of rotavirus in a Zetasizer ZS90, by pouring 100 μL of the rotavirus stock in a disposable micro cuvette (ZEN0118). The rotavirus population

can be considered as monodispersed if the hydrodynamic size does not exceed 110 nm with a polydispersivity index (PDI or wide parameter of the cummulant analysis) lower than 0.2 (one peak distribution population).

- 2.10 Properly discard every disposable material that has been in contact with MA-104 cells or rotavirus (e.g., 50 mL centrifuge tubes, pipettes, bottle-top CA membrane filters, PVDF membrane) in biohazard bags for further 30 minutes gravity autoclave process. Autoclave the approximately 2.18 L effluents produced from this dialysis-concentration process along with every non-disposable material that has been in contact with MA-104 cells or rotavirus (e.g., Amicon ultrafiltration cell, 500 mL and 1 L Pyrex bottles) in 30 minutes liquid process.
- 2.11 Conduct an infectivity assay with the samples collected, as described in the next section, to assess the loss of rotavirus particles during the process of stock concentration and purification.

3 Focal forming unit infectivity assay^{1,2}

- 3.1 After cell confluence confirmation of the 150 cm² flask originally destined for FFU assay (Section 1), start the process of splitting cells and setting up 24-well tissue culture plates as follows: place a CELL MEM bottle and a PBS bottle at 37°C for 2 hours.
- 3.2 Thaw a bottle of Trypsin/EDTA solution (originally at -20°C) at 37°C in a water bath.
- 3.3 Remove the CELL MEM solution from the confluent MA-104 cells in the 150 cm² flask by pipetting with a new 25 mL sterile polystyrene disposable serological pipette using a Drummond portable Pipet-Aid. Immediately rinse the MA-104 cells twice with 7 mL of PBS by pipetting with a new 10 mL sterile polystyrene disposable serological pipette

- using a Drummond portable Pipet-Aid. Dispose this used PBS and CELL MEM solution in the MEM WASTE container.
- 3.4 Add 3 ml of the Trypsin/EDTA solution to the monolayer of MA-104 cells and rock the flask to evenly coat the cells with the Trypsin/EDTA solution.
 - 3.5 Incubate the flask at 37°C and in a 5% CO₂ environment for approximately 5 minutes.
 - 3.6 After the 5 minutes, gently hit the flask with the palm of the hand to detach cells from the flask. Then, carefully monitor under the microscope (10X) the dissociation of cells from the substrate of the flask. If a considerable fraction of the cells are still attached to the substrate, place again the flask into incubation for additional 2 minutes, and constantly monitor the progress of detachment of cells. As similarly described in the previous section, if over-exposure to Trypsin/EDTA, cells may not be able to attach to a new substrate again.
 - 3.7 Once confirmed the detachment of the majority of cells, add 70 mL of MEM CELL by pipetting with a new 25 mL sterile polystyrene disposable serological pipette using a Drummond portable Pipet-Aid. Titrate the cell-solution with the pipette to avoid fast sedimentation of cells due to their large size.
 - 3.8 Pipette 1 mL of the cell-solution to every well of three 24-well tissue culture plates (BD Falcon# 08-772-1H).
 - 3.9 Return the PBS and CELL MEM bottle to -4°C and the Trypsin/EDTA bottle to -20°C.
 - 3.10 Incubate the three 24-well tissue culture plates at 37°C and in a 5% CO₂ environment for 48 hours. Repeat the procedures described in the previous sections for media renewal and periodically monitor the growth of cells under a microscope (10X) until confluence. To achieve confluence of MA-104 cells in culture plates usually takes several days.

- 3.11 When cells in the 24-well plates are confluent, follow the next protocol for infection of cells with rotavirus, one plate at a time.
- 3.12 Place one microcentrifuge Safe-Lock Tube containing trypsin solution (already aliquoted in the previous section), a MEM bottle, and a PBS bottle at 37°C for 2 hours. Be careful not to confuse MEM with CELL MEM.
- 3.13 As described in the previous sections, trypsinise all your rotavirus samples with 10 µL of trypsin solution per 1.0 ml of virus sample and incubate for 30 minutes at 37°C.
- 3.14 In the meantime, properly mark (codify) 1 mL microcentrifuge Safe-Lock Tube for serial dilutions of rotavirus samples. Recommended dilutions for rotavirus samples are: 1/5, 1/10, 1/50, 1/100, 1/500, and 1/1,000.
- 3.15 Serially dilute trypsinised rotavirus samples in MEM solution in the prepared microcentrifuge tubes to a final volume of 500 µL (for example: dilution 1/10 contains 50 µL of trypsinised rotavirus sample and 450 µL MEM solution).
- 3.16 Remove the media from every well of the plate and rinse twice with 2 mL of PBS per well. A 12-channel pipetter (Eppendorf# 13-688-512, 30 to 300 µL) is highly recommended at this step of this process.
- 3.17 The distribution of the wells in tissue culture plates follows the next notation: rows are labeled A, B, C, and D; while columns are labeled 1, 2, 3, 4, 5, and 6. Add 100 µL of previously diluted rotavirus samples to each well, keeping track of the location of the each diluted sample.
- 3.18 It is highly recommended to pipette 100 µL of only MEM solution to well D6 as a negative control (i.e., no FFU should be detected after further immunocytochemistry analysis in this well).

- 3.19 Incubate the plate at 37°C and in a 5% CO₂ environment for 30 minutes.
- 3.20 Remove the viral solution from each well. Rinse each well with 1 mL MEM solution. Once again, it is highly advisable to use a multichannel pipetter for these steps.
- 3.21 Add 1 mL MEM solution per well and Incubate the plate at 37°C and in a 5% CO₂ environment for 16 to 18 hours.
- 3.22 Return the PBS and MEM bottle to -4°C, and properly discard every disposable material that has been in contact with MA-104 cells (e.g., pipetter tips, flasks) or rotavirus in biohazard bags for further 30 minutes gravity autoclave process. Autoclave the effluents produced from this rotavirus production process (e.g., MEM and PBS) along with every non-disposable material that has been in contact with MA-104 cells or rotavirus in 30 minutes liquid process.
- 3.23 The immunochemical detection of virus-infected cells (FFU infectivity assay) is conducted following the next protocol:
- 3.24 Prepare 200 mL of the 9:1 methanol:glacial acetic acid, by adding 180 mL of Methanol to 20 mL of glacial acetic acid in a 250 mL Pyrex beaker. Prepare 200 mL of 70% ethanol solution, by adding 140 mL of ethanol to 60 mL of de-ionized water in a 250 mL Pyrex beaker. Prepare 200 mL of 50% ethanol solution, by adding 100 mL of ethanol to 100 mL of de-ionized water in a 250 mL Pyrex beaker. Prepare 1 liter of wash buffer by adding 15.15 g TRIS-HCl (Fisher Scientific# PR-H5121), 20.45 g NaCl, 3.47 g TRIS-base (Fisher Scientific# PR-H5133), and 2.5 mL Triton X-100 (Fisher Scientific# NC9903183) to 1 L of deionized water (wash buffer must be kept at -4°C until used). The solutions described above were prepared in large volumes for multiple FFU assays and can be stored for long periods of time. Label the containers.

- 3.25 The next solutions were prepared in small volumes for approximately one infectivity assay. Prepare 8 mL of 3% H_2O_2 solution by adding 800 μL of 30% H_2O_2 (Fisher Scientific# H325-100) to 7.2 mL of wash buffer in a 15 mL conical centrifuge tube. Prepare 8 mL of 5% normal goat serum (NGS, Fisher Scientific# NC9270494) by adding 400 μL of NGS to 7.6 mL of wash buffer in a 15 mL conical centrifuge tube. Prepare 8 mL of rabbit anti-human rotavirus antibody solution (termed in this study as 1st antibody) by adding 80 μL of 1st antibody (AbB Serotec# AHP1360) to 7.9 mL of wash buffer in a 15 mL conical centrifuge tube. Prepare 8 mL of bio-tinylated goat anti-rabbit IgG solution (termed in this study as 2nd antibody) by adding 120 μL of NGS and 40 μL of 2nd antibody to 7.9 mL of wash buffer in a 15 mL conical centrifuge tube. Properly label all containers.
- 3.26 The timing of every upcoming steps must be followed rigorously using a chronometer. In addition, once the FFU assay is started, it cannot be interrupted until completing the entire process (approximately 4 hours). The process of “incubation” during immunocytochemistry is conducted at ambient temperature on a rocking platform (Fisher Scientific# 13-878-475) unless otherwise indicated. Furthermore, it is highly advisable to use a multichannel pipetter during the entire infectivity assay.
- 3.27 Remove the MEM solution from all the wells and rinse twice with 1 mL of PBS solution per well.
- 3.28 Fix the cells by adding 1 mL of 9:1 methanol:glacial acetic acid solution per well for 2 minutes. Remove immediately the fixing solution and place it in a separate labeled-container for further proper disposal due to high its toxicity.

- 3.29 Rehydrate cells by adding 500 μ L of 70% ethanol to every well and incubate for 5 minutes. After removing the 70% ethanol solution, continue the rehydration process by adding 500 μ L of 50% ethanol and incubate for 5 minutes. Remove the 50% ethanol solution.
- 3.30 Quench any endogenous peroxidase activity by adding 150 μ L 3% H_2O_2 solution per well and incubate for 10 minutes. Remove the 3% H_2O_2 solution.
- 3.31 Add 500 μ L of wash buffer per well and incubate for 10 minutes. Remove the wash buffer solution.
- 3.32 Add 150 μ L of 5% NGS solution per well to inhibit any nonspecific primary antibody binding and incubate for 20 minutes. Remove the 5% NGS solution.
- 3.33 Add 150 μ L of 1st antibody solution to each well and incubate at 37°C for 1 hour. Remove the 1st antibody solution.
- 3.34 Add 500 μ L of wash buffer per well and incubate for 10 minutes. Remove the wash buffer solution.
- 3.35 Add 500 μ L of wash buffer per well and incubate for 10 minutes. Remove the wash buffer solution.
- 3.36 Add 150 μ L of 2nd antibody solution to each well and incubate for 20 minutes.
- 3.37 During incubation of the 2nd antibody solution, prepare 8 mL of Vectastain ABC solution (Fisher Scientific# NC9313719) by adding 160 μ L of reagent A and 160 μ L of reagent B to 7.6 mL of wash buffer in a 15 mL conical centrifuge tube. In addition, prepare 8 mL of DAB solution (KLP DAB kit, Fisher Scientific# NC9068240) by adding 3 drops of TRIS buffer, 2 drops of DAB, 2 drops of H_2O_2 (these 3 reagents are included in the DAB

- kit) to 8 mL of deionized water in a 15 mL conical centrifuge tube. Remove the 2nd antibody solution.
- 3.38 Add 500 μ L of wash buffer per well and incubate for 10 minutes. Remove the wash buffer solution.
- 3.39 Add 500 μ L of wash buffer per well and incubate for 10 minutes. Remove the wash buffer solution.
- 3.40 Add 150 μ L of Vectastain ABC solution to each well and incubate for 20 minutes. Remove the Vectastain ABC solution.
- 3.41 Add 500 μ L of wash buffer per well and incubate for 10 minutes. Remove the wash buffer solution.
- 3.42 Add 500 μ L of wash buffer per well and incubate for 10 minutes. Remove the wash buffer solution.
- 3.43 Add 150 μ L of DAB solution to each well and incubate for 20 minutes. Remove the DAB solution and dispose in a separate labeled-container for further proper disposal due to its toxicity.
- 3.44 Add 500 mL of deionized water to each well.
- 3.45 Properly discard every disposable material that has been in contact with MA-104 cells or rotavirus in biohazard bags for further 30 minutes gravity autoclave process. Autoclave the effluents produced from this immunocytochemistry process along with every non-disposable material that has been in contact with MA-104 cells or rotavirus in 30 minutes liquid process. Properly store glacial acetic acid/methanol solution, 70% and 50% ethanol solutions in chemical cabinets in their corresponding sections.

- 3.46 Use a 10X microscope to inspect the integrity of the monolayer of cells in each well. If the process was conducted carefully, no significant detachment should be evident.

4 Preparation of natural organic matter (NOM) samples

- 4.1 Prepare 500 mL of 1 mM NaHCO₃ solution by adding 0.042 g of NaHCO₃ to 500 mL of DDI water (18 MΩ-cm resistivity). Measure the pH of this solution, which should be 8.3. Filter this solution through a disposable sterile 45 mm diameter bottle-top 0.22 μm cellulose acetate (CA) membrane filter (Corning) into a 500 mL 45 mm diameter neck sterile Pyrex media bottle. The pH of the solution should not experience any variation.
- 4.2 Add 10 mg of the NOM sample (originally kept in a desiccator at ambient temperature) to 50 mL of the previously prepared 1 mM NaHCO₃ solution in a sterile 50 mL conical centrifuge tube (BD Falcon). Cover the NOM solution from the light with aluminum foil and rotate using a Lab tube/vial Rotator (Glas Col #099A RD4512, Terre Haute, USA) at 6 rpm overnight.
- 4.3 Filter the NOM solution through a disposable sterile 33 mm diameter bottle-top 0.22 μm cellulose acetate (CA) membrane filter (Corning) into a sterile 50 mL conical centrifuge tube (BD Falcon). Take 1 mL of the NOM sample in an Eppendorf Snap-Cap 2 mL Microcentrifuge Safe-Lock Tube for further total organic carbon (TOC) measurement. Aliquot the NOM solution in five sterile 15 mL conical centrifuge tube (BD Falcon), label properly, cover from light with aluminum foil, and finally store at -4°C.
- 4.4 Measure the TOC of the NOM sample using a Phoenix 8000 TOC analyzer (Dohrmann, USA).

5 Cleaning of silica surfaces⁵

- 5.1 Prepare 2% Hellmanex solution by diluting 5 mL of Hellmanex (Hellma Analytics, USA) solution in 245 mL of DI water in a sterile 250 mL Pyrex bottle. In addition, prepare 100 mL of sulfuric acid/nochromix solution by adding 30 g nochromix/L (dose: 3 g nochromix) to 98% sulfuric acid in a 250 mL sterile Pyrex bottle.
- 5.2 Silica surfaces were obtained from Q-sense (Sweeden) with a surface area of approximately 0.7 cm².
- 5.3 Cleaning procedure of silica surfaces were conducted as follows: carefully place the silica surface in a Teflon holder (Q-Sense Sensor Holder, Sweden) using tweezers (AFM Cantilever Tweezers, NM-SS, TedPella, USA). Pour 50 mL of 2% Hellmanex solution in a sterile 100 mL Pyrex beaker. Immerse the Teflon holder with the silica surface in the 2% Hellmanex solution for 120 minutes. Remove the Teflon holder from the 2% Hellmanex solution. Using tweezers remove the silica surface from the Teflon holder and rinse with DI water in excess. Dry the surface using ultrapure nitrogen gas (N₂).
- 5.4 Using tweezers, place the silica surface in a (60 mm diameter x 15 mm height) sterile Pyrex petri dish (Corning #08-747A). Using a 1 mL Pyrex serological pipette (Corning #13-671-101C), pipette 400 µL of sulfuric acid/nochromix solution on the silica surface, cover the petri dish, and store at -4°C for 24 hours. Remove the sulfuric acid/nochromix solution with a 1 mL Pyrex serological pipette (properly dispose this solution) and rinse the silica surface with DI water in excess (using tweezers). Dry the surface using ultrapure nitrogen gas (N₂).
- 5.5 Using tweezers, place the silica surface at the center of a microscope glass slide (3"x1"x1.0mm, Fisher #12-550-343, USA). Insert the glass slide in an Ozone/UC

chamber (BioForce Nano-Sciences Inc., Ames, IA) and oxidize the colloidal probe for 30 minutes.

6 Cleaning of new AFM colloidal probes

- 6.1 Before starting the cleaning procedure of the AFM probes, measure the sensitivity and spring constant of the AFM silica colloidal probes as describe in the section above.
- 6.2 Pipette 7 mL of 70% ethanol to a new 47 mm sterile disposable tight-fit lid petri dish (BD Falcon #08-757-105).
- 6.3 It is highly recommended to use a microscope (10X) for the manipulation of the AFM silica colloidal probes.
- 6.4 Using tweezers (AFM Cantilever Tweezers, NM-SS, TedPella, USA), carefully immerse the silica colloidal probe (once again always grab it by the supporting chip and do not actually touch the cantilever) in the ethanol solution for 2 hours.
- 6.5 Pipette 7 mL of DI water to a new 47 mm sterile disposable tight-fit lid petri dish (BD Falcon #08-757-105).
- 6.6 Remove the silica colloidal probe from the ethanol solution and immerse in DI water for 2 hours.
- 6.7 Remove the colloidal probe from DI water and place it at the center of a microscope glass slide (3"x1"x1.0mm, Fisher #12-550-343, USA). Under a microscope (10X), carefully dry the support chip (cantilever base usually made of silica) with Kimwipes without touching the cantilever.
- 6.8 Oxidize the colloidal probe (along with the glass slide) in an Ozone/UC chamber (BioForce Nano-Sciences Inc., Ames, IA) for 30 minutes.

6.9 Store the clean colloidal probe in a sterile glass bottom culture petri dish (35 mm petri dish, 14 mm microwell, MatTek #P35G-0-14-C) until further coating.

7 Measuring sensitivity and spring constant of AFM colloidal probes

7.1 Obtain 1 μm (diameter) silica (SiO_2) colloidal probes (silicon nitride cantilever 0.06 N/m, Novascan #PT.SiO2.SN.1).

7.2 A MFP-3D Stand Alone (SA) Atomic Force Microscope (Asylum Research, USA) will be used in this study.

7.3 Turn on the Molecular Force Probe 3D controller. Subsequently, turn on the Laser switch and wait 30 minutes for the laser to warm up.

7.4 Turn on the Fiber lite MI-150OR High Intensity Illuminator (Dolan Jenner, USA) and set the intensity controller to 100%.

7.5 Load (Igor Pro-based) MFP-3D software (Asylum Research, USA).

7.6 Carefully remove the Head and place it upside-down next to the Base.

7.7 Remove the standard cantilever holder by pushing the black pin located at the front to release the holder.

7.8 Under a microscope (10X) and using tweezers (AFM Cantilever Tweezers, NM-SS, TedPella, USA), carefully place the silica colloidal probe (always grab it by the supporting chip and do not actually touch the cantilever itself) on the holder and secure it using a small Phillips screwdriver (usually 2 soft turns are enough to prevent breaking the cantilever).

7.9 Place the cantilever holder back in the head, making sure to push the black pin to secure the holder.

- 7.10 Place a previously cleaned calibration grid (rinsed in 70% ethanol, DI water, and dried with ultrapure N₂) on the stage (top of the base) and secure it at the corners with 2 small magnets.
- 7.11 Carefully place the Head back on top of the base.
- 7.12 The stage is micrometer driven for mechanical alignment of the silica colloidal probe and calibration grid. Therefore, manually align the head by rotating the 3 knobs that controls the three legs of the head. Allow a separation distance of only a couple of millimeters between the calibration grid and the cantilever.
- 7.13 In the MAIN tab, click IMAGING MODE, and select CONTACT mode, and set the SETPOINT to 1 volt.
- 7.14 Select INCREASING and RELATIVE by clicking on these options.
- 7.15 Adjust the SCAN RATE to 0.3 Hz. This rate results in a VELOCITY of 600 nm/s, which is a parameter commonly used in these studies.
- 7.16 Adjust the FORCE DISTANCE to 1 μ m.
- 7.17 Turn on VIDEO CAPTURING, by clicking the VIDEO icon. An image of the cantilever will be visualized. Adjust the focus of the image with the CAMERA knob located at the rear of the head. If necessary, adjust the field diaphragm located at the front of the base for a better image.
- 7.18 The cantilever must look black in color. If yellowish, the cantilever is probably bended (and therefore no longer useful). To rule out this possibility, repeat the silica colloidal probe mounting process.
- 7.19 Aim the laser light to the very tip of the cantilever with the X and Y knobs located at the sides of the head. Slightly move the laser across the tip of the cantilever for maximizing

- the SUM signal (constantly monitor the SUM at the SUM AND DEFLECTION METER window). A maximized SUM usually ranges from 4 to 6 (depending on the cantilever).
- 7.20 Adjust the deflection to zero with the DEFLECTION KNOB located at the side of the head, always monitoring the SUM AND DEFLECTION METER window.
 - 7.21 Manually place a static neutralizer close to the cantilever holder (this is only necessary in air scanning and not in liquid scanning)
 - 7.22 At this point we must remember that there is an approximate separation distance of a couple of millimeters between the AFM probe and the calibration grid.
 - 7.23 Click ENGAGE at the SUM AND DEFLECTION METER window. The Z VOLTAGE will go up to 150.
 - 7.24 Manually approach the AFM probe to the calibration grid by lowering the head with the front knob until the Z-VOLTAGE at the SUM AND DEFLECTION METER window reaches approximately 70. A beep will alert when reaching this level (hitting the SETPOINT of 1 volt).
 - 7.25 Click WITHDRAW at the SUM AND DEFLECTION METER window.
 - 7.26 Click SINGLE FORCE at the MAIN window. A new window will open and a force versus distance curve (approaching on red and retraction on black) will be generated. Focus on approaching regime only (red curve).
 - 7.27 Click CONTROL+I, and a small window will pop-up. Drag the hollowed-circle icon (labeled A) to the beginning of the approaching curve (force=0, where there is no interaction between the AFM probe and the calibration grid). Similarly, drag the hollowed-squared icon (labeled B) to approximately 500 nm from the beginning of the approaching curve.

- 7.28 On the FORCE window, at the CAL tab, click SENSITIVITY, and select VIRTUAL DEFL LINE. This option corrects the slope of approaching curve during the “no interaction” regime (slope should be = 0).
- 7.29 Click WITHDRAW at the SUM AND DEFLECTION METER window (always withdraw before generating a new force versus distance curve).
- 7.30 Click again SINGLE FORCE at the MAIN window. A new force versus distance curve will be generated. Click again CONTROL+I, and a small window will pop-up. This time drag the hollowed-circle icon (labeled A) to the end of the approaching curve, which corresponds to the end of the contact regime between the AFM probe and the calibration grid. Similarly, drag the hollowed-squared icon (labeled B) to approximately the beginning of the contact regime. The contact region between the AFM probe and the calibration grid is characterized by a perfectly linear regime.
- 7.31 On the FORCE window, at the CAL tab, click SENSITIVITY, and select DEFL INVOLS. This option calculates the sensitivity of the cantilever. Write down the value of the sensitivity (in units of nm/V) displayed at the DEFL INVOLS cell in the CAL tab.
- 7.32 Raise the head using the front knob.
- 7.33 At the THERMAL tab, click CAPTURE THERMAL DATA and a new window displaying the thermal spectra of the cantilever will pop-up.
- 7.34 At ZOOM CENTER, select the approximate location of the center of the most prominent peak (in units of Hz). This value is highly dependent on the cantilever and is usually mentioned by the vendor in the technical specifications.
- 7.35 At ZOOM WIDTH, select the approximate width of the most prominent peak (in units of Hz).

- 7.36 Click INITIALIZE FIT. This fit will be conducted on the selected peak and will result on the calculation of the spring constant of the cantilever. Write down the value of the SPRING CONSTANT (in units of pN/nm) displayed at the DEFL INVOLS cell in the CAL tab.
- 7.37 Close the THERMAL window.
- 7.38 Remove the head and place it upside down next to the base.
- 7.39 Remove the cantilever holder as previously describe. In addition, using tweezers and under a microscope (10X), remove the silica colloidal probe from the holder and carefully place it in an AFM probe box. Label this silica colloidal probe and record the values of sensitivity and spring constant.
- 7.40 Turn off the software, turn off the laser switch, set the intensity controller to 0, turn off the high intensity illumination switch, and finally turn off the power of the molecular force probe 3D controller.

8 NOM coating protocol of silica surfaces⁶

- 8.1 Prepare 50 mL of HEPES buffer by adding 100 mM NaCl (0.292 g NaCl) and 10 mM N-(2-hydroxyethyl) piperazine-N'-2-ethanesulfonic acid (0.130g HEPES) to 50 mL of DI water in a 50 mL conical centrifuge tube.
- 8.2 Prepare PLL solution by dissolving poly-L-lysine (PLL) hydrobromide (Fisher # ICN10269180) in HEPES buffer at a final concentration of 0.1 g/L in the original PLL glass container.
- 8.3 The coating protocol of silica surfaces will be conducted following the layer-by-layer procedure as follows: place the silica surface back in the sterile Pyrex petri dish and pipette 400 μ L of PLL solution on the surface and allow to coat for 8 hours. Remove the

PLL solution by pipetting. Rinse twice the now PLL-coated surface by pipetting 400 μ L of DI water. This rinsing procedure must be conducted carefully to avoid touching the surface.

8.4 Pipette 400 μ L of NOM stock solution on the PLL-coated silica surface and allow to coat for 8 hours. Remove the NOM solution by pipetting. Rinse twice the now NOM-coated surface by pipetting 400 μ L of DI water. This rinsing procedure must be conducted carefully to avoid touching the surface.

8.5 Using double-sided tape, immediately glue the silica surface to the center of a microscope glass slide (3"x1"x1.0mm, Fisher #12-550-343, USA)

8.6 Pipette 200 μ L of DI water on the NOM-coated silica surface to keep the NOM hydrated (do not allow the NOM layer to dry). Desiccation of NOM may affect its interactions with rotavirus, and therefore produce non-representative force vs. distance profiles.

8.7 Immediately use this sample for NOM experimentation.

9 Rotavirus coating protocol of AFM colloidal probes⁶

9.1 The coating protocol of AFM colloidal probes will be conducted following the layer-by-layer procedure as follows: pipette 400 μ L of PLL solution in a sterile glass bottom culture petri dish (35 mm petri dish, 14 mm microwell, MatTek #P35G-0-14-C).

9.2 Pipette 7 mL of DI water into 2 new 47 mm sterile disposable tight-fit lid petri dish (BD Falcon #08-757-105).

9.3 It is highly recommended to use a microscope (10X) for the manipulation of the AFM silica colloidal probes.

9.4 Using tweezers carefully place the clean AFM silica colloidal probe in the PLL solution and allow to coat for 8 hours.

- 9.5 Using tweezers carefully remove the now PLL-coated silica colloidal probe from the PLL solution and place it in the first petri dish containing DI water for 3 to 5 minutes for rinsing purposes.
- 9.6 On a separate new sterile glass bottom culture petri dish, pipette 400 μL of rotavirus stock solution.
- 9.7 Remove the PLL-coated silica colloidal probe from the petri dish containing DI water and immerse it in the rotavirus solution and allow to coat for 8 hours.
- 9.8 Remove the rotavirus-coated silica colloidal probe from the rotavirus solution and place it in the second petri dish containing DI water for 3 to 5 minutes for rinsing purposes.
- 9.9 Immediately start AFM experiments and do not allow the rotavirus-coated silica colloidal probe to dry. Desiccation of rotavirus may affect its interactions with NOM, and therefore produce non-representative force vs. distance profiles.
- 10 Probing rotavirus-coated probes on NOM-coated silica surface with Atomic force microscopy⁶**
 - 10.1 Turn on the Molecular Force Probe 3D controller. Subsequently, turn on the Laser switch and wait 30 minutes for the laser to warm up.
 - 10.2 Turn on the Fiber lite MI-150OR High Intensity Illuminator (Dolan Jenner, USA) and set the intensity controller to 100%.
 - 10.3 Load (Igor Pro-based) MFP-3D software (Asylum Research, USA).
 - 10.4 Carefully remove the Head and place it upside-down next to the Base.
 - 10.5 Remove the standard cantilever holder by pushing the black pin located at the front to release the holder.

- 10.6 Under a microscope (10X) and using tweezers (AFM Cantilever Tweezers, NM-SS, TedPella, USA), remove the (recently prepared) rotavirus-coated silica colloid from DI water and place it in a microscope glass slide. Carefully dry the support chip with Kimwipes without touching the cantilever. By drying the support chip, it will become easier to place the AFM probe on the holder.
- 10.7 If the next steps are conducted quick enough then the cantilever, and therefore the rotavirus-coated colloid, will remain wet.
- 10.8 Using tweezers, place the rotavirus-coated silica colloidal probe (always grab it by the supporting chip and do not actually touch the cantilever itself) on the holder and secure it using a small Phillips screwdriver (usually 2 soft turns are enough to prevent breaking the cantilever).
- 10.9 Place the cantilever holder back in the head, making sure to push the black pin to secure the holder.
- 10.10 Place a NOM-coated silica surface (already glued in a microscope glass slide) on the stage (top of the base) and secure it at the corners with 2 small magnets.
- 10.11 Carefully place the Head back on top of the base.
- 10.12 The stage is micrometer driven for mechanical alignment of the cantilever and calibration grid. Therefore, manually align the head by rotating the 3 knobs that controls the three legs of the head. Allow a separation distance of only a couple of millimeters between the calibration grid and the rotavirus-coated silica probe.
- 10.13 With the left hand lift the head from the front (the 2 back legs must be in contact with the stage while the front leg is lifted).

- 10.14 With the right hand pipette approximately 200 μL of the desired electrolyte solution on top of the NOM-coated silica surface without touching the substrate.
- 10.15 Slowly lower the head, allowing the holder to carefully immerse in the 200 μL of electrolyte solution.
- 10.16 In the MAIN tab, click IMAGING MODE, and select CONTACT mode, and set the SETPOINT to 1 volt.
- 10.17 Select INCREASING and RELATIVE by clicking on these options.
- 10.18 Adjust the SCAN RATE to 0.3 Hz. This rate results in a VELOCITY of 600 nm/s, which is a parameter commonly used in these studies.
- 10.19 Adjust the FORCE DISTANCE to 1 μm .
- 10.20 Turn on VIDEO CAPTURING, by clicking the VIDEO icon. Similarly to air conditions (described in the previous section), an image of the cantilever will be visualized in the electrolyte solution. Adjust the focus of the image with the CAMERA knob located at the rear of the head. If necessary, adjust the field diaphragm located at the front of the base for a better image.
- 10.21 The cantilever must look black in color. If yellowish, the cantilever is probably bended (and therefore no longer useful). To rule out this possibility, repeat the rotavirus-coated silica colloidal probe mounting process.
- 10.22 Aim the laser light to the very tip of the cantilever with the X and Y knobs located at the sides of the head. Slightly move the laser across the tip of the cantilever for maximizing the SUM signal (constantly monitor the SUM at the SUM AND DEFLECTION METER window). Similarly to air conditions, a maximized SUM usually ranges from 4 to 6 (depending on the cantilever).

- 10.23 The DEFLECTION value at the SUM AND DEFLECTION METER window, should display unstable decreasing values with time (this unstable regime occurs in solution due to the stabilization of the cantilever to the electrolyte conditions). Before adjusting the deflection to zero (in the next step), wait at least 15 minutes until deflection stabilizes in a fix value.
- 10.24 Adjust the deflection to zero with the DEFLECTION KNOB located at the side of the head, always monitoring the SUM AND DEFLECTION METER window.
- 10.25 In the FORCE window, manually input the values of sensitivity and spring constant obtained for this specific cantilever during the previous section.
- 10.26 At this point we must remember that there is still an approximate separation distance of a couple of millimeters between the AFM probe and the calibration grid.
- 10.27 Click ENGAGE at the SUM AND DEFLECTION METER window. The Z VOLTAGE will go up to 150.
- 10.28 Lower the head with the front knob until the Z-VOLTAGE at the SUM AND DEFLECTION METER window reaches approximately 70. A beep will alert when reaching this level (hitting the SETPOINT of 1 volt).
- 10.29 Click WITHDRAW at the SUM AND DEFLECTION METER window.
- 10.30 Click SINGLE FORCE at the MAIN window. A new window will open and a force versus distance curve (approaching on red and retraction on black) will be generated. Focus on approaching regime only (red curve).
- 10.31 Click CONTROL+I, and a small window will pop-up. Drag the hollowed-circle icon (labeled A) to the beginning of the approaching curve (force=0, where there is no interaction between the AFM probe and the calibration grid). Similarly, drag the

- hollowed-squared icon (labeled B) to approximately 500 nm from the beginning of the approaching curve.
- 10.32 On the FORCE window, at the CAL tab, click SENSITIVITY, and select VIRTUAL DEFL LINE. This option corrects the slope of the approaching curve during the “no interaction” regime (slope should be = 0).
- 10.33 Click WITHDRAW at the SUM AND DEFLECTION METER window (always withdraw before generating a new force versus distance curve).
- 10.34 Click again SINGLE FORCE at the MAIN window. A new force versus distance curve will be generated. Click again CONTROL+I, and a small window will pop-up. This time drag the hollowed-circle icon (labeled A) to the end of the approaching curve, which corresponds to the end of the contact regime between the rotavirus-coated probe and the NOM-coated silica surface. Similarly, drag the hollowed-squared icon (labeled B) to approximately the beginning of the contact regime. The contact region between the rotavirus-coated silica colloidal probe and the calibration grid is characterized by a perfectly linear regime.
- 10.35 In the small window generated right below the force versus distance curve, notice the values of ΔX and ΔY , which represents the slope of the contact region between the rotavirus-coated silica colloidal probe and the NOM-coated silica surface.
- 10.36 The ratio of these 2 values (ΔX and ΔY) must be close to 1 ($\pm 5\%$). This indicates that the previous measurement of sensitivity of the clean colloidal silica probe was correct and in good agreement with the now rotavirus-coated silica colloidal probe. If there is a noticeable difference between both sensitivities, then probably the cantilever was affected by the coating process (although this possibility rarely occurs).

- 10.37 Click WITHDRAW at the SUM AND DEFLECTION METER window.
- 10.38 At this point, we have calibrated the necessary parameters for conducting force versus distance curves (e.g., spring constant, sensitivity, virtual defl line, defl invols, scan rate, and force distance).
- 10.39 Subsequently, at the AR SAVE PANEL, choose a BASE NAME for the force versus distance curves to be generated and a PATH in the hard disk. Click SAVE CURVES TO DISK at the MAIN menu/SAVE tab.
- 10.40 By clicking FORCE CURVE at the MAIN window, a new force versus distance curve will be generated and it will be automatically saved in the PATH declared.
- 10.41 Remove the head and place it upside down next to the base.
- 10.42 Remove the cantilever holder as previously describe. In addition, using tweezers and under a microscope (10X), remove the cantilever from the holder and carefully place it in a cantilever box.
- 10.43 Turn off the software, turn off the laser switch, set the intensity controller to 0, turn off the high intensity illumination switch, and finally turn off the power of the molecular force probe 3D controller.

11 *References*

1. Rolsma, M. D.; Gelberg, H. B.; Kuhlenschmidt, M. S., Assay for Evaluation of Rotavirus-Cell Interactions - Identification of an Enterocyte Ganglioside Fraction That Mediates Group-a Porcine Rotavirus Recognition. *Journal of Virology* **1994**, 68, (1), 258-268.
2. Rolsma, M. D.; Kuhlenschmidt, T. B.; Gelberg, H. B.; Kuhlenschmidt, M. S., Structure and function of a ganglioside receptor for porcine rotavirus. *Journal of Virology* **1998**, 72, (11), 9079-9091.

3. Gutierrez, L.; Li, X.; Wang, J. W.; Nangmenyi, G.; Economy, J.; Kuhlenschmidt, T. B.; Kuhlenschmidt, M. S.; Nguyen, T. H., Adsorption of rotavirus and bacteriophage MS2 using glass fiber coated with hematite nanoparticles. *Water Research* **2009**, 43, (20), 5198-5208.
4. Gutierrez, L.; Mylon, S. E.; Nash, B.; Nguyen, T. H., Deposition and Aggregation Kinetics of Rotavirus in Divalent Cation Solutions. *Environmental Science & Technology* **2010**, 44, (12), 4552-4557.
5. Liu, Y.; Janjaroen, D.; Kuhlenschmidt, M. S.; Kuhlenschmidt, T. B.; Nguyen, T. H., Deposition of cryptosporidium parvum oocysts on natural organic matter surfaces: Microscopic evidence for secondary minimum deposition in a radial stagnation point flow cell. *Langmuir* **2009**, 25, (3), 1594-1605.
6. Gutierrez, L.; Nguyen, T. H., Interactions between Rotavirus and Suwannee River Organic Matter: Aggregation, Deposition, and Adhesion Force Measurement. *Environmental Science & Technology* **2012**, 46, (16), 8705-8713.